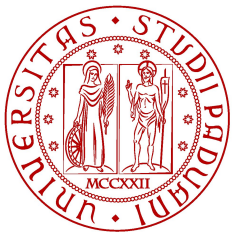

UNIVERSITÀ
DEGLI STUDI
DI PADOVA

Sede Amministrativa: Universitá degli Studi di Padova

Dipartimento di Ingegneria Civile, Edile e Ambientale (ICEA)

SCUOLA DI DOTTORATO DI RICERCA IN
SCIENZE DELL'INGEGNERIA CIVILE ED AMBIENTALE
Indirizzo Comune
XXVI CICLO

Sediment yield in rivers at different time-scales

Direttore della Scuola: Chiar.mo Prof. Stefano Lanzoni

Supervisori: Chiar.mo Prof. Andrea Defina

Chiar.mo Prof. Giampaolo Di Silvio

Dottoranda: Mariateresa Franzoia

Aknowledgements

I would like to express my sincere gratitude to my advisor, Professor Giampaolo Di Silvio, for having encouraged in me a passion for the topic of the sediment transport, for his guidance, caring and patience. Special thanks also to Professor Andrea Defina.

I really appreciate the feedback offered by Professor Roberto Ranzi during the revision of my thesis.

I would also like to express my gratitude to Corila for their financial support.

Special thanks to the staff of Corila and Cnr-Ismar, who helped me to develop some researches; furthermore I have greatly benefited from the help of the staff of ArpaV for the collection and interpretation of data. A deep appreciation goes to Michael Nones who helped me to take the first steps in my PhD carrier, for his support and patience.

My debt is also to the XXVI–PhD team and to the ex–biblioteca office team for the time spent together and for the support given to me.

Abstract

The present thesis is devoted to a particular topic regarding the fluvial sub-systems, namely the evaluation of the annual amount of sediment yield through a given cross-section of a river. This problem has been largely investigated in literature and the resulting models can be classify in different groups depending on the morphological characteristics they take into account and their complexity. In any case the large quantity of data required is always the main problem. With this work we want to find simple relationships that require the lesser number of data as possible, so we have made our evaluations at a basin-scale and assumed for the river the Local Uniform Flow hypothesis (LUF). Accordingly, each river reach is defined by its length, width, slope and bottom composition, while the watershed area is collapsed in its barycentre which coincides with the upstream end of the LUF reach.

A basic state, called equilibrium and represented by a stationary rating curve (a monomial relation between the solid and the liquid discharge of Engelund-Hansen type) is first identified, with the purpose to evaluate the deviations of the real solid transport from the equilibrium value, deviations that depend on the time-scale considered. In particular we have developed three models, valid in three different time-scales.

For the short-term analysis we use the 1-D deterministic solution of the harmonic river which provides the delay and attenuation of the perturbation of the solid transport with respect to the equilibrium condition. In other words we link the actual deviations of the solid transport recorded downstream with previous perturbations of the liquid discharge, happened upstream.

For a pluri-annual time-scale we integrate the 1-D morphodynamic model to a zero-dimensional model. As the water and sediments inputs to the river are concentrated

in its upstream end, the width of the entire river is assumed to be constant, whilethe slope and the grain-size composition are considered to be variable in time. The resulting mathematical model is implicit and non-linear, but at this time-scale we simplify it in order to find a simple and generic analytical solution for the pluri-annual morphological evolution of the river.

Finally, for very long-term analysis we integrate numerically the exact 0-D morphodynamic model to predict the morphological reactions of a river at geological time-scale. In this case we schematize the river with two contiguous LUF channel, representing the highland and the lowland parts of the real watercourse respectively. In this way, this model can simulate the typical behaviour of natural rivers showing a grain-size segregation (fining) in the downstream direction, accompanied by smaller slopes, without the computational costs necessary for a complete one-dimensional model.

Some comparisons and numerical applications have been made.

Sommario

Questa tesi é dedicata ad un tema particolare che riguarda i sotto-sistemi fluviali, vale a dire la valutazione dell'importo annuo di produzione di sedimenti attraverso una determinata sezione fluviale. Questo problema é stato ampiamente studiato in letteratura e i modelli sviluppati possono essere classificati in diversi gruppi a seconda delle caratteristiche morfologiche di cui tengono conto e della loro complessitá. In ogni caso, il problema principale é sempre la grande quantitá di dati richiesti. Con questo lavoro vogliamo trovare delle semplici relazioni che richiedano il minor numero di dati possibile, per questo abbiamo sviluppato le nostre valutazioni ad una scala spaziale di bacino ed assunto per il fiume l'ipotesi flusso localmente uniforme (LUF). Di conseguenza ogni tratto fluviale é definito dalla sua lunghezza, dalla larghezza, dala pendenza e dalla composizione granulometrica del fondo, mentre l'estremitá a monte del canale LUF coincide col baricentro del bacino in cui si assume sia concentrata l'intera area.

Prima si identifica una condizione di base, chiamata di equilibrio e rappresentata da una curva stazionaria (una relazione monomia tra le portate solida e liquida di tipo Engelund-Hansen), con lo scopo di valutare le deviazioni del trasporto solido reale dal valore di equilibrio, deviazioni che dipendono dalla scala temporale considerata. In particolare abbiamo sviluppato tre modelli, validi per tre diverse scale temporali.

Per l'analisi a breve termine usiamo la soluzione deterministica armonica 1-D del fiume, che fornisce il ritardo e l'attenuazione della perturbazione del trasporto solido rispetto alla condizione di equilibrio. In altre parole, colleghiamo le deviazioni effettive del trasporto solido registrate a valle con le precedenti perturbazioni della portata liquida avvenute a monte.

Per una scala pluriannuale integriamo il modello morfodinamica 1-D ad un modello zero-dimensionale. Dato che gli ingressi di acqua e sedimenti al fiume sono concentrati alla sua estremitá a monte, la larghezza dell'intero fiume é ipotizzata costante, mentrela pendenza e la composizione granulometrica sono considerate essere variabili nel tempo. Ne risulta un modello matematico implicito e non lineare, ma a questa scala temporale lo possiamo semplificare al fine di trovare una soluzione analitica semplice e generica per l'evoluzione morfologica pluriennale del fiume.

Infine, per un'analisi a lungo termine integriamo numericamente il modello morfodinamico 0-D esatto per valutare le reazioni morfologiche di un fiume a scala temporale geologica. In questo caso si schematizza il fiume con due canali LUF contigui, che rappresentano rispettivamente il tratto montano e e il tratto di pianura del reale corso d'acqua. In questo modo, questo modello puó simulare il comportamento tipico dei fiumi naturali mostrando una differenziazione granulometrica (affinamento) verso valle accompagnata da pendenze minori, senza i costi computazionali necessari per un modello unidimensionale completo.

Sono stati fatti alcuni confronti e applicazioni numeriche.

Contents

Chapter 1

Introduction

The amount of sediment conveyed by a river through a given cross-section during a period of time (***sediment yield***) is somehow connected with, but not identical to, the amount of sediments detached from the watershed surface (***sediment production***) during the same period of time. Usually, the evaluation of the sediment production lies in the specialization of a number of disciplines, depending upon the dominant mechanism of the detachment (wind erosion in desert areas, surface erosion from inland, mass erosion from inclined slopes, intermediate forms, etc...); while the evaluation of the sediment transported by a watercourse resides traditionally in the proficiency of fluvial engineering. In this thesis the attention has been especially (although not exclusively) given to the sediment transported by the river, with the implicit presumption that the hydrological, morphological and grain-size features of the river itself are somehow "imprinted" by the sediment production from the watershed surface, not only contemporary but in all the preceding time. This presumption is obviously related to the concept of *equilibrium* (only in a hypothetical full equilibrium conditions there is a coincidence between sediment production and sediment yield) and therefore on the relate concept of *space-* and *time-scale*.

These preliminary ideas will be then briefly discussed in the following paragraphs.

1.1 Concept of equilibrium

In the present text "equilibrium" is defined as a stationary condition of the system under consideration, related to a specific space- and time-scale of the processes involved. As far as sedimentary systems [Allen, 1974] are concerned (like watercourses, estuaries, littorals, etc...), we may state that the entire system, or any part of it (sub-system), is in equilibrium if it does not change its shape (morphology) when averaged over a convenient interval of time. To define an equilibrium condition is then necessary to specify both the significant length of the (sub-)system (space scale) and the duration of the relevant morphodynamic process controlled by this length (time scale). The two scales are mutually related, depending upon the sub-system considered.

For a watercourse, the overall system is its hydrographic basin and the significant space-scale may be represented by the river length or, as we will see later (section 5), by a more significant "filling volume". The time-scale of the relevant morphodynamic process (altimetric and planimetric evolution of the entire hydrographic network) may be represented by the "filling time " of this volume by the sediment production from the watershed surface. The filling time of a large river is extremely long (up to 10^4 years) and its equilibrium can only be defined as an (eventual) stationary condition averaged over such a long period.

Beside the overall system (river watershed), however, one may also consider the following progressively smaller sub-systems and the corresponding significant space scale. The relevant morphodynamic process is indicated between brackets while the corresponding response time is scaled with the ratio between the space scale and the sediment flux (water velocity times volumetric concentration):

- length of the reach between subsequent main tributaries (evolution of the bottom profile and composition);
- width of the reach (evolution of river mega-forms: braids and meanders);
- depth of the reach (evolution of river meso-forms: dunes);
- height of the laminar boundary layer (evolution of river micro-forms: ripples);

- sediment grain-size (entrainment, transport and deposition of particles).

The evolution of the various (sub-)systems could be simulated, in principle, by solving the appropriate partial differential equations in time and space that describe each relevant process. As all the processes are mutually interacting, all the equations should be in general considered coupled and solved together. This approach, in practice, is obviously unfeasible and several simplifications, to be discussed later, are to be introduced.

The first basic simplification (more or less implicitly presupposed in most morphodynamic problems) consist in decoupling the different processes, by postulating that the respective time- and space-scale are substantially different. In this way, if we are interested in simulating the time-history of a certain sub-system (e.g., the evolution of the dune pattern when the river flow changes) we shall suppose that, during the evolution period, both the super-ordinate (larger) and sub-ordinate (smaller) sub-systems are in "equilibrium". In particular we assume that the super-ordinate sub-systems (braids, meander, river reach, hydrographic network) are strictly stationary, while the sub-ordinate sub-systems (ripples, particles dynamics) maintain a statistical configuration instantaneously adapted to the water flow. In other words, for simulating the dune pattern evolution, both the larger and the smaller sub-systems do not need to be explicitly reproduced by solving partial differential equations but they can be accounted for by simple algebraic (i.e. "equilibrium") equations.

1.2 Fluvial (sub-)systems at different scales

The space- and time-scales discussed above characterize the various sub-systems of a river in *relative* terms, inasmuch as they refer to the specific quantity (e.g. the river depth for dunes) that controls the respective morphodynamic process. By considering the actual dimensions of the river, however, the *absolute* space-scale may range over tens order of magnitude from the experimental devices of a laboratory, up to the fluvial watershed of continental size. In terms of time-scale, the range may in principle be even much wider, from fraction of seconds in laboratory experiments to eras or periods

of the geological evolution. In the graph of Figure 1.1 [Di Silvio, 2008] the time-scale as been conventionally limited by the last glaciations (Würm glaciation), after which the climatic conditions can be considered reasonably stationary.
In the same graph are shown the typical domains of interest for laboratory experiments, hydraulic structures and environmental engineering, as well as for geological sciences involving much longer time-scales. The straight lines,corresponding to the ratio between *absolute* space- and time-scale, represent the velocities of the respective morphological process, without reference however to the specific sub-system controlled by the *relative* scale.

For applications to *hydraulic structures* the relevant sub-system is usually the river width, or even (for single localized elements) the river depth. Depending upon the river size the corresponding *absolute* space-scale may range between meters and kilometers, while the time-scale varies between second and days.

For *hydraulic models* in laboratory the space- and time- scale of the structure would be correspondingly reduced according to, say, the Froude similitude. While for *basic experiments* the absolute size is very often even smaller, as they may include smaller (sub-ordinate) sub-systems like the laminar boundary layer or even the particles grain-size.

For *environmental engineering*, by contrast, the absolute scales largely increase, as the relevant system is usually the entire watershed or, at least, the river reach between two subsequent main tributaries. Indeed, in order to predict the effects of large river works (e.g. a dam) it is necessary to include in the simulation a substantial part of the river down to the coast, where the negative effects are expected to show up, albeit not immediately, and protection or mitigation measures should be timely taken. The reaction time of large rivers is in fact very long and in some cases the anthropogenic perturbations produced by the river works tend to interact with the natural perturbations produced by climatic changes. In such a case the simulations for environmental engineering should be extended well beyond the conventional limit of stationary climatic conditions and more into the domain of *geological sciences*. On the other hand the analysis of fluvial paleo-morphology as consequence of geological

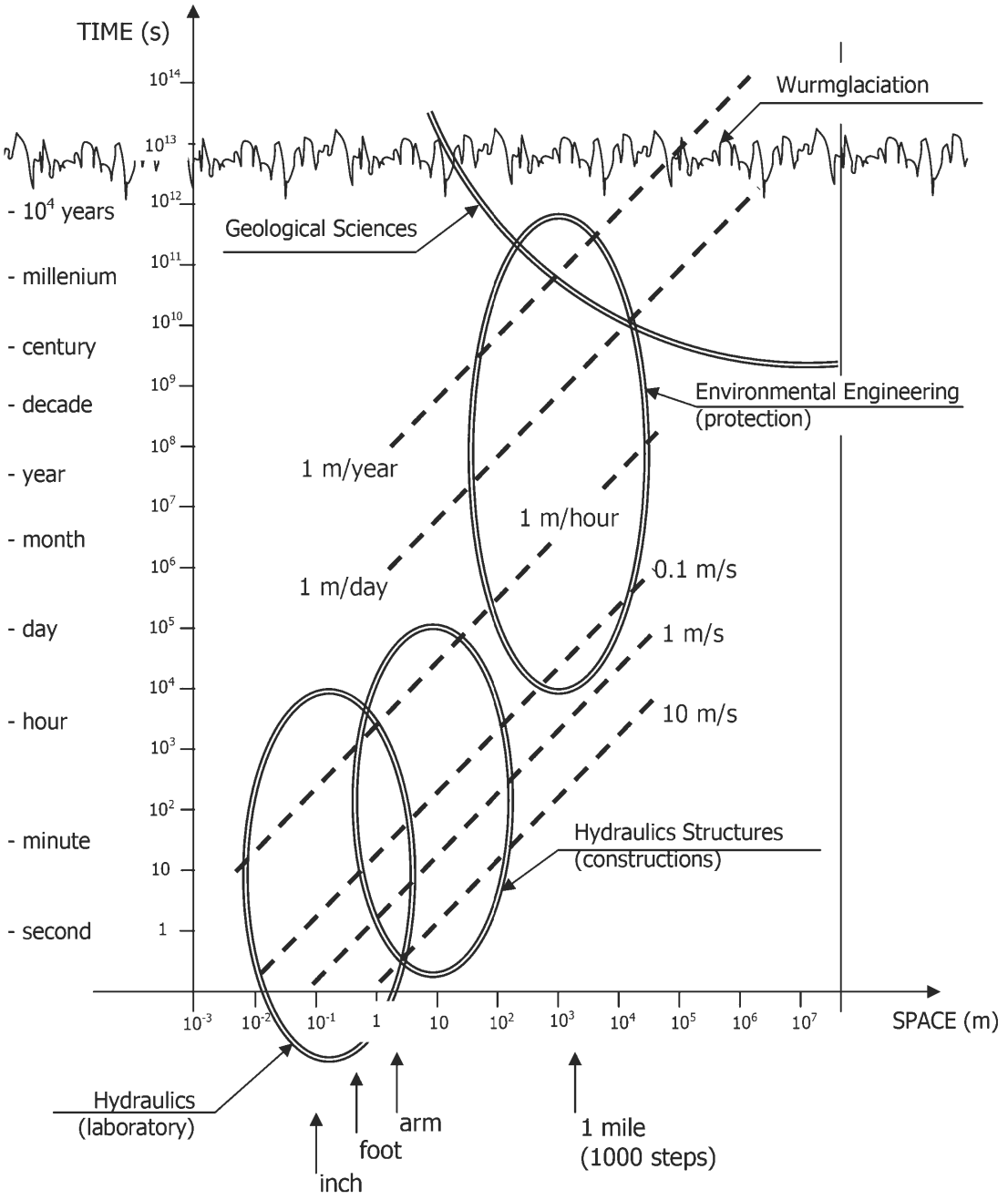

Figure 1.1: A graphical representation of the absolute time- and space-scales for fluvial systems with typical zones of interest of various applications [Di Silvio, 2008].

forcing (climate and tectonics) are nowadays well developed [Allen and Heller, 2012] and could in principle be fruitfully combined with fluvial mathematical modeling .

1.3 Scope and structure of the thesis

The present thesis is devoted to a particular topic regarding the fluvial sub-systems, namely the evaluation of the annual amount of sediments transported by the river (*sediment yield*) through a given cross-section. Of course, an experimental evaluation can be made by a continuous recording of solid discharge (both in suspension and as bed load) integrated over the year, and this is in fact what it is made (more or less accurately) in a great number of gauge stations around the world. However, a part of from the difficulties of measuring accurately all the requested quantities, the available records are far from being sufficient in terms of number of stations, length of records and reliability of data.

In the practice the continuous measurements of the sediment transport, especially bed load, are difficult and not so precise. Also for the suspended load we had in the past only the analysis of periodic manual samples, an expensive practice that often could not be done during a flood event. Today optical automatic instruments, that measure continuously the turbidity of the flow, or acoustic devices, as the ADCPs (Acoustic Doppler Current Profilers), are typically used. In order to have TSM (Total Suspended Matter) concentration data, a transformation law is calibrated thanks to periodic samples from which the direct value of the concentration is known (as performed by Gentile et al. [2010] and in Di Silvio et al. [2011]). In any case gauging stations of this type are few and generally they work only for short periods, with no possibility to create statistically valid records. Here we just mention that in Asian watershed there is a different situation: the large rivers flowing in China or in Vietnam are better monitored (always measuring only the suspended material) and the long series of data are used in literature to evaluate their sediment contribution and how it is influenced by the human activities [Walling, 2006, Le et al., 2007, Zhang et al., 2011].

Another important source of data for the evaluation of the integrated sediment yield over relatively log periods is represented by repeated bathymetric surveys of reservoirs

that intercept the sediment transport.

In the present thesis an alternative procedure to evaluate the sediment yield of a particular basin is considered. This method is based on the use of appropriate mathematical models that predict the detachment of sediments from the watershed slopes (**sediment production**) and their subsequent movement along the hydrographic network (**sediment transport**), from the thinnest ephemeral drainage print of the overland flow, down to the considered cross-section of the river.

Existing models of both sediment production and sediment transport can be classified according to the time- and space-scale they refer to. Moreover, three main categories of modelling approach are generally identified: empirical, conceptual or physically based models. A wide description and differentiation between these three types of models is given by Merritt et al. [2003]. They sets that the distinction is not sharp but often models are hybrids between two of these classes: often physically based rainfall-runoff models are coupled with empirical relationship used to model erosion and sediment transport. Depending on the type of model, we need more or less detailed information about the territory and the climatic conditions.

A lot of works has been done to predict the **sediment production** of a catchment. The processes involved are quite known, but uncertainly predictable from the quantitative view point. Indeed there is no a typical detachment rate for a specific region because large local variations occur. Moreover the soil losses at one scale are not representative for the losses at another scale because of the extremely variable "delivery ratio" [De Vente and Poesen, 2005].

In literature there are several different procedures to calculate the long-term surface erosion rate from a hill-slope, from the classical USLE formula [Wischmeier and Smith, 1978], to its subsequent numerous adaptations (RUSLE, MUSLE, etc...); all of them depending on rainfall intensity, runoff, soil erodibility, vegetation cover and slope angle. The most significant (and uncertain) factor for surface erosion is the vegetation cover, which may vary over many orders of magnitude when we pass from bare soil to a well managed forest. It should be noted, however, that surface erosion is not the only active mechanism of sediment production; for forested watershed, for instance, mass

movement (landslides and debris flows) plays a definitely dominant role.

Sediment production from the watershed slopes represents the boundary conditions for the transport in the hydrographic network of the rivers, which can be simulated in principle by the complete one-dimensional (1-D) model described in Chapter 2.

Unluckily, the available information are in general very few and uncertain also for implementing a complete 1-D model of the river. To cope with the usual scarcity of data a series of simplifications for the 1-D model have been introduced, which will be described in the same Chapter 2. One of the basic simplifications is the transformation of the 1-D approach into zero-dimensional (0-D) approach, which permits the evaluation of the annual amount of sediments transported by the river (sediment yield) through a given cross-section, taking into account the general lack of morphological information we are dealing with. In fact 0-D models can simulate the behaviour of the entire hydrographic basin, and thus predict the sediment yield at different time-scales: from daily/monthly scale, to annual, pluri-annual, up to geological scale too. By the models proposed here we tried to find a direct evaluation of the sediment yield, from the typical information available for most of the natural rivers: mean river width, mean bottom slope and, most difficult, mean bed composition, as well as long records of the liquid discharge.

The structure of the thesis is developed as follows.

Chapter 2 - The one-dimensional morphodynamic model and its simplifications, after a brief description of the complete one-dimensional formal model, presents an analytical solution, proposed by Fasolato et al. [2009], based on two main hypothesis: we will take into account two representative classes of the nonuniform sediment grain-sizes and we will consider a configuration of long-term equilibrium. Moreover a particular rating curve to calculate the "equilibrium" solid transport as a function of the principal mean morphological characteristics and the liquid discharge will be proposed. The analytical solution is then simplified, assuming the Local Uniform Flow hypothesis (LUF) (see section 2.6.2), in order to evaluate the deviations from the long-term equilibrium configuration

of the instantaneous measured solid transport at a gauge station caused by variable boundary conditions at the upstream and downstream ends of the channel. Namely we consider the watershed area collapsed in its "barycenter", which is the upstream end of the LUF channel, so considering a zero-dimensional model of the basin.

Then three principal models for the sediment yield evaluation are investigated, increasing step by step the considered time-scale. All the models proposed consider the basin-scale as a space-scale.

Chapter 3 - Long-term equilibrium model with short-term perturbations: this model is the application of the deterministic analytical solution described in the Chapter 2 through specific procedures of calibration of the model against a set of measured data. A particular attempt to evaluate the boundary conditions represented by the sediment and water input concentrated at the upstream end of the channel in dependence of the downstream measures is proposed.

Chapter 4 - Long-term non-equilibrium model: with this model we investigate an intermediate time-scale. Renouncing to the hypothesis of the existence of a long-term equilibrium, we admit that the rivers are pluri-annually evolving and only a short-term (annual) equilibrium can be identify. The one-dimensional model is integrated to a zero-dimensional model, more representative for the basin scale and for the time-scale considered. Then numerical observations lead to particular simplifications in order to find an original analytical solution for the morphodynamic evolution of the river. With measured data we made some attempts to use this analytical solution in order to evaluate the term of the sediment input at the upstream end of the river.

Chapter 5 - Morphological reactions rivers at geological scale: in this Chapter the integrated 0-D model is used for very long-term simulations in order to evaluate the morphological reactions of a schematic river to long-term perturba-

tions of the boundary conditions. In order to represent the typical concave profile, the model is split in two reaches standing for the highland (mountain) and the lowland (plain) courses respectively, generally recognizable in a natural river.

Chapter 6 - Conclusive remarks and prospective: some conclusive remarks and prospective for possible developments of this research are reported.

Chapter 2

The one-dimensional morphodynamic model and its simplifications

2.1 The one-dimensional morphodynamic model

The system describing the one-dimensional morphodynamic model (Figure 2.1) is composed by the continuity equation of the water flow, the momentum balance along the stream (De St. Venant equation simplified considering equal to 1 the Coriolis coefficients) , the continuity equation of the sediment (Exner equation, which express the sediment exchange between the flow and the bottom) and the sediment balance per each size fraction i of the active layer (Hirano equation (1971)):

$$\begin{cases} \dfrac{\partial Q}{\partial x^*} + \dfrac{\partial (BY)}{\partial t^*} = 0 \\ \dfrac{\partial}{\partial x^*}\left(Y + H + \dfrac{Q^2}{2gA^2}\right) = -\dfrac{1}{g}\dfrac{\partial U}{\partial t^*} - j \\ \dfrac{\partial (BY)}{\partial t^*} = -\displaystyle\sum_{k=1}^{N} \dfrac{\partial P}{\partial x^*} \\ \dfrac{\partial (\beta_k \delta B)}{\partial t^*} = -\dfrac{\partial P_k}{\partial x^*} - \beta_k^* \left(\dfrac{\partial (BY)}{\partial t^*} - \dfrac{\partial (\delta B)}{\partial t^*}\right) \end{cases} \tag{2.1}$$

where x^* is the longitudinal axes of the river and t^* is the time, Q is the liquid discharge, H is the bed elevation above a reference, B, Y and $A = BY$ are respectively the width, the mean water depth and the area of the cross section, U is the mean velocity of the flow, j is the slope of the energy line, P is the solid transport, δ is the thickness of the active layer. The mass balance of the sediments consider two layer: the transport layer and the mixing layer, in which the suspended transport and the bed load transport take place respectively [Hirano, 1971]. The sediment is composed by N grain size, each of which is present in the bottom with a β_k percentage, in the transport with a α_k percentage and below the active layer with a β_k^* percentage.

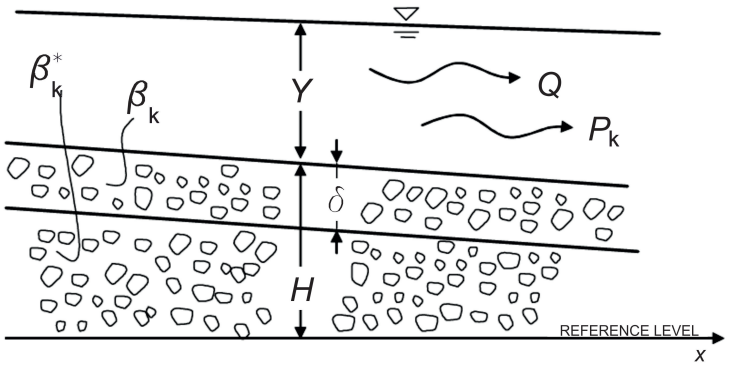

Figure 2.1: Scheme and nomenclature of the 1-D morphodynamic model of a river.

The previous system is closed by a uniform flow empirical formula and by a solid transport formula. For the first we can use the Chézy formula (2.2) or the Gauckler-Strickler (2.3) formula:

$$Q = \chi A (Yj)^{1/2} \tag{2.2}$$

$$Q = k_s A Y^{2/3} j^{1/2} \tag{2.3}$$

where χ and k_s are respectively the Chézy and the Gauckler-Strickler roughness coefficients. They empirically express the ratio between mean and friction velocity, in its turn linked to the relative or absolute size of the roughness of the bottom. If we admit

that the roughness of the bottom is represented by the term d_{90} (the diameter of the sediment class larger than the 90% of the entire sample of sediment) we can use the following relationships:

$$k_s = \frac{26}{d_{90}^{1/6}} \qquad \chi = 26\left(\frac{Y}{d_{90}}\right)^{1/6}$$

The total solid transport of each component d_k of the grain-size distribution can be approximated with a transport formula of the Engelund-Hansen type [Engelund and Hansen, 1967]:

$$P_k(t) = \alpha_{EH}\frac{Q^m(t)\ j(t)^n}{B(t)^p\ d_k^q} \tag{2.4}$$

where the coefficient α_{EH} and the exponent m are site-specific dimensionless calibration parameters while the values of the exponents n, p and q depend on the value of m, calculated from a dimensional analysis considering which uniform flow equation is used. In particular in the Table 2.1 the values for the exponents n, p, and q are reported in the case we had considered the Chézy formula (2.2) or the Gauckler-Strickler formula (2.3).

Table 2.1: Values of the exponents in the equation (2.4)

uniform flow formula	$\boldsymbol{n}$	$\boldsymbol{q}$	$\boldsymbol{p}$
Chézy	m	$m-1$	$\frac{3}{2}(m-1)$
Gauckler-Strickler	$\frac{7}{6}m$	$m-1$	$\frac{3}{2}(m-1)$

In this case, with multiple grain-size composition, the rating curve has to be applied to each grain-size. Then the total transport $P(t)$ is given by the sum

$$P(t) = \sum_{k=1}^{N} P_k(t) = \alpha_{EH}\frac{Q^m(t)\ j(t)^n}{B(t)^p\ d_{eq}^q}$$

where d_{eq} is an equivalent diameter representing the non-uniform movable bottom of the river. This value will not be simply the mean diameter of the grain-size composition: we use the relation (2.4) modified like in Di Silvio and Peviani [1991], where the effect of the mutual influence of grain of different sizes is taken into account through the

hiding-exposure coefficient ζ_k [Egiazaroff, 1965], reported in the equation (2.6):

$$P_k(t) = \alpha_{EH} \frac{I(t)^n}{B(t)^p} \frac{\beta_k(t)\zeta_k(t)}{d_k^q} Q^m(t) \tag{2.5}$$

$$\zeta_k(t) = \left(\frac{d_k}{\sum_1^N \beta_k(t) d_k} \right)^s \tag{2.6}$$

An explicit evaluation of the d_{eq} will be made in the section 2.5 for the particular case of $N = 2$.

The monomial relation between the solid and the liquid discharge, like the (2.4), is properly valid only for an immediate adaptation of the transport to the local conditions. It is possible however to identify a particular length along the river after which the concentration of the sediment in the water column is completely adapted; in analogy with the uniform flow relationship, which are only valid when the flow is fully developed.

2.2 Boundary conditions

In order to solve the 1-D model just exposed we have to set the boundary conditions of the system. The number of necessary prescribed boundary conditions depends on the number N of grain-size fractions that are put into account and on the type of the motion of the sediment that is considered, either total or suspended [Sieben, 1997]. As said in the previous section the transport is considered as total. In this case we need to prescribe the liquid input $Q(x^* = 0, t)$ and the N components of the solid input $G_k(x^* = 0, t)$ upstream in addition to one boundary condition downstream that depend on the flow regime. For super-critical flow ($F_r \geq 1$) the bottom elevation downstream $H(x^* = L, t)$ has to be prescribed; for sub-critical flow ($F_r < 1$) the water elevation $(H(x^* = L, t) + Y(x^* = L, t))$ has to be prescribed.

A fundamental requirement for a model representing the sediment transport is the sediment input $G_k(x^* = 0, t)$, i.e. the sediment production of the basin.

Models that simulate the sediment production and models that simulate the sediment transport could in principle be combined, provided that their simulation is relatively accurate, for example in order to evaluate the effects of relevant human interventions on the watershed area [Ranzi et al., 2012]. Because of the large scale considered and the extreme variability of the conditions upon the surface of a basin, in this work we will concentrate the attention on the process of the sediment transport, knowing that a detailed model for the sediment production always need a more precise (2-D) description of the real situation all over the watershed.

Indeed, if we are able to model the entire network of the watercourse in the basin, we would be allowed to take into account only the sediment transport process by considering that the smallest upstream creeks are in equilibrium conditions: namely that the input (sediment production) is equal to the output (sediment to the downstream network).

2.3 Simplifications: the Local Uniform Flow (LUF) hypothesis

Numerical solutions of the model described in the section 2.1, more or less simplified, have been already proposed by numerous authors (for example Bellos and Hrissanthou [2003] applied to experimental laboratory data or Fang et al. [2008] applied on the Hongshui River in China measurements).

In the following we will introduce further simplifications for the waterflow (De St. Vanant) equations. First we will assume the instantaneous propagation of the liquid wave to simplify the continuity equation, then the quasi-steady flow conditions are assumed to simplify the momentum balance equation. This conditions are always valid if we have a flood wave shorter than the distance between two principle tributaries.

The resulting water flow equations are the following:

$$\begin{cases} \dfrac{\partial Q}{\partial x^*} = 0 \\ \dfrac{\partial}{\partial x^*}\left(Y + H + \dfrac{Q^2}{2gA^2}\right) = -j \end{cases} \tag{2.7}$$

A last simplifying hypothesis, virtually necessary for long-term simulations at basin scale, is considering the energy slope equal to the bottom slope, when it is averaged over a convenient length. The so called Local Uniform Flow (LUF) assumption allows notable simplifications of the analysis, but it is not always applicable. Validity limits will be discussed in the section 2.6.2.

The liquid flow (LUF) equations become:

$$\begin{cases} \dfrac{\partial Q}{\partial x^*} = 0 \\ \dfrac{\partial H}{\partial x^*} = \dfrac{\partial}{\partial x^*}\left(Y + \dfrac{Q^2}{2gA^2}\right) \end{cases} \tag{2.8}$$

2.4 Solid transport equation and sediment rating curve

In laboratory the solid transport equation is calibrated in strictly equilibrium conditions. For a certain configuration of the flume (prescribed slope and grain-size composition) in a closed circuit, there is a unique relationship between liquid and solid discharge (sediment rating curve) of the type :

$$P(t) = MQ^m(t) \tag{2.9}$$

where M is a constant coefficient and m a constant exponent depending on the flume configuration (the bottom slope i, the channel width B and the grain-size d), as expressed by the Engelund-Hansen type relationship [Engelund and Hansen, 1967] (2.4):

$$M \propto \frac{i^n}{B^p d^q} \tag{2.10}$$

In nature the profile and bed composition of rivers hardly attain equilibrium con-

ditions at basin scale, except for very small watershed (see section 1.1).

Even if we are not properly in equilibrium conditions, however, the measured sediment transport at a gauging station in a certain point of a river (usually at the closure of a particular watershed area) can be recognize to be approximately on phase with the behaviour of the correspondent liquid discharge recorded at the same cross section, provided that time-averages values are considered at an appropriate time-scale. In this regard we consider a time-scale short enough in order to neglect natural changes (subsidence or tectonic uplift; climatic forcing) but long enough in order to consider correspondingly enough large space-scale to neglect the variations of the micro- (e.g. ripples and particles) and meso-forms (e.g. dunes) (see section 1.1). Although the rivers are influenced by seasonal, annual and pluri-annual fluctuation of the boundary conditions, we postulate that at reach scale the mean morphological characteristics (mean longitudinal and planimetric profiles, mean bottom composition) remain unchanged over the selected observation time. Indeed we improperly call this configuration as the "equilibrium" state, and calibrate a rating curve [Asselman, 2000], also called equilibrium curve, namely the average relation between liquid and suspended sediment concentration for a certain location.

The most commonly used sediment rating curve find the sediment concentration C of the flow as a power function of the liquid discharge Q, of the type:

$$C(t) = MQ^{m'}(t) \tag{2.11}$$

where the quantities M and m' are calibrated against a set of data; m' is dimensionless, while the dimension of M depends on the value of m' [Syvitski et al., 2000]. As the solid discharge is given by the multiplication of the concentration and the liquid discharge, we find again:

$$P(t) = C(t)Q(t) = MQ^{(m'+1)}(t) = MQ^{m}(t) \tag{2.12}$$

This relation is reported in the Figure 2.2.

A lot of studies find site-specific calibration parameters by a linear interpolation

(Asselman [2000] is one of the most cited work in the early years) minimizing the root square error of the logarithmic relation: $log(P(t)) = log(M) + m\ log(Q(t))$. We will resume this topic at the section 3.2. Only just to emphasize the fact that this formula is strictly site-specific, i.e. strictly connected to the specific environment and period which the data referred to.

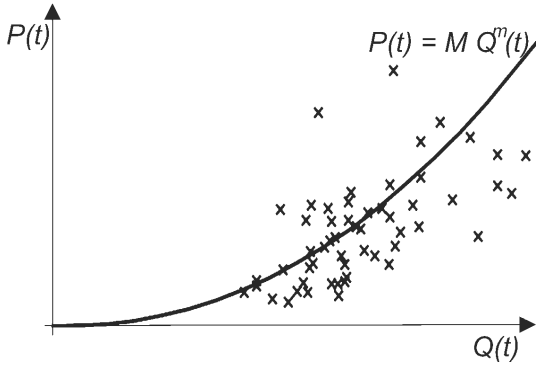

Figure 2.2: Example of the relation between the solid and the liquid discharges: rating curve.

Physical interpretation of these rating curve have been made. For example Müller and Förstner [1968] found that the coefficient M increase with the meteorological events intensity or with the erodibility of the channels. Asselman [2000] sad that the exponent m (or m') represents the erosive power of the river, with large values being indicative for rivers with a strong increase in erosive power and in sediment transport capacity when discharge increases, While high values of the coefficient M occur in areas characterised by intensively weathered materials, which can be easily eroded and transported. However m and M parameters of sediment rating curves are obviously inversely correlated.

The parameter M include information that convert liquid discharge in sediment discharge and we call it the *morphodynamic parameter*. If we consider a relation of Engelund-Hansen type [Engelund and Hansen, 1967] (2.4) we can link the morphodynamic parameter directly to the time-averaged morphology of the river represented by the time-averaged width B, the time-averaged slope I and the time-averaged-grain size of the sediment d:

$$M = \alpha_{EH} \frac{I^n}{B^p d_{eq}^q} \tag{2.13}$$

2.5 Two representative grain-size classes

In sake of simplicity we consider only two representative diameter of the sediment, representing respectively the fine d_f and the coarse d_c fraction of the sediment. We say that the composition of the bottom is β for d_f and $(1-\beta)$ for d_c. Similarly the composition of the transported sediments is α for d_f and $(1-\alpha)$ for d_c. Knowing that $P(t) = \sum P_k(t)$, we can express the equivalent diameter of the grain size of the bottom through the relation of the hiding-exposure coefficient and defining $d = d_f/d_c$, a sort of a measure of the level of uniformity of the grain-size of the bottom:

$$d_{eq}(t)^q = \frac{\beta(t)((1/d)^{q-s} - 1) + 1}{d_c^q(\beta(t)(d-1)+1)^s} \tag{2.14}$$

Moreover we can also express the composition of the transport α, i.e. $\alpha = P_f(t)/P(t)$, in relation with the composition of the bottom β:

$$\alpha(t) = \frac{\beta(t)(1/d)^{q-s}}{\beta(t)((1/d)^{q-s} - 1) + 1} \tag{2.15}$$

We can now write the total transport of the river as:

$$P(t) = \alpha_{EH}\frac{I(t)^n}{B(t)^p d_{eq}(t)^q}Q^m(t) = M(t)Q^m(t) \tag{2.16}$$

where M, the *morphodynamic parameter*, incorporates all the morphological characteristics of the river in a simpler monomial relation. Substituting the expression (2.14) in the (2.16) to get the complete evaluation of the morphodynamic parameter $M(t)$, we get to:

$$M(t) = \frac{\alpha_{EH}}{B^p d_c^q}\ I(t)^n\ \frac{\beta(t)((1/d)^{q-s} - 1) + 1}{(\beta(t)(d-1)+1)^s} = Cost\ I(t)^n\ c_1(\beta(t)) \tag{2.17}$$

where we have called $c_1(\beta)$ the following expression:

$$c_1(\beta(t)) = \left(\frac{d_c}{d_{eq}(\beta(t))}\right)^q = \frac{\beta(t)((1/d)^{q-s} - 1) + 1}{(\beta(t)(d-1)+1)^s} \tag{2.18}$$

The evaluation of the values of the exponents n, q and p is made as described in section 2.1 .

2.6 Linearization of the equations and harmonic solution

To take into account the short-term perturbations of boundary conditions with respect to the equilibrium configuration, an analytical solution for the equations (2.1) has been found by Fasolato et al. [2009]. They have taken into account the linearized system and they have assumed the instantaneous propagation of the liquid flow and the quasi-steady flow conditions as exposed in the section 2.1 (see equations (2.7)).

We suppose that the monitored river is in equilibrium conditions as explained in the previous paragraph, actually that it has a reference geometry configuration consisting in a finite rectangular channel of constant width B and constant energy slope J; all the irregularities in space and in time of the parameters, with respect to the averaged values, are caused by short-term small perturbations at the boundary conditions. Thus, any variable $\Xi(t)$ of the morphodynamic 1-D system (2.1), described in the section 2.1, can be linearized as the sum of the equilibrium value $\bar{\Xi}$ and a perturbation $\Xi'(t)$. The dimensionless perturbation of the variable is $\xi(t) = \frac{\Xi(t)-\bar{\Xi}}{\bar{\Xi}}$.
Considering the dimensionless perturbations as small perturbations (namely much smaller than one), the one-dimensional morphodynamic model (once the boundary conditions of the system are known) can be linearized. Below (2.19) the system (2.1) is written in terms of dimensionless perturbations and dimensionless coordinates, namely $x = x^*/\bar{Y}$ and $t = t^*\,\bar{U}/\bar{Y}$. We have introduced the following dimensionless parameters: $\alpha_F = (1 - F_r^2)$, where F_r is the Froude number; $\epsilon = (3/2)EF_r^2$, where $E = 2g/\chi^2$ is the resistance coefficient; $\eta = (1-d)/(1+d)$ and $\eta^* = (1-d^*)/(1+d^*)$, where $d = d_f/d_c$ and $d^* = d^{1-s}$, is associated with the hiding-exposure coefficient ζ (see eqaution (2.6));

$S^* = 1 - (\eta^*)^2$; $\psi = \bar{P}/\bar{Q}$ is the sediment concentration; $\Delta = \delta/\bar{Y}$ is the relative thickness of the mixing layer.:

$$\begin{cases} \dfrac{\partial q}{\partial x} = 0 \\ \alpha_F \dfrac{\partial y}{\partial x} + \dfrac{\partial h}{\partial x} - (1-\alpha_F)\dfrac{\partial b}{\partial x} = \epsilon \left(y + \dfrac{2}{3}b - \dfrac{2}{3}q \right) \\ \dfrac{\partial h}{\partial t} + \psi \dfrac{\partial p}{\partial x} = 0 \\ p = 6q - 6y + (\eta^* + s\eta)\bar{\beta}_1 - 5b \\ \dfrac{\partial \bar{\beta}_1}{\partial t} + \dfrac{\psi}{\Delta}\left(S^* \dfrac{\partial \bar{\beta}_1}{\partial x} + \eta^* \dfrac{\partial p}{\partial x} \right) = 0 \end{cases} \tag{2.19}$$

Fasolato et al. [2009] found a deterministic harmonic solution for the system (2.19) considering the dimensionless boundary conditions as sinusoidal waves. In particular we have five boundary conditions: the solid transport $p(x = 0, t)$ and the bottom composition $\beta(x = 0, t)$ at the upstream end, the bottom level $h(x = l, t)$ and the water level $(h+y)(x = l, t)$ at the downstream end and the liquid discharge $q(t)$. These sinusoidal boundary conditions are characterized by the angular frequency $\omega = \frac{2\pi}{T_w}\frac{\bar{Y}}{\bar{U}}$, where T_w is the period of the typical flood event wave. The particular solution, given by the equilibrium state of the river, is:

$$\begin{cases} \bar{\beta}_1(x) = 0 \\ p(t) = 2q(t) \\ y(x,t) = \dfrac{2}{3}q(t) - \dfrac{5}{6}b(x) \\ h(x) = \left(1 - \dfrac{\alpha_F}{6}\right) b(x) - \dfrac{\epsilon}{6} \int_0^x b(x)dx \end{cases} \tag{2.20}$$

The homogeneous solution of each parameter $\xi(x, t)$, can be expressed as the sum of three basic damped harmonic waves that convey along the stream the boundary condition. These waves are three sinusoidal expressions, two propagating downstream

($n = 1,\ 2$ in the following expression) and one propagating upstream ($n = 3$):

$$\xi(x,t) = \sum_{n} = 1^{3} \xi_{c_n}\ e^{i\ k_n\ x\ -\ i\ \omega\ t} \tag{2.21}$$

This solution is valid for all the perturbations ($p(x,t)$, $y(x,t)$, $h(x,t)$ and $\beta(x,t)$) but $q(x,t)$, which propagation is instantaneous and undamped.

Each amplitude ξ_{c_n} of the resulting perturbation wave is effected by all the amplitudes ξ_c of the boundary conditions, through a linear combinations of their values.

2.6.1 Dominant boundary conditions and dominant perturbations

Fasolato et al. [2009] found that one perturbation wave ($n = 1$) is predominant with respect to the other two ($n = 2, 3$) for relatively short wave period of the boundary conditions, similar to the period of the typical flood event. This wave is propagating downstream and the other two become negligible.

Moreover they found that for any variations of the boundary conditions, the consequent disturbance propagating along the river related to the bottom elevation $h(x,t)$ and to the water depth $y(x,t)$ are negligible with respect to the disturbance related to the solid transport $p(x,t)$ and to the bottom composition $\beta(x,t)$.

Finally, for flows with $F_r > 0,2$, only the boundary conditions for the solid transport $p(x = 0,t)$ and for the bottom composition $\beta(x = 0,t)$ have notable effects in the propagating perturbations, meanwhile the boundary conditions for the water discharge and the bottom elevation are negligible.

2.6.2 Validity of the LUF hypothesis

The celerity and the attenuation length of the three waves of the harmonic solution can be evaluated only numerically. They characterize the river reaction of the river to the perturbations introduced at the boundary with respect to the equilibrium state.

Making suitable average along quite long reaches of the river, we can simplify the problem thinking that each reach has local uniform flow (LUF), thus we substitute the energy slope with the bottom slope of the reach. Having sinusoidal boundary conditions

characterized by a period T_w, Fasolato et al. [2011] advise that this assumption can be made only if the characteristic parameter $\bar{\epsilon} >> 1$:

$$\bar{\epsilon} = \frac{EF_r^2 \psi \bar{U}}{8\pi\Delta^2 \bar{Y}} T_w \tag{2.22}$$

where $E = 2 \cdot 9.81/\chi^2$ is the dimensionless resistance coefficient, F_r is the mean Froude number of the current, ψ is the mean concentration of the flow, $\bar{U}$ is the mean velocity, Δ is the relative thickness of the active layer and $\bar{Y}$ is the mean water depth.

With the LUF hypothesis is possible to find explicit formulations for the celerity (c_{f_i}) and the attenuation lengths (L_{f_i}) of the three dumped waves propagating along the reach from the boundaries. We consider only the first wave as the faster and more persistent than the other two (see section 2.6.1): the correspondent propagation celerity c_{f_1} and attentuation length L_{f_1} are

$$c_{f_1} = \frac{\psi}{\Delta}\gamma \qquad L_{f_1} = \frac{\epsilon\psi^2}{6\Delta^3\omega^2}\frac{\gamma^4}{(\gamma - S^*)} \tag{2.23}$$

where $\gamma = 1 - s\eta\eta^*$.

For the particular solution in equilibrium state the geometry of the river can be characterized by its width $B(x)$, composed by a series of N sinusoidal curves with wave length λ_k and amplitude b_{c_k}. The mean bed elevation $\bar{H}$ is a function of $B(x)$. The relative error between the exact (found numerically) and the LUF solution decrease for increasing Froude number and dimensionless wave length $\lambda_k/\bar{Y}$ of the river width oscillation $b(x)$, but it is not effected by the amplitude of the curves. We can decide a lower threshold of the wave length λ_{lim} that provide acceptable relative errors. Thus, we identify a characteristic length, called *morphological box*, $L_{box} = \lambda_{lim}/4$ that acts like an averaging operator filter: only variations longer than L_{box} can be reproduced with the LUF hypothesis. L_{box} increases with decreasing Froude number of the flow.

Similarly is possible to find a temporal averaging operator filter from the analysis of the homogeneous solution. The relative error between the exact and the LUF solutions is always lower than 10% for both the celerity and the attenuation length if $\bar{\epsilon} > 10$, consistently with the assumption that $\bar{\epsilon} >> 1$ (see equation (2.22)). With this

result we can define a threshold temporal evolution window T_{wind} for the period of the perturbations imposing $\bar{\epsilon}_{lim} = 10$:

$$T_{wind} = \frac{T_{wave}}{4} = \frac{20\pi\Delta^2\bar{Y}}{EF_r^2\psi\bar{U}} \tag{2.24}$$

Perturbations with duration larger than T_{wind} can be reproduced by the LUF solution. T_{wind} depend on both hydraulic and geometric parameters, but Froude number and wave period are most important.

The LUF hypothesis lead to have a univocal relation between the solid transport and the bottom slope (variable only in "morphological" time) instead the energy slope (variable in "hydraulic" time). Moreover with this assumption we can make long-term simulations on long and large rivers. This condition is necessary to work at basin-scale.

2.7 Transfer of the short-term perturbations

In order to evaluate the instantaneous solid transport in a specific cross-section we utilize the linearized 1-D model of the reach (see section 2.6) for transferring the perturbations from the upstream end (corresponding to the hypothetical barycenter of the watershed area of the river) to the gauge station or to the sea. Maintaining all the simplifications and assumptions taken into account by Fasolato et al. [2011], we will finally use the simplified 1-D LUF linearized solution to evaluate the values of the perturbation waves of the sediment transport in correspondence of the investigated cross-section of the river (more details in section 3.3).

Chapter 3

Long-term equilibrium model with short-term perturbations

3.1 Long-term and short-term sediment transport

In the present Chapter 3 we want to use the 1-D LUF deterministic solution for the harmonic river proposed by Fasolato et al. [2011] and discussed in the Chapter 2 to evaluate the short-term fluctuations of the solid transport recorded at a gauge station with respect to the basic configuration (equilibrium condition) that we postulate at a longer time-scale. As we are dealing with a long reach, we can correctly suppose for the long-term basic transport a monomial relationship between the solid and the water flux at the gauge station (see sediment rating curve, equation (2.5)). To describe the short-term perturbations with respect to the equilibrium configuration, we must take into account the variations of the boundary conditions at the upstream end. In accordance with Fasolato et al. [2009] the most important boundary conditions that produce deviations of the solid transport at the gauge station are those relative to the total solid input and to the bed composition (see in 2.6.1).

Keep in mind that the deterministic analytical solution for the 1-D morphodynamic model was found by Fasolato et al. [2009] and Fasolato et al. [2011] under specific hypothesis:

- instantaneous water flow propagation (quasi-steady flow);

- existence of a stationary configuration of the river reach (long-term equilibrium) and linearization of the equations about the long-term equilibrium value considering only small perturbations;
- the sediment is composed by only two grain size representative classes;
- Local Uniform Flow (LUF) conditions.

3.2 Calibration of the equilibrium sediment rating curve

In order to calibrate the parameters m and M against available data different methods have been investigated.

As said in paragraph 2.4, the calibration is usually made by a linear interpolation, minimizing the root square error of the logarithmic relation: $log(P(t)) = log(M) + m\ log(Q(t))$. The problem now is that often we have not records of the solid transport at the same temporal scale of the records of the liquid discharge; and it can be shown that we can find a different calibration of the log-relation for each temporal scale we consider. For example if we calibrate the log-relation for the Adige river with three different temporal scales, daily, monthly and annual, we get to the result of the Table 3.1:

Table 3.1: Calibration of the relation $log(P(t)) = log(M) + mlog(Q(t))$ for the Adige river in the period 1932-1941 with records of data at different temporal scales.

	m	M
daily records	2.16	1.23 x 10^{-7}
monthly records	2.62	9.45 x 10^{-9}
annual records	1.08	8.41 x 10^{-5}

This is due not only to a statistical intrinsic problem (the analysis depends on the number of data: to have same results of a statistical analysis we should analyse an infinite number of values), but also because the records we are analysing are not independent random data but have some interrelations, especially when we deal with short-temporal scale.

We can define an *equivalent liquid discharge* as that liquid discharge powered to m that, multiplied by M, provides the mean annual solid transport at the gauge station

(obviously different from the mean annual liquid discharge). Knowing the daily ($t = d$) averaged liquid discharge, we power to m these values and define their annual ($t = y$) average as the annual equivalent liquid discharge ($\overline{Q^m}(y)$). The correct parameter M is then given by the quotient between the mean annual solid transport and the mean annual equivalent discharge:

$$M = \frac{\overline{P(y)}}{\overline{\overline{Q^m}(y)}} \tag{3.1}$$

To choose the exponent m that provides the best fitting, namely to assess which is the *best* fitting of the resulting annual transport, we have different methods to quantify the accuracy of the result. We use the classical Root Mean Square Error (RMSE), that is a dimensional value. Referring to Moriasi et al. [2012], we can test the results with Nash-Sutcliffe efficiency (NSE), which is very commonly used and which ranges between $-\infty$ and 1, that indicate perfect fit, while negative values indicate that the mean observed value is a better predictor than the simulated value. It is calculated with the normalization of the RMSE, dividing this value by the sum of the square of the differences between the observed data and the mean observed value. Instead, the Relative-RMSE normalize the RMSE with the sum of the square of the observed data, and provides values from 0 (best fit) to ∞. The results are very different from results obtained with RMSE-observations standard deviation ratio (RSR), which standardizes RMSE using the observations standard deviations and ranges from 0 (best fit) to ∞. It find a best fit for values that NSE says to be unacceptable performance as shown in the Figure 3.1.

Thus the NSE has been taken as decision parameter.

3.3 Transferring short-term perturbations to the gauge station

With this model we correct the equilibrium prediction of the instantaneous solid transport $P(t)$ with the amplitude of the perturbations propagated downstream with the first wave (the other two are negligible, as mentioned in the paragraph 2.6.1).

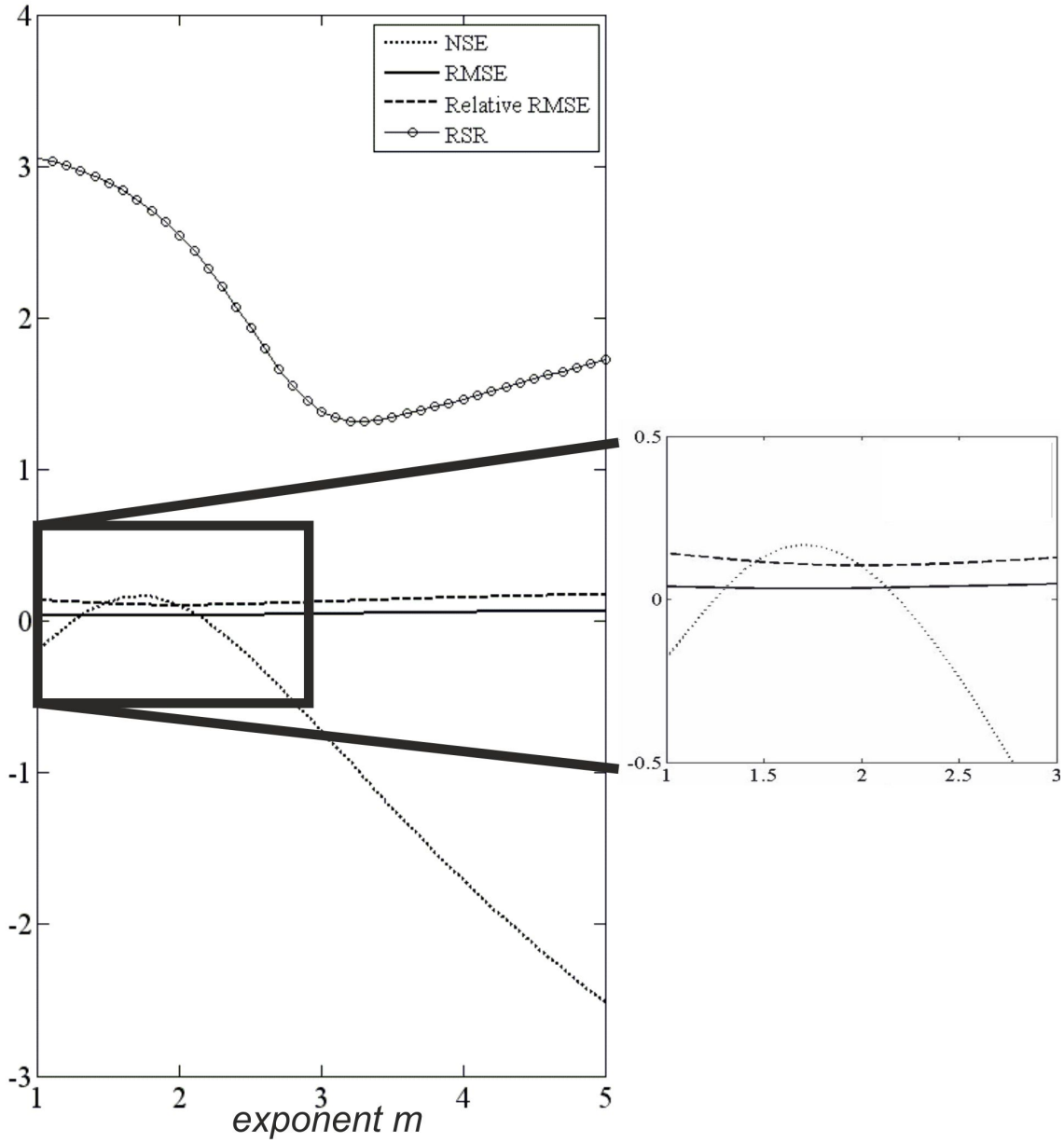

Figure 3.1: Example of the behaviour of the different method to quantify the accuracy of the model with different value of m. The dot-line represent the NSE, the solid line is the RMSE, the dash-line is the relative RMSE and the circles represent the RSR.

The perturbation of the solid transport travels along the LUF-reach much slowly than the liquid wave (having an instantaneous propagation). In this way the chronological sequence of the records $P(t)$ in the gauge station contain the information about the past solid transport in the upstream end.

The equilibrium prediction of the instantaneous solid transport is $P(t) = MQ^m(t)$, where M is the equilibrium morphodynamic parameter given by (2.17). In non-equilibrium conditions we have also a perturbation $P'(t)$ of the morphological characteristics. We can write:

$$P(t) = MQ^m(t) + P'(t) = MQ^m(t)(1 + p_{c,1}(t) + m_{c,1}(t)) \tag{3.2}$$

where $p_{c,1}(t)$ and $m_{c,1}(t)$ are the amplitudes of the non-dimensional perturbations at the gauge station (see Figure 3.2), respectively due to the deviations from the equilibrium conditions of solid input and morphological characteristics of the upstream boundary.

According to Fasolato et al. [2009] the only two boundary conditions that have notable effect downstream are those related to the total transport and to the grain size composition. For calculating the perturbations $p_{c,1}(t)$ and $m_{c,1}(t)$ we use the formulation given in that work.

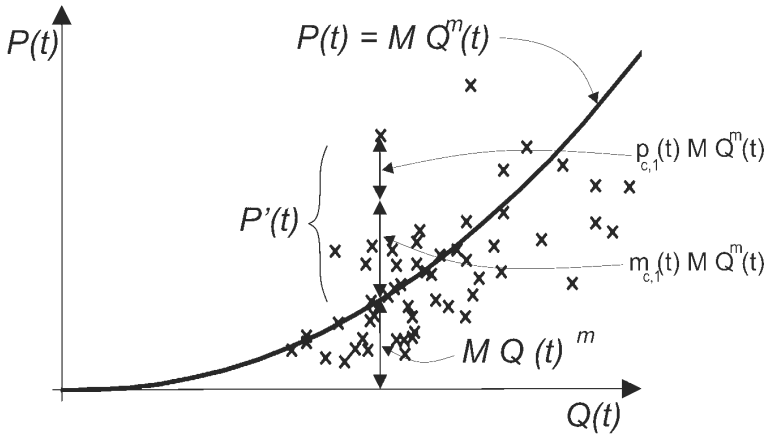

Figure 3.2: Long-term sediment rating curve in equilibrium conditions and identification of absolute perturbations for an arbitrary measure.

The propagation along the LUF reach takes a certain time, called k, that can be

known when we know the length of the reach and the celerity of the wave, given by (2.23) [Fasolato et al., 2011].

When we know the boundary conditions of the total sediment input $p_c(t)$ and of the bottom composition $\beta_c(t)$ in $x = 0$ (barycenter of the basin), all the amplitude of the perturbations are calculated through a linear combination of all the amplitude of the boundary conditions [Fasolato et al., 2009]:

$$\begin{cases} p_{c,1}(t-k) = A_1 m_c(t-k) + B_1 p_c(t-k) \\ m_{c,1}(t-k) = D_1 m_c(t-k) + E_1 p_c(t-k) \end{cases} \tag{3.3}$$

In Fasolato et al. [2009] we find the values for the coefficients: $A_1 = 0.70$, $B_1 = 0.30$, $D_1 = 0.40$ and $E_1 = 0.60$. When the perturbations wave have been formed they propagate downstream and arrive in $x = L$ (at the gauge station) after k time and damped. We can calculate the damping coefficient α_{att} knowing the length L of the reach and the attenuation length (given by (2.23)), defined as the distance over which the amplitude of the wave is reduced by a factor of $1/e$. So we have:

$$\begin{cases} p_{c,1}(t) = \alpha_{att}\, p_{c,1}(t-k) \\ m_{c,1}(t) = \alpha_{att}\, m_{c,1}(t-k) \end{cases} \tag{3.4}$$

3.4 Boundary conditions

For the application of this model to a natural river we need to know the boundary conditions $p_c(t-k)$ and $m_c(t-k)$, which represent the amplitude of the sinusoidal dimensionless fluctuations of the sediment input and morphology characteristics due to complex natural phenomena in the basin area. There are a lot of work trying to measure the production of sediment by a watershed area, related to the climatic conditions in more or less complicated model. A large discussion about the principal models of sediment production and their problem or advantage has be done both by De Vente and Poesen [2005] and Aksoy and Kavvas [2005]. The models can be classify in different

groups depending on the morphological characteristics they take into account and their complexity. In any case the large quantity of data required is always the main problem. Moreover the analysis of a large record of data made by De Vente and Poesen [2005] found out that the relations between the typical characteristics taken into account in the models can be very different from a river to another one: for example the relation between the unit sediment yield and the basin area is not always negative, but it can be also positive. As our scope is to find simple relationship that require the lesser number of data as possible, we tried to develop simple relationships to evaluate the short-term variable boundary conditions at the system only dependent on the LUF liquid discharge. Note that this relationship, together with other empirical formulations, will be calibrated against the measurements by an ARMA procedure (see 3.5).

3.4.1 Mathematical formulations for the boundary conditions

In our model the basin is concentrated in its barycenter, and the stream is a LUF channel without any other input after the upstream end. So we can consider the records of the liquid discharge $Q(t)$ downstream as an indicator of the climatic conditions upstream, strictly bound to the sediment production.

We consider two hypothetical formulations that provides the variations in time of boundary conditions $p_c(t)$ and $m_c(t)$ only knowing the liquid discharge at the gauge station.

Dimensionless perturbation of the solid transport: $p_c(t)$

This parameter describe the variations of the sediment transport directly induced by the time-depending floods. We consider that $p_c(t)$ is proportional to the dimensionless deviations from the equilibrium solid transport in the closure section:

$$p_c(t) = a_1^* \frac{MQ^m(t) - \overline{MQ^m}}{M\overline{Q^m}} = a_1^* \frac{Q^m(t) - \overline{Q^m}}{\overline{Q^m}} \tag{3.5}$$

where a_1^* is a calibration parameter.

Dimensionless perturbation of the morphological characteristics: $m_c(t)$

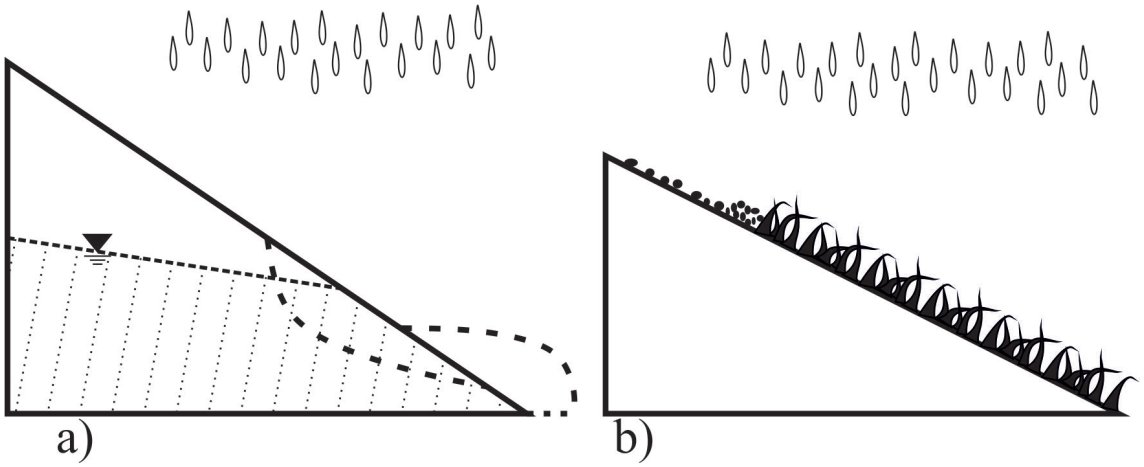

Figure 3.3: Schematic representation of two main mechanisms of sediment production leading to a fining of the bottom composition of the river: a) mass erosion; b) surface erosion with the effect of the vegetazion cover

For Fasolato et al. [2009] a relevant factor governing this perturbation is the variation of the bed composition of the input. We think that a remarkable fining of the bed occurs when a landslide falls from the slopes of the basin (Figure 3.3, a). We formulate $m_c(t)$ proportional to a cumulative term of the water flux, somehow correlated, in its turn, with long-term rainfall and thus with the accumulation of water in the slopes, the main cause of the mass erosion. The cumulative term does not identify single events, but it is a continuous function because the landslide can occur in any point of the basin. Each basin is characterized by a specific filling time p of the slopes of the basin that determines the landslides occurrence. Moreover we assume that the landslide creates a sort of sediment storage that progressively empties with a linear evolution regulated by a non-dimensional erodibility coefficient E_u; thus at every time step $m_c(t)$ depends also on the value of m_c at the previous time:

$$m_c(t) = a_2^* \left[\frac{\sum_{i=t-p}^{i=t} \left(Q(i) - \overline{Q}\right)}{\overline{Q}} + \frac{m_c(t - \Delta t)}{(1 + E_u)} \right] \tag{3.6}$$

where a_2^* is a calibration parameter and $E_u/\Delta t$ is according to the size $10^{-6} \frac{1}{sec}$ [Crosato, 2007].

This approach is obviously related to sediment production by mass-movements. Wherever the main mechanism of sediment production is surface erosion, bounded to high values of kinetic energy of the rainfall, we can consider an alternative relation for m_c. In this case an important role is played by the vegetation cover, which delay the response (Figure 3.3, b), and the cumulative formulation is maintained:

$$m_c(t) = a_2^* \left[\frac{\sum_{i=t-p}^{i=t} \left(R^{r_m}(i) - \overline{R^{r_m}} \right)}{\overline{R^{r_m}}} + \frac{m_c(t-\Delta t)}{(1+E_u)} \right] \tag{3.7}$$

where R is the erosivity factor in the USLE formula [Wischmeier and Smith, 1978].

3.5 Final deterministic solution

We can substitute the formulations of the boundary conditions (3.5) and (3.6) (or (3.7)) in the equations (3.3). Then, using the transferring formulations (3.4), we can finally evaluate the instantaneous solid transport at the gauge station with the equation (3.2). The final resulting formulation is:

$$\begin{aligned}
P(t) &= MQ^m(t) \left\{ 1 + \alpha_{att}\, p_{c,1}(t-k) + \alpha_{att}\, m_{c,1}(t-k) \right\} = \\
&= MQ^m(t) \left\{ 1 + \alpha_{att} \left[A_1\, m_c(t-k) + B_1\, p_c(t-k) \right] + \right. \\
&\left. + \alpha_{att} \left[D_1\, m_c(t-k) + E_1\, p_c(t-k) \right] \right\} = \\
&= MQ^m(t) \left\{ 1 + \alpha_{att} \left[(B_1 + E_1)\, p_c(t-k) + (A_1 + D_1)\, m_c(t-k) \right] \right\} = \\
&= MQ^m(t) \left\{ 1 + \alpha_{att} \left[a_1^* \left(B_1 + E_1 \right) \frac{Q^m(t-k) - \overline{Q^m}}{\overline{Q^m}} + \right. \right. \\
&\left. \left. + a_2^* \left(A_1 + D_1 \right) \left(\frac{\sum_{i=t-k-p}^{i=t-k} \left(Q(i) - \overline{Q} \right)}{\overline{Q}} + \frac{m_c(t-\Delta t)}{(1+E_u)} \right) \right] \right\}
\end{aligned} \tag{3.8}$$

The proportionality coefficients a_1^* and a_2^* are calibrated against a set of measured data by means of the ARMA procedure.

To achieve the best reproduction of the deviations from the equilibrium formula, we applied the ARMA procedure not to the absolute formula, but just to the dimensionless

deviations from the equilibrium conditions, i.e.:

$$\frac{P(t) - MQ^m(t)}{MQ^m(t)} = p_{c,1}(t) + m_{c,1}(t) \tag{3.9}$$

The ARMA procedure will be explained in Appendix B.

3.6 Splitting the watershed in sub-basins

The main course of large rivers is formed by a series of portions characterized by very different morphological characteristics, in part because of different lithological situations occurring along hundreds of kilometers and in part because it is fed by large tributaries coming from different watershed. So we can identify a subdivision of the complete basin in two or more sub-basins, each one representable by LUF conditions and that can be modeled by the same scheme just described. Each sub-basin has its boundary conditions, both by its proper watershed area and by its tributaries. These variable boundary conditions creates waves perturbation that travel, dumped, along the LUF channel up to the confluence with the LUF channels of the other sub-basin. The main channel of each sub-basin is characterized by a different wave celerity and attenuation length (with regard to the characteristics of the sub-basin), and obviously by a different time-delay k. At the confluences the waves are summed to create a single wave perturbation.

Given N_B sub-basins, the final equation (3.8) will be modified as follows:

$$\begin{aligned} P(t) = MQ^m(t) \Bigg\{ 1 + \sum_{i=1}^{N_B} [\alpha_{att,i} \; ((A_1 + D_1)\, m_{c,i}(t - k_i) + \\ + (B_1 + E_1)\, p_{c,i}(t - k_i))] \Bigg\} \end{aligned} \tag{3.10}$$

As mentioned before, at the section 2.2, the borderline case is modeling the entire network of the watercourse in the basin.

This procedure is in principle applicable only if we have the direct measurements of the liquid discharge at the closure section of each LUF channel identified. This

condition is generally never verified.

Obviously the best alternative is the calibration of an accurate hydrological model against the record of measured total liquid discharge at the closure cross-section of the entire basin. As we do not have a precise description of the watershed area, as well as measurements of the local daily rainfall and temperature, necessary to give acceptable results, we have applied a more compact approximate model.

The watershed area has been split in macro-regions of the basin that are relatively uniform and substantially different from each other: for example we can easily distinguish a mountain region from a plain region. In this case the two sub-basins are characterized, inter alia, by different mean elevation and so by different mean daily temperature. In particular they will react in a totally different way as far as the temporary storage of the rainfall in the snow pack and the consequent release, phenomena that sensibly discriminate the seasonal trend of the liquid discharge coming from the two sub-basins identified. On the other hand, when we average over a long number of years,the effect of the temporary storage in the snow pack is negligible; so that we assume the watershed surface of each sub-basin S_B as a relative measure of its importance in the contribution of the averaged total liquid discharge $\bar{Q}$ measured at the gauge station:

$$\frac{\overline{Q_B}}{\bar{Q}} = \frac{S_B}{S} \tag{3.11}$$

where $\overline{Q_B}$ is the averaged liquid flow of each sub-basin identified with the subscript B, S_B represents the surface of the sub-basin and S is the area of the entire basin. In order to evaluate the instantaneous waterflow $Q_B(t)$ as a function of $\overline{Q_B}$, the following water balance of the snow-pack has been written (3.12), exclusively based on the

temperature distribution $T_B(t)$ over the sub-basin.

$$\begin{aligned}
&\text{If} \quad T_{B,i}(t) < 0 \rightarrow s_{now,B,i}(t) = c_B Q(t) \frac{S_{B,i}}{S} \\
&\text{If} \quad T_{B,i}(t) > 0 \rightarrow s_{now,B,i}(t) = 0 \\
&S_{now,B,i}(t) = \frac{S_{now,B,i}(t-1) + s_{now,B,i}(t)}{1 + \rho_{B,i}(t)} \\
&Q_{melt,B,i}(t) = \rho_{B,i}(t)\ S_{now,B,i}(t) \\
&Q_B(t) = c_B \left[Q(t) \frac{S_B}{S} + \sum_{i=1}^{N} Q_{melt,B,i}(t) \right]
\end{aligned} \tag{3.12}$$

where $s_{now}(t)$ is the " snow precipitation", S_{now} indicates the accumulated storage of snow, i indicates the altitude/temperature zone and c_B is a calibration parameter set such to verify that $\sum_{b=1}^{N_B} Q_B(t) = Q(t)$. The correction parameters $\rho_{B,i}$ are expressed as the ratio between the mean daily temperature $T_{B,i}$ and the mean yearly temperature of that area $\bar{T}_{B,i}$. This evaluation is normalized as follows:

$$\rho_B(T(t)) = \rho_B(t) = \sum_{i=1}^{N} \rho_{B,i}(t) = \sum_{i=1}^{N} \frac{exp\left(\frac{T_{B,i}(t)}{\bar{T}_{B,i}}\right)}{max\left[exp\left(\frac{T_{B,i}(t)}{\bar{T}_{B,i}}\right)\right]} \tag{3.13}$$

The sub-basins identified could in principle be characterized by a different type of vegetation cover. This characteristic is important because the presence of the vegetation on the basin influences the carrying capacity of the slopes and the surface erosion, as shown by numerous formulations (e.g. U.S.L.E. Wischmeier and Smith [1978]).

In particular we think that the temperature could be again a distinguishing parameter assuming that the growth of the vegetation is proportional to the local temperature. We define a new correction parameter $V_{B,i}(t)$ function of the local temperature $T_{B,i}(t)$ in the altitude/temperature zone i, of the mean temperature of each sub-basin and of

a typical limit-growth temperature $T_{B,lim}$ for the vegetation type considered:

$$V_{B,i}(t) = \frac{T_{B,i}(t) - T_{B,lim}}{\bar{T}_{B,i}} \tag{3.14}$$

The correction parameter is then normalized such that it varies between zero (no vegetation) and 0.95 (quasi-completely vegetated slopes). The value of the liquid discharge coming from the sub-basin B is reduced with respect to the presence of vegetation by the multiplication for the factor $[1 - V_{B,i}(t)]$

3.7 Numerical applications to the Adige river

The Adige River (Figure 3.4) has its source at the elevation of 1586 m s.l. from an artificial hydropower reservoir, close to Resia pass (Bolzano, Italy). It flows eastbound to Bolzano, where the principal watercourse, Isarco River, joins. Then it flows through the cities of Trento and Verona. The watershed area finish near Alberedo d'Adige (Verona, Itlay), after about 290 km, and then continues along the north-eastern part of Italy as a confined pensile river, parallel to the Po River, down to the Adriatic Sea. With about 415 km in length, it is the second longest river in Italy, after the Po River. With a catchment area of 12 200 km^2, the Adige River is the third Italian watershed, behind the Po River and the Tiber River. It has a great influence to the adjacent environment which is extremely man-made.

This river has mountain characteristic in the high part of its basin, while assuming alluvial characteristics already dowstream the city of Bolzano.

3.7.1 Geomorphological data and calibration

Historically the water level of the Adige river was constantly monitored in many gauge stations and through the discharge rating curve it is possible to evaluate the correspondent liquid discharge. We can also find some records of the concentration of the suspended load but only for two stations and for two distinct limited periods. The gauge station on the San Lorenzo bridge in Trento recorded concentrations data from 1932 to 1941 (call this period as **'30*s***) and from 1958 to 1973 (call this period as $'60s$). The other gauge station is on the bridge of the *SP1* road, near Boara Pisani and has worked from 1929 to 1941 (**'30*s***) and from 1958 to 1972 ($'60s$). The available data are collected in the SIMN (the old national service managing the hydro and sea gauge stations in Italy up to 2001) publications of the Hydrological Annals as monthly mean solid suspended concentrations (SSC $[mg/l]$).

We assume that the total solid transport is quasi completely composed by the measured suspended load, as there are not measures of the bed load. This hypothesis is reliable in a context of a gauge station placed in a quite lowland part of the river [Asselman, 2000], as in this case (and not for a torrent type of stream).

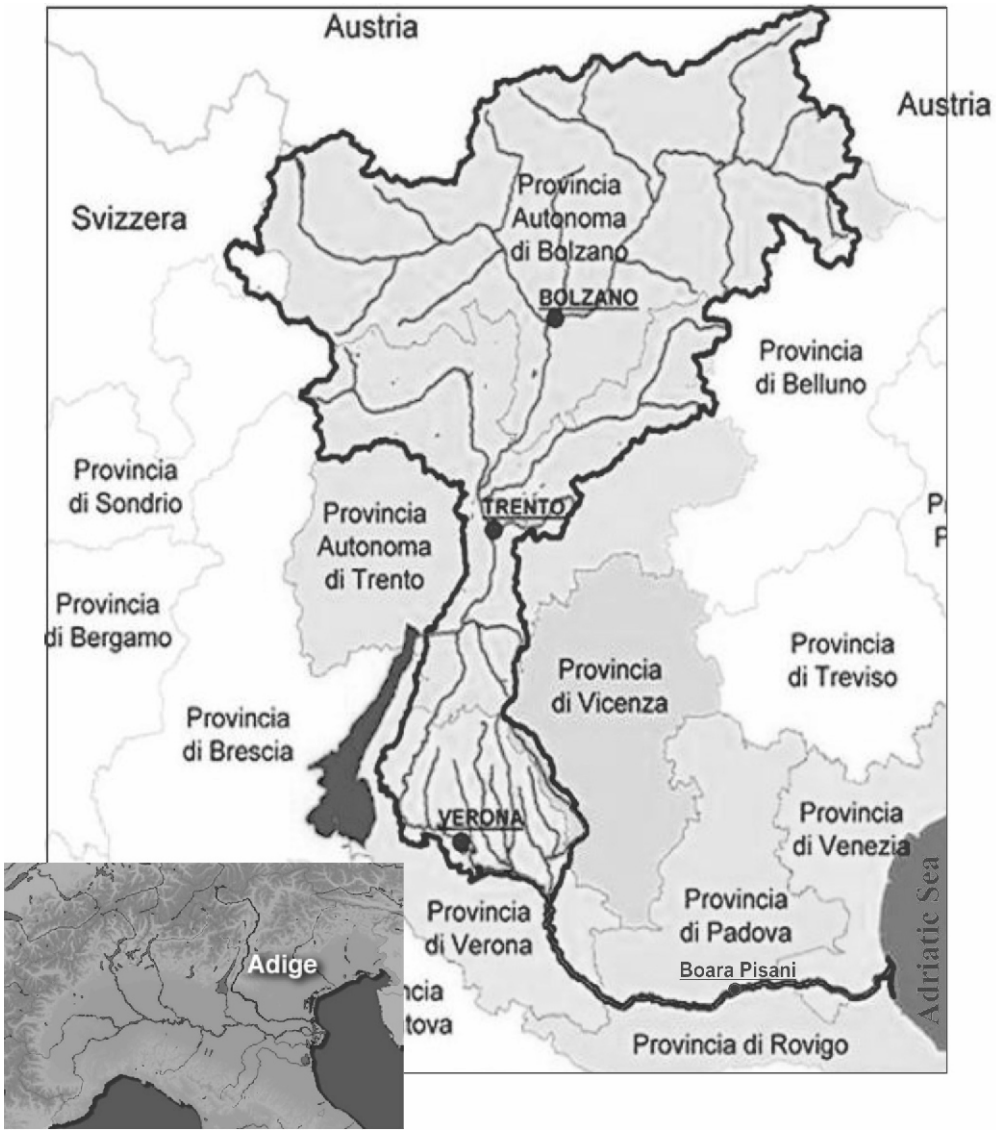

Figure 3.4: Map of the Adige watershed

The mathematical model evaluate the volumetric solid discharge of the solid transport referred to a certain liquid discharge (see equations(3.8)). We convert the SSC series in volumetric solid discharge $[m^3/s]$ (equation (3.15)) by the multiplication with the instantaneous liquid discharge and dividing for the product of the mean density of the sediments δ (assumed that the material is essentially siliceous material we set $\delta = 2600\ kg/m^3$) and the full index $(1 - n)$ (assumed a debris porosity (void index) $n = 0.35$). These assumptions are not precise but they will be corrected by the calibration parameter, both of the equilibrium formula (α_{EH} in (2.13)) and of the perturbation equations (a_1^* and a_2^* in (3.8)).

$$P(t) = \frac{SSC\ Q(t)}{\delta\ n} \tag{3.15}$$

As the morphological data are refereed to current measurements (and so they are not temporally coherent with liquid discharge and solid concentration data), they are not properly valid in order to calculate the morphodynamic parameter M (2.13), the celerity and the attenuation length (2.23) of the perturbation waves. Moreover the barycenter of the basin is identify by an empirical evaluation, so we do not precisely know the length of the LUF channel. For these reasons we must calibrate (and not calculate) the morphodynamic parameter M and we can not trust to the analytical evaluation of the delay k of the perturbation waves.

We consider the records coming from different stations as records coming from two different rivers characterized by a different morphology.

However, recent works about the balance of the sediments of the Adige river (Di Silvio et al., 2008, Nones et al., 2009) have shown that for the morphological boxes (see section 2.6.2) the principal morphological quantities (equivalent grain-size diameter, width, slope) are not substantially changed during the last century.

"Trento" LUF reach: The watershed surface closed at the cross section in Trento has peculiar mountain characteristics. In Bolzano (about 50 km before Trento station) the Adige River meet its principle tributary Isarco River, which has a mean slope and

a mean water flow greater than the upstream part of the Adige itself. Then we can say that the Adige River for the LUF ending in Trento has two main courses. We assumed a unique LUF length of 75 km and a slope of about 3.8‰, that correspond as considering the barycenter in Ponte Gardena (or Merano, if we follow the Adige river main course instead the Isarco).

"Boara Pisani" LUF reach: The basin closed at the cross-section in Boara Pisani has more lowland characteristics. Similarly for Trento, the barycenter is identified corresponding about in the city of Salorno, between Trento and Bolzano, for have a plausible length and slope of the LUF channel but neglecting in part the fact that a lot of sediment input comes from the rivers flowing from the Lessini mountain (Alpone, Chiampo, etc ...) after Verona. The resulting LUF is about 240 km with a slope of about 0.9 ‰.

The LUF reaches closing at the two gauging stations of Trento and of Boara Pisani are shown in the Figure 3.5

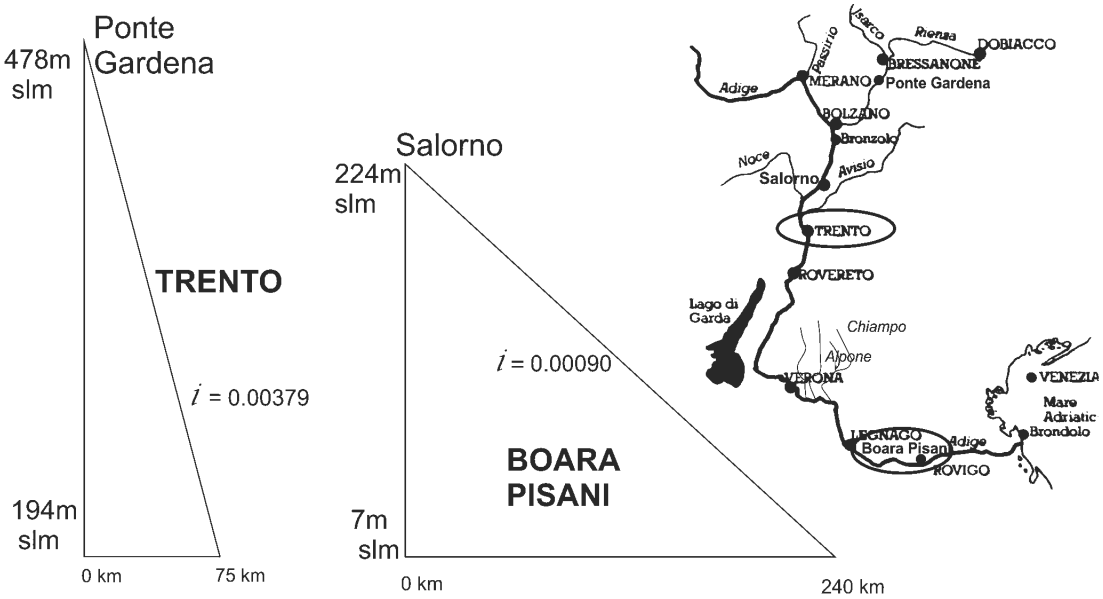

Figure 3.5: The two scheme of the Adige river: a) the LUF channel closing at Trento gauge station; b) the LUF channel closing at Boara Pisani gauge station.

3.7.1.1 Grain-size composition

For Adige river we have some grain-size measurements made by the Autonomous Province of Bolzano and by the Basin Autority of the Adige river. These data refer to samples picked up from the main course in Marlengo and in Merano (near the confluence of the Passirio river), in Cortina d'Adige and in Salorno (between Bolzano and Trento), in Dolcè (near Garda lake in the Province of Verona), in Zevio (south of Verona) and finally some measurements in Boara Pisani are acquired from Brunelli [1987].

Then, assuming that the grain-size curve has a normal distribution, the two representative classes (see section 2.5) are identified by the diameter that corresponds to the cumulative percent passing equal to 16 % for the fine class and equal to 84 % for the coarser class. For Adige river we have $d_f = 2.2\ mm$ and $d_c = 42.4\ mm$.

Finally we have the actual representative grain-size composition finding the real percent passing of this two classes in the average particle size distribution obtained respectively for the Adige river closing in Trento and closing in Boara Pisani. The resulting data are summarized in the Table 3.2.

Table 3.2: Representative current grain-size composition of river Adige closing in the gauging station of Trento and the river closing in Boara Pisani.

	d_i $[mm]$	β_i in Trento [%]	β_i in Boara Pisani [%]
$fine$	2.2	24.08	30.32
$coarse$	42.4	75.92	69.68

3.7.2 Results

Though a Fourier analysis we found that the principal sinusoidal wave of both the liquid flow and the solid transport has a period equal to one year. The second and the third waves have respectively period of six and three months. These results respect the limit of application of the LUF hypothesis found by Fasolato et al. [2009] (see (2.22) in section 2.6.2), having that the $T_w \geq 4\ T_{wind}$, calculated such that $\bar{\epsilon} = 10$, lead to shorter values (see Table 3.3).

3.7.2.1 Calibration of the equilibrium formula

As we said, the exponent m is considered as a characteristic parameter of the river. By contrast the long-term equilibrium is considered valid only for one period at a time ($'30s$ and $'60s$), while the two periods considered are rather separated by a period of time characterized by a great human activity over the basin (reservoirs construction, interventions for the erosion control, mines, etc ...). For this reason the calibrations of the equilibrium formula is preliminarily made putting together the records of data referred to the two different periods in order to identify the m exponent of the river. Then the two temporal series are separated in order to calibrate the other parameters.

The results are shown in Table 3.3, where are reported also the NSE of the evaluation of the solid transport with the calibrated equilibrium formula and the minimum period of the periodical boundary conditions representing the threshold for the application of the LUF hypothesis (see secion 2.6.2). Finally are reported the celerity of the perturbation waves (both dimensionless and in the dimensional form through the multiplication with the mean flow velocity U), the consequent delay k of the wave to arrive at the gauge station from the barycenter of the basin along the LUF reach, the attenuation length (both dimensionless and in the dimensional form through the multiplication with the mean water depth Y) and the correspondent attenuation parameter α_{att}.

3.7.2.2 ARMA calibration of the non-equilibrium perturbations

The ARMA procedure works in order to calibrate the coefficients a_1^* and a_2^* of the formulation (3.8). But in that formulation there are also other parameter, measurable in principle, that are unknown. In particular there are the mean characteristic filling time of the slope of the basin p and the erodibility coefficient E_u. Moreover, as already explained above, the available morphological data are not referred to the same period which the solid measures are referred to. This means that the evaluated delay k would be not so precise, also because the length of the LUF channel can not be perfectly appreciated.

In order to evaluate the best set of parameter a recursive procedure was be devel-

Table 3.3: Results of the calibration of the equilibrium formula for Adige river

	Trento		**Boara Pisani**	
L $[km]$	75		240	
m	2.1		1.8	
	'30*s*	**'60*s***	**'30*s***	**'60*s***
M	2.025 x 10^{-7}	1.595 x 10^{-7}	7.530 x 10^{-7}	8.170 x 10^{-7}
NSE of the calibrated equilibrium formula	58.28 %	46.37 %	74.19 %	62.50 %
$\bar{P}$ $[m^3/s]$	0.032	0.017	0.022	0.015
$\overline{Q^m}$ $[m^3/s]$	1.47 x 10^5	1.05 x 10^5	2.95 x 10^4	1.89 x 10^4
$\bar{Y}$ $[m]$	1.244	1.152	1.667	1.442
$\bar{U}$ $[m/s]$	3.021	2.907	1.926	1.792
$min[T_w]$ $[d]$	12	19	42	46
α_{EH}	0.00089	0.00064	0.02406	0.02612
$c_{f_1}[\backslash]$	0.00176	0.00105	0.00192	0.00166
$c_{f_1}\bar{U}$ $[km/y]$	168	97	116	94
k $[d]$	163	284	753	937
$L_{f_1}[\backslash]$	2.55 x 10^7	9.85 x 10^6	1.74 x 10^6	1.50 x 10^6
$L_{f_1}\bar{Y}$ $[km]$	31712	11342	2899	2161
α_{att}	0.996	0.989	0.875	0.840

oped, where different combinations of the values of the parameter, each one varying in a appropriate range, was taken into consideration. For each set of k, p and E_u, the ARMA procedure could be applied in order to find the best a_1^* and a_2^* for the model defined. The ARMA procedure finds the couple a_1^* and a_2^* such to minimize the root square error of the relative deviation of the measured data from the equilibrium evaluation (see (3.9)). Then the correct set of parameter has to be chosen.

As for the decision of the best calibration of the equilibrium formula discussed in the section 3.2, the method to judge the goodness of a model is not univocal. In general we chose the set of parameters that gives the best NSE of the data, because we want to give a greater importance to the peak of the solid transport than to the low values, considered that the ARMA procedure has already adjusted the results to the relative values.

Is important to note that sometimes good results come out with one or both of the ARMA parameter negative. But negative parameters were excluded because of the physical interpretation of the boundary conditions (see section 3.4.1).

A first trial application of the recursive procedure kipping the delay k equal to the one resulting from the analytical evaluation (made with the current morphological characteristics) (see Table 3.3) can be indicative for the characterization of the values of p and Eu. Unluckily in this way no positive (and so acceptable) ARMA parameters was found for the first period of the gauge station of Trento. For the other three records the results are reported in the Table 3.4, where also the NSE and the RSR of the equilibrium results are reported for simplicity of comparison.

This method can be better applied if we would have the right morphology parameter in order to calculate the correct k. For the Adige river here we use the recursive procedure also for the delay k, finding the results reported in the Table 3.5. The Figures 3.6, 3.7, 3.8 and 3.9 show the chronological sequence of the monthly solid transport data against the results calculated with the equilibrium and calculated with the combination of the ARMA and recursive procedures for the four series of data. As example, only for the first period ($'30s$) of Trento is reported the Figure 3.10. It shows the graphs that compare the measured values with the results calculated with

Table 3.4: Preliminary results of the ARMA procedure for the river Adige (also the NSE and the RSR of the equilibrium results are reported for simplicity of comparison).

	Trento	**Boara Pisani**	
	'60*s*	**'30*s***	**'60*s***
k $[d]$	284	753	937
p $[d]$	7	525	252
E_u	0.2	2.5	0.2
a_1^*	0.07655	0.16070	0.04897
a_2^*	0.00411	0.00023	0.00027
NSE	45.32 %	74.22 %	61.99 %
equilibrium NSE	46.37 %	74.19 %	62.50 %
RSR	0.739	0.508	0.616
equilibrium RSR	0.732	0.508	0.612

the equilibrium formula and the results calculated with the ARMA/recursive model respectively: on the left a) compares the results in the log scale and shows the number of data included in an interval equal to $+/-10\,\%$; on the right b) compares the results in the absolute scale, with the interpolation line of both the results.

Table 3.5: Results of the combination of the ARMA and recursive procedures for the river Adige (also the NSE and the RSR of the equilibrium results are reported for simplicity of comparison).

	Trento		**Boara Pisani**	
	'30*s*	**'60*s***	**'30*s***	**'60*s***
k $[d]$	1151	425	1146	1127
p $[d]$	420	14	889	700
E_u	2.5	0.1	0.0	2.5
a_1^*	0.20962	0.00747	0.28656	0.13406
a_2^*	0.00057	0.00632	0.00004	0.00033
NSE	70.8 %	47.6 %	78.6 %	64.0 %
equilibrium NSE	55.5 %	46.4 %	74.2 %	62.5 %
RSR	0.541	0.724	0.463	0.600
equilibrium RSR	0.667	0.732	0.508	0.612

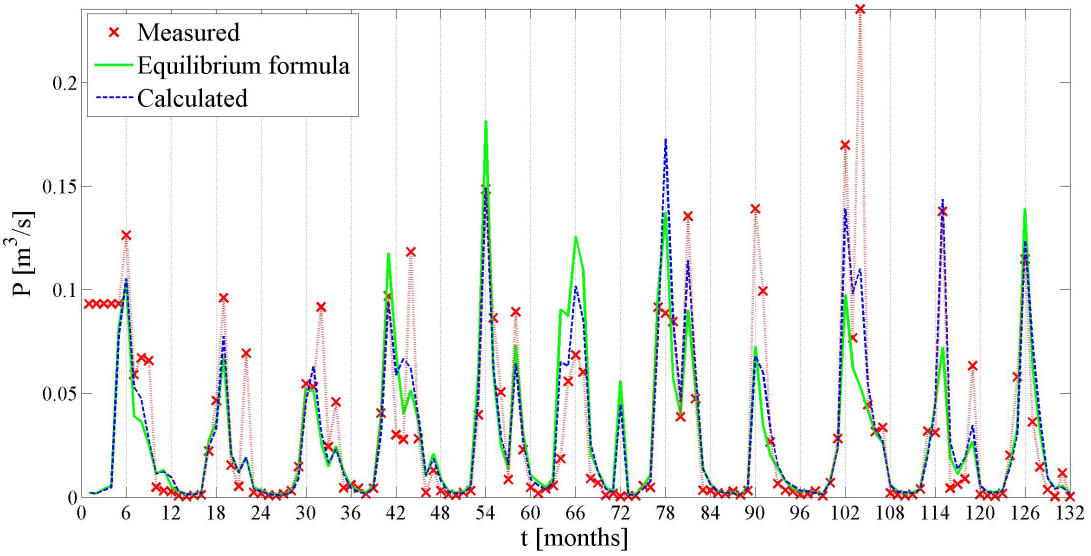

Figure 3.6: Comparison between the chronological series of suspended solid discharge measured (red crosses), evaluated with the equilibrium formula (green line) and calculated with the complete model (blue dotted line) calculated with the complete model (blue dotted line) calculated with the complete model (blue dotted line) calculated with the complete model (blue dotted line) for the first period ($'30s$) of **Trento**.

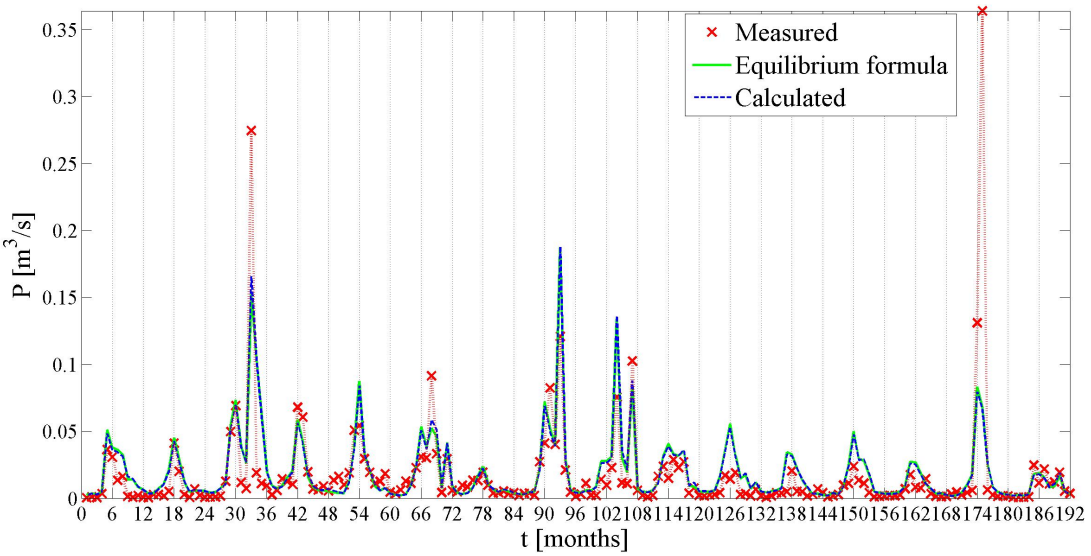

Figure 3.7: Comparison between the chronological series of suspended solid discharge measured (red crosses), evaluated with the equilibrium formula (green line) and calculated with the complete model (blue dotted line) calculated with the complete model (blue dotted line) calculated with the complete model (blue dotted line) calculated with the complete model (blue dotted line) for the first period ($'60s$) of **Trento**.

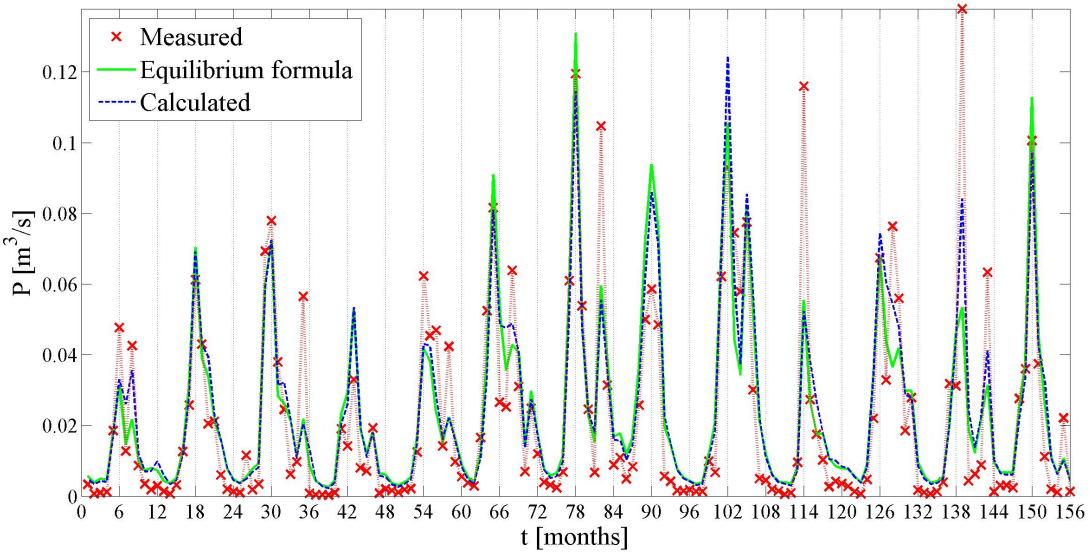

Figure 3.8: Comparison between the chronological series of suspended solid discharge measured (red crosses), evaluated with the equilibrium formula (green line) and calculated with the complete model (blue dotted line) calculated with the complete model (blue dotted line) calculated with the complete model (blue dotted line) calculated with the complete model (blue dotted line) for the first period ($'30s$) of **Boara Pisani**.

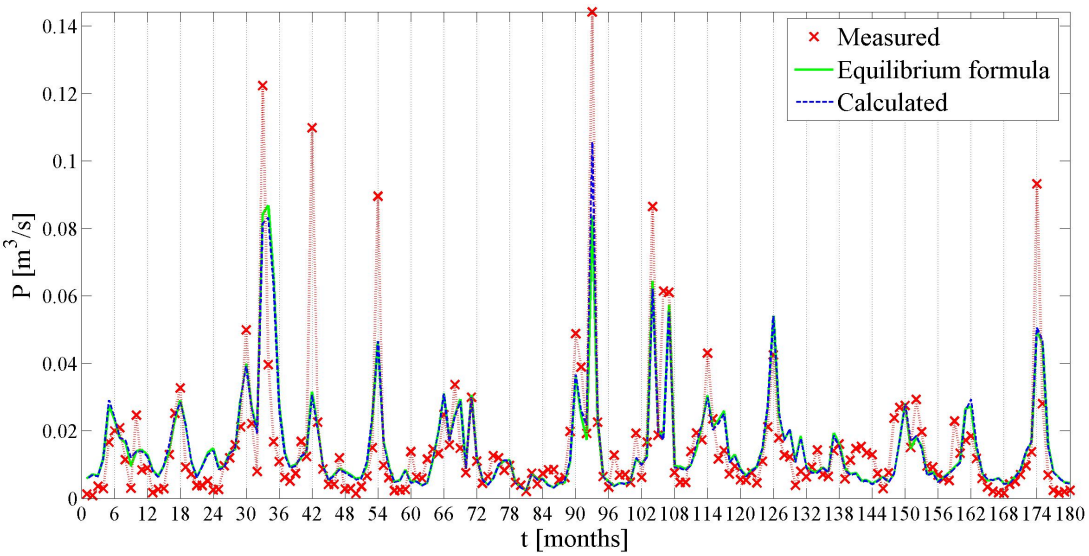

Figure 3.9: Comparison between the chronological series of suspended solid discharge measured (red crosses), evaluated with the equilibrium formula (green line) and calculated with the complete model (blue dotted line) calculated with the complete model (blue dotted line) calculated with the complete model (blue dotted line) calculated with the complete model (blue dotted line) for the first period ($'60s$) of **Boara Pisani**.

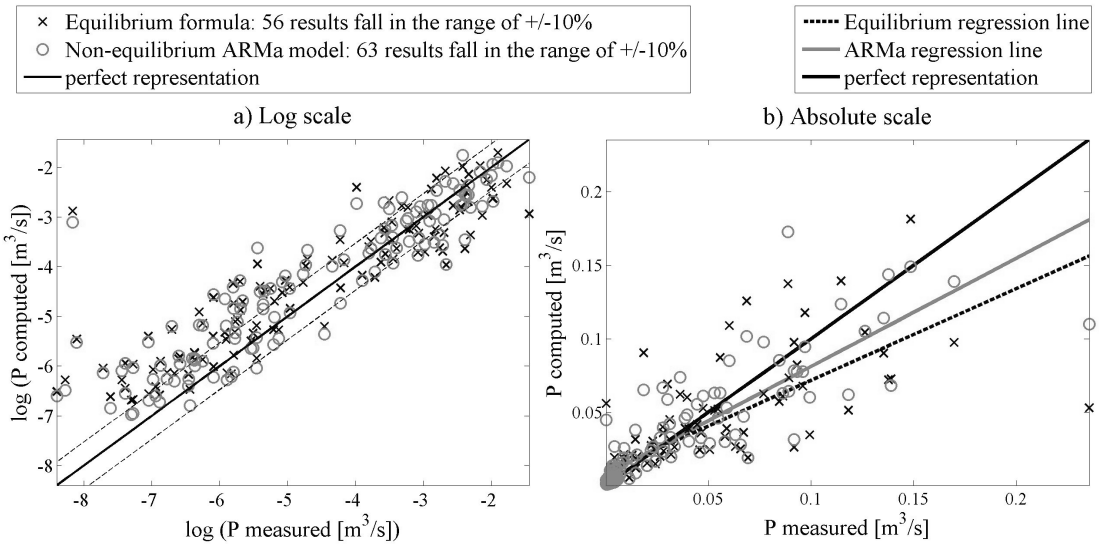

Figure 3.10: Suspended solid transport measured vs calculated (with equilibrium formula (crosses) and with the complete ARMA model (cicles)) for the first period ($'30s$) of Trento in the log-scale (a) and in the absolute scale (b). In the log-scale graph (a) the dotted lines identify a range of $+/-10\%$ with respect to the perfect representation.

3.7.2.3 Sensitivity analysis and discussion

The results from the Table 3.5 shows that the ARMA/recursive procedure gives an improved result both in terms of NSE (greater) and in therm of RSR (smaller) with respect to the evaluation of the solid transport calculated with the equilibrium formula. From the Figures 3.6, 3.7, 3.8 and 3.9 we see, especially for the $'30s$, that there are some peaks of the measured solid discharge which are very much better interpreted by the new model. In the Figure 3.10 the calculated data are compared with the measures and we can see that the cloud of measured/calculated points are closer in the case of the new model; moreover in the absolute scale (b) in Figure 3.10) the regression line for the ARMA/recoursive model results closer to the perfect representation.

For the recursive procedure we have developed an automatic method and, as already said, the set of parameters providing the best NSE is chosen as the result.

But a sensitivity analysis of the results shows that there are many sets of parameters that gives similar response. In particular is important to observe that generally similar results come out (i.e. provides positive ARMA parameters) for a certain range of k, but the same range is repeated periodically every year, demonstrating that the boundary conditions calculated on the measured values respect the sinusoidal behaviour with annual period.

Moreover, even if acceptable results are provided for almost all the values of p and E_u, the corresponding NSE varies with a p and E_u with a consistant inclination that may give us some useful information, even if different for every data set and not yet very clear. NSE increases with increasing E_u only for the first periods ($'30s$) of both the stations (more evident for Trento), while decreases with E_u increasing for the second periods ($'60s$). With increasing p the results for Boara Pisani do not show particular tendency, and seem to be independent about it, apart from some preferences for very low ($< 100\ days$) and very high values ($> 2\ years$). For Trento instead the dependence on p is strong, expecially for the first period, and also in this case the dependence seems to have a peculiar annual periodic behaviour (see Figure 3.11). These observations are valid despite the results presented in the Table 3.5, where the best NSE is chosen: as we can see from the Figure 3.11 the NSE variance is very low.

The delay k found with the recursive procedure is always greater than the one analytically evaluated with Fasolato et al. [2011]. Moreover, especially for the gauge station of Trento, k presents lower values in the second period, while from the analytical calculation we found an inverse tendency. Probably this is due by the fact that for the calculation of the celerity of the perturbation waves we consider the same morphology of the river, while from the first to the second period the reduction of the solid transport along the river, caused mainly by the huge human intervention, lead to an armouring of the bed that in its turn lead to an increasing speed of the propagating waves.

In any case, a direct inspection of the results shows that the propagation celerity (and so the delay k) of the perturbations is hardly precisely constant as assumed by the harmonic approach, basically because the input is not precisely sinusoidal. Yet the inaccurate delay of the solid transport perturbations may also depend on the different delay of the inputs coming from different area of the watershed (and not all concentrated in the barycenter). In order to put it into account, some tests have been made by splitting the watershed in sub-basins.

3.7.2.4 Improvement of the model by dividing the area in sub-basins

Taking a look to the map of the river Adige (see Figure 3.4), is possible to identify many important tributaries: Rienza, Passirio, Noce and Avisio in the upper part and all

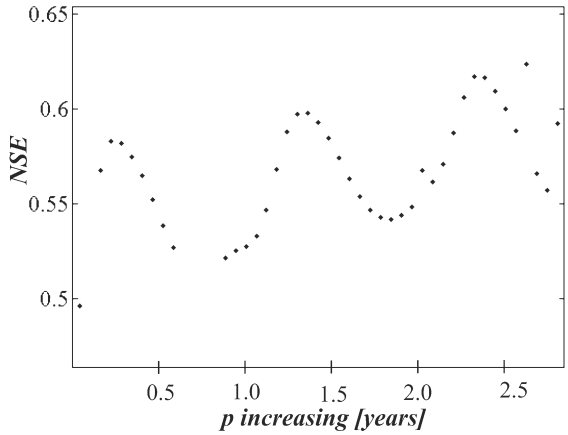

Figure 3.11: Example of the tendency of the NSE with p increasing. given k and E_u.

the rivers coming from the Lessini mountain (Alpone, Chiampo, etc ...) downstream Verona.

For sake of simplicity we do a simple division in two great sub-basins of the watershed area In this way we schematize the river in two LUF reach conveying in a unique gauge station, as shown in the Figure 3.12.a. Properly this scheme lead to have 3 different LUF channel. In order to reduce the computational time the barycenter of the second sub-basin is collapsed into the confluence, reducing the number of the LUF channel to 2 (Figure 3.12.b).

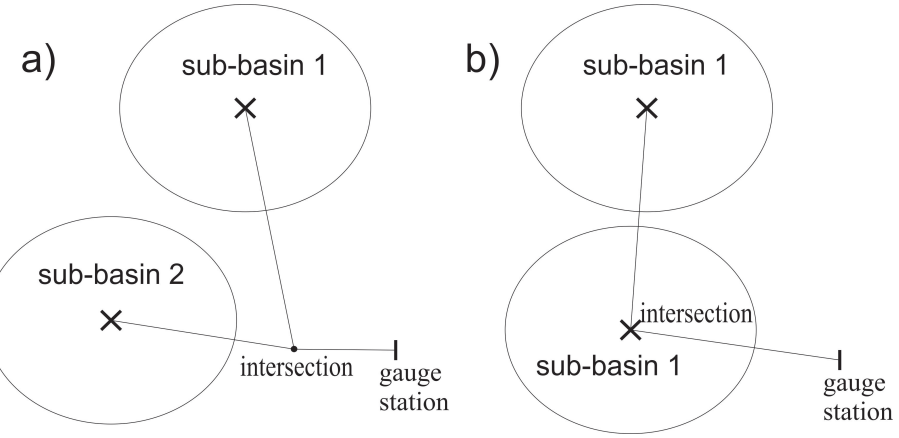

Figure 3.12: Schematic of Adige river divided in two principle sub-basins: a) Schematic of the river closing at Trento; b) Schematic of the river closing at Boara Pisani

Trento gauge station

As said in the section 3.7.1, the Adige river is composed by two "main" courses up to Bolzano. Moreover there are other two great tributaries flowing onto the Adige river just before the Trento gauge station: the torrent Noce from the right side (about 10 km before the gauge station) and the torrent Avisio from the left side (about 7 km before the gauge station). These two rivers convey to the Adige a great part of solid transport.

The first sub-basin correspond to the upper part of the surface, properly the Isarco and the upper-part of Adige watershed area. The second sub-basin is a great southern basin that combine the watershed area of both Noce and Avisio.

Boara Pisani gauge station

In this case we distinguish the mountain part with an ideal barycenter in Bolzano from the portion with more flat features. This second part has not a main course, but a lot of little torrent. We can for example collapse its barycenter in correspondance of the city of Rovereto, at the confluence of the Leno torrent.

Some simulations have be done with this new configuration but, as already said, considering that we do not know the correct morphology of the different LUF channels, the computational time required for the recursive method began to be important. Moreover the improvements obtained can be simply attributed to the increasing number of the addends of the mathematical model (see equation (3.10)).

3.8 Numerical applications to the Po river

The Po River represented in the Figure 3.13 is the longest and largest river of Italy: it springs from a stony hillside at Pian del Re, a flat place at the head of the Val Po under the northwest face of Monviso (in the Cottian Alps), it flows across northern Italy for 652 km and then finally reach the Adriatic Sea, southern Venice, forming a wide delta (with hundreds of small channels). It has a drainage area of 74000 km^2. The river flows through many important Italian cities, including Torino, Piacenza and Ferrara.

Also in this case is then possible to recognize and differ the mountain part from the plain. But now the mountain part may be further subdivided recognizing that the Po river is feeded both from medium-large river flowing from the Alps and from rivers with typical turrential behaviour flowing from the Apennines.

The river is subject to heavy flooding, consequently over half its length is controlled with levees.

In this section is briefly presented the same analysis made in the previous section 3.7 for the Adige river, now made for the Po river.

3.8.1 Geomorphological data and calibration

From the collection of the Hydrological Annals of the SIMN we have very long series of liquid discharge and some series of the solid discharge along the main course: in Piacenza, just before the confluence of the torrent Trebbia, the solid concentration was measured from 1956 to 1975 and again from 1977 to 1985; in Boretto from 1968 to 1972 and from 1976 to 1985; in Pontelagoscuro, near the delta on the Adriatic sea from 1968 to 1985, but the year 1974. As for the calibration for the Adige river, we assume that the total solid transport is quasi completely composed by the measured suspended load (section 3.7.1).

3.8.1.1 Grain-size composition

We get the data about the sediment composition from the grain-size cartography of the Basin Authority of the Po river. From these data we can evaluate the average

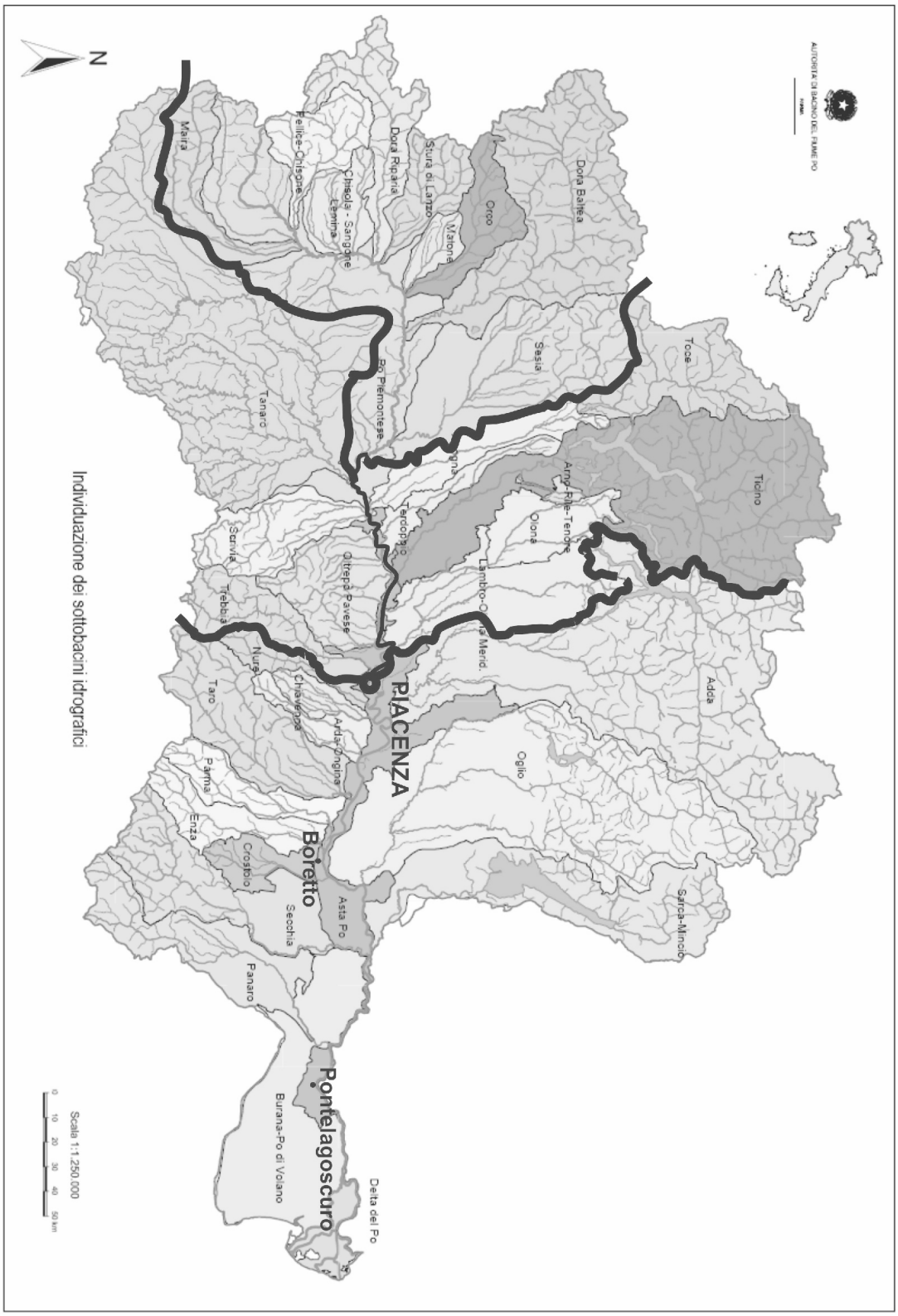

Figure 3.13: Basin of the river Po and its tributaries and the identification of the three considered gauge station. The bold black lines represent an hypothetical subdivision in three principal sub-basins proposed in section 3.8.2.4.

finer diameter d_{16} and the average coarser diameter d_{84} for the entire river and then calculate the respective bed composition for the entire river closing in the different gauge stations (see table 3.6).

Table 3.6: Representative actual grain-size composition of river Po closing at the gauge station of Piacenza, Boretto and at the closet of the river in Pontelagoscuro.

d $[mm]$	β_i in Piacenza [%]	β_i in Boretto [%]	β_i in Pontelagoscuro [%]
0.72	29.97	55.17	70.03
11.66	70.03	44.83	29.97

3.8.2 Results

Also in this case though a Fourier analysis we found that the principal sinusoidal wave of both the liquid flow and the solid transport has a period equal to one year. The second and the third waves have respectively period of six and three months. These results respect the limit of application of the LUF hypothesis found by Fasolato et al. [2009] (see (2.22) in section 2.6.2), having that the $T_w \geq 4\ T_{wind}$, calculated such that $\bar{\epsilon} = 10$, lead to shorter values (see Table 3.7).

3.8.2.1 Calibration of the equilibrium formula

In the Table 3.7there are the results of the calibration of the equilibrium formula, its corresponding NSE and the resulting delay k and attenuation coefficient α_{att}.

In this case the no-datum period (about 4 years for all the three stations) is maybe short enough in order to calibrate the model as we had a unique series of data. In the Table 3.7 the calibration for both the two distinguished periods and the unique period are shown.

3.8.2.2 ARMA calibration of the non-equilibrium perturbations

Also in this case there are all the problems about the available morphological data discussed for the Adige river (section 3.7.2.2). Moreover here we have a bigger and more differentiated watershed area. For these reasons here below, in the Table 3.8, we will present directly the final results obtained by the application of the combination of the

Table 3.7: Results of the calibration of the equilibrium formula for Po river

	Piacenza			**Boretto**			**Pontelagoscuro**		
L $[km]$	212100			317100			432100		
m	1.9			1.4			1.5		
	56-73	77-85	56-85	57-72	76-85	57-85	56-73	77-85	56-85
M	8.88 x 10^{-8}	7.78 x 10^{-8}	8.47 x 10^{-8}	7.34 x 10^{-6}	6.20 x 10^{-6}	6.96 x 10^{-6}	3.45 x 10^{-6}	2.15 x 10^{-6}	2.88 x 10^{-6}
NSE of the calibrated equilibrium formula	60.12 %	67.28 %	61.12 %	63.70 %	53.22 %	58.34 %	68.03 %	49.49 %	55.03 %
$\bar{P}$ $[m^3/s]$	0.0598	0.0701	0.0632	0.1740	0.1832	0.1775	0.2278	0.1790	0.2096
$\overline{Q^m}$ $[m^3/s]$	6.70 x 10^5	8.84 x 10^5	7.72 x 10^5	2.39 x 10^4	2.99 x 10^4	2.58 x 10^4	6.60 x 10^4	8.23 x 10^4	7.18 x 10^4
$\bar{Y}$	1.79	1.97	1.87	1.99	2.21	2.06	2.15	2.37	2.23
$\bar{U}$	1.84	1.92	1.88	1.74	1.84	1.77	1.65	1.73	1.68
$min[T_w]$ $[d]$	75	77	78	48	57	51	62	95	72
α_{EH}	0.0090	0.0079	0.00863	0.1572	0.1329	0.1489	0.1395	0.0870	0.1167
$c_{f_1}[\backslash]$	0.0014	0.0015	0.0014	0.0032	0.0029	0.0031	0.0035	0.0024	0.0030
$c_{f_1}\bar{U}$ $[km/y]$	83	89	84	177	168	174	181	129	161
k $[d]$	933	869	921	655	689	665	870	1218	980
$L_{f_1}[\backslash]$	6.67 x 10^5	6.41 x 10^5	6.28 x 10^5	1.98 x 10^5	1.45 x 10^5	1.79 x 10^6	1.49 x 10^6	6.27 x 10^5	1.09 x 10^6
$L_{f_1}\bar{U}$ $[km]$	1198	1260	1177	3950	3213	3692	3215	1488	2442
α_{att}	0.7667	0.7757	0.7636	0.8788	0.8550	0.8714	0.8124	0.6671	0.7669

ARMA and the recursive procedures. The Figure 3.14 shows the chronological sequence of the monthly solid transport data against the results calculated with the equilibrium and calculated with the combination of the ARMA and recursive procedures for the total period (1956-1985) for the station in Piacenza. In this case this tipe of graph is less clear than the case of the Adige river (see section 3.7.2.2), because the great range of variability of the solid transport and because of the minor differentiation between the two calculations. So here the Figures 3.15, 3.16 and 3.17 are presented. They show the graphs that compare the measured values with the results calculated with the equilibrium formula and the results calculated with the ARMA/recursive model respectively: on the left a) compares the results in the log scale and shows the number of data included in an interval equal to $+/-10\,\%$; on the right b) compares the results in the absolute scale, with the interpolation line of both the results.

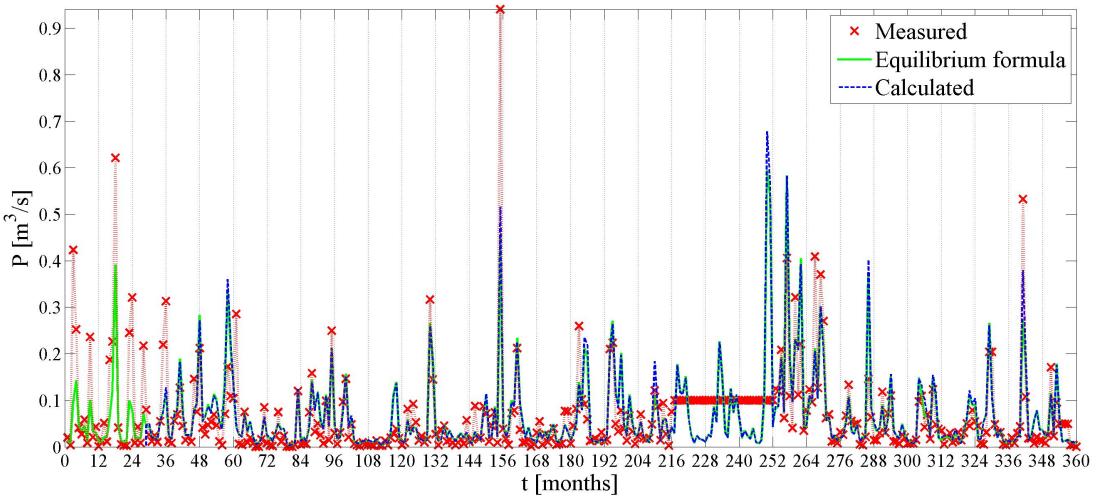

Figure 3.14: Comparison between the chronological series of suspended solid discharge measured (red crosses), evaluated with the equilibrium formula (green line) and calculated with the complete model (blue dotted line) calculated with the complete model (blue dotted line) for the total period of **Piacenza**

3.8.2.3 Sensitivity analysis and discussion

The better results obtained for the Piacenza gauge station are probably to attribute to the fact that this station is just before the confluence of the last four important Apennian affluent, which have a large contribution about the solid transport of the Po

Table 3.8: Results of ARMA combined with recursive procedures for the river Po (also the NSE and the RSR of the equilibrium results are reported for simplicity of comparison).

	Piacenza			**Boretto**			**Pontelagoscuro**		
	56-73	77-85	56-85	57-72	76-85	57-85	56-73	77-85	56-85
k $[d]$	1886	303	1678	866	11	1436	1452	449	1765
p $[d]$	525	133	616	497	49	798	826	14	917
E_u	0.0	2.5	0.0	2.5	2.5	0.0	2.5	0.8	0.8
a_1^*	0.1417	0.0699	0.0939	0.2956	0.0795	0.0937	0.54681	0.14028	0.28369
a_2^*	$9.67 \text{ x } 10^{-5}$	$4,42 \text{ x } 10^{-4}$	$1.73 \text{ x } 10^{-5}$	$1,34 \text{ x } 10^{-4}$	$2.63 \text{ x } 10^{-5}$	$2.93 \text{ x } 10^{-5}$	$63.20 \text{ x } 10^{-4}$	$1.97 \text{ x } 10^{-5}$	$2.54 \text{ x } 10^{-5}$
NSE	63.54 %	67.55 %	63.18 %	65.43 %	40.73 %	59.10 %	62.38 %	36.32 %	56.27 %
equilibrium NSE	59.42 %	64.84 %	61.12 %	62.37 %	50.34 %	58.34 %	62.61 %	33.29 %	55.03 %
RSR	0.6038	0.5697	0.6068	0.5880	0.7699	0.6394	0.6133	0.80	0.6613
equilibrium RSR	0.6370	0.5930	0.6236	0.6134	0.7047	0.6455	0.6115	0.8167	0.6706

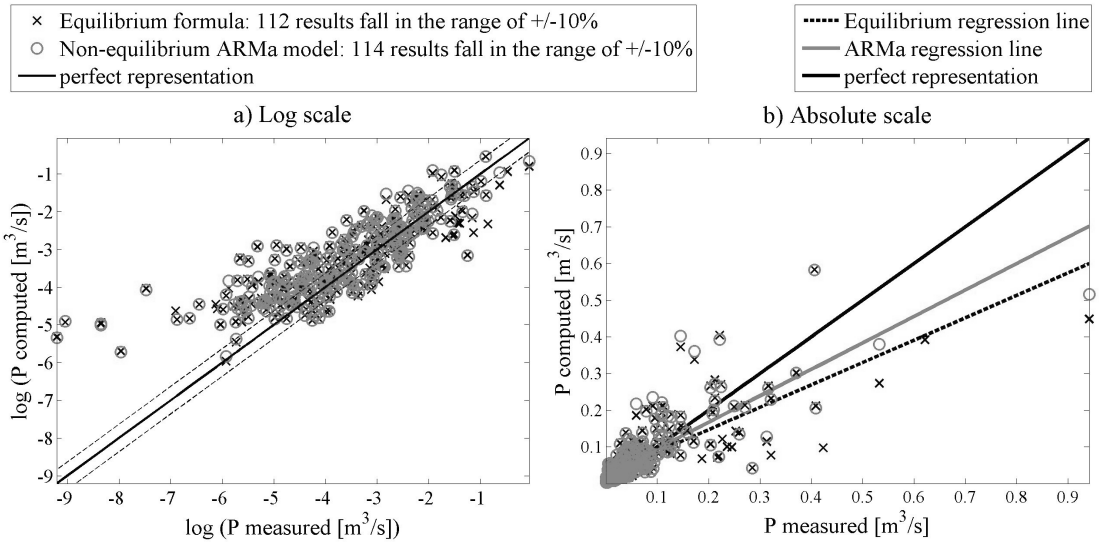

Figure 3.15: Suspended solid transport measured vs calculated (with equilibrium formula (crosses) and with the complete ARMA model (circles)) for the total period of **Piacenza** in the log-scale (a) and in the absolute scale (b). In the log-scale graph (a) the dotted lines identify a range of $+/-10\%$ with respect to the perfect representation.

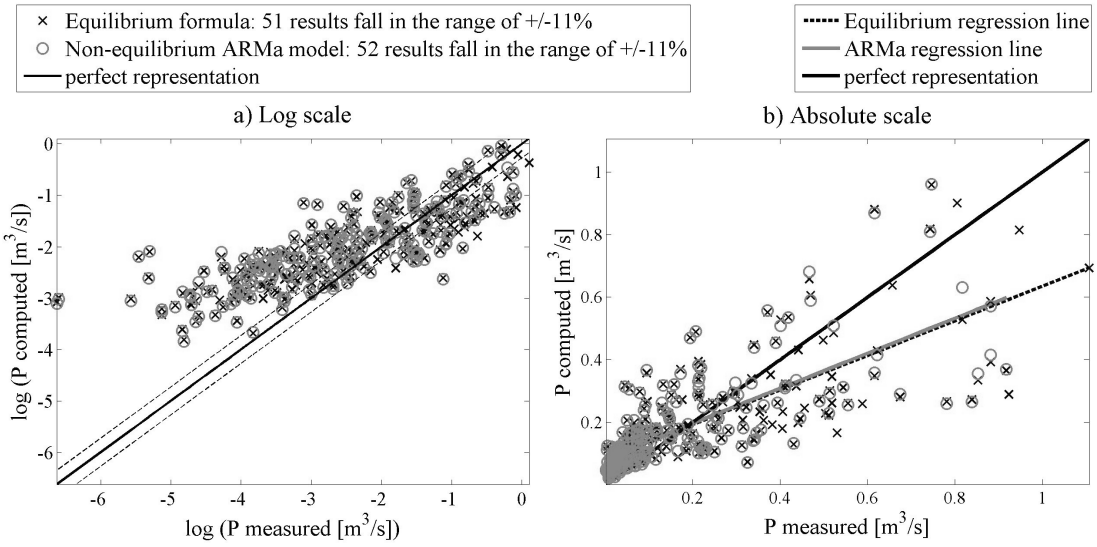

Figure 3.16: Suspended solid transport measured vs calculated (with equilibrium formula (crosses) and with the complete ARMA model (circles)) for the total period of **Boretto** in the log-scale (a) and in the absolute scale (b). In the log-scale graph (a) the dotted lines identify a range of $+/-10\%$ with respect to the perfect representation.

river: for Syvitski and Kettner [2007] more than the 50 % of the solid transport of the Po river arrives from the rivers and torrents draining the southern Apennian hinterlan. For this reason the following two gauge stations, Boretto and Pontelagoscuro, are worstly represented by a unique LUF channel.

Also for the results obtained here for the Po river we can do the same type of discussion done for the Adige river in the section 3.7.2.3. In particular we find that similar results come out (i.e. provides positive ARMA parameters) for a certain range of k and the same range is repeated periodically every year.

3.8.2.4 Improvement of the model by dividing the area in sub-basins

Some simulations with a preliminary hypothetical subdivision of the basin closing in Piacenza in three principle sub-basins have be done. This subdivision is made by the identification of a first great upstream sub-basin with mountain characteristics and with the city of Torino as barycenter. The second sub-basin incorporates the Apennian affluent represented with the Tanaro torrent. The last sub-basin incorporates the Alpine affluent represented by the Ticino river. These three principal sub-basins are identified with the thick black line in the map of the basin in the Figure 3.13.

In this way five principle LUF channel can be identified, as shown in the Figure 3.18.

Is interesting to note that during the LUF channel 123 of the Figure 3.18 in the reality the river, from braided, become meandering, because the conjunction of two facts: the great contribution in liquid discharge from Ticino river and the decreasing of the slope due by a pre-Quaternary stone formation.

As said for the Adige river (see section 3.7.2.4), these simulations take great computational time and the results may be not representative of the real behaviour of the river because the lack of information about the real morphology.

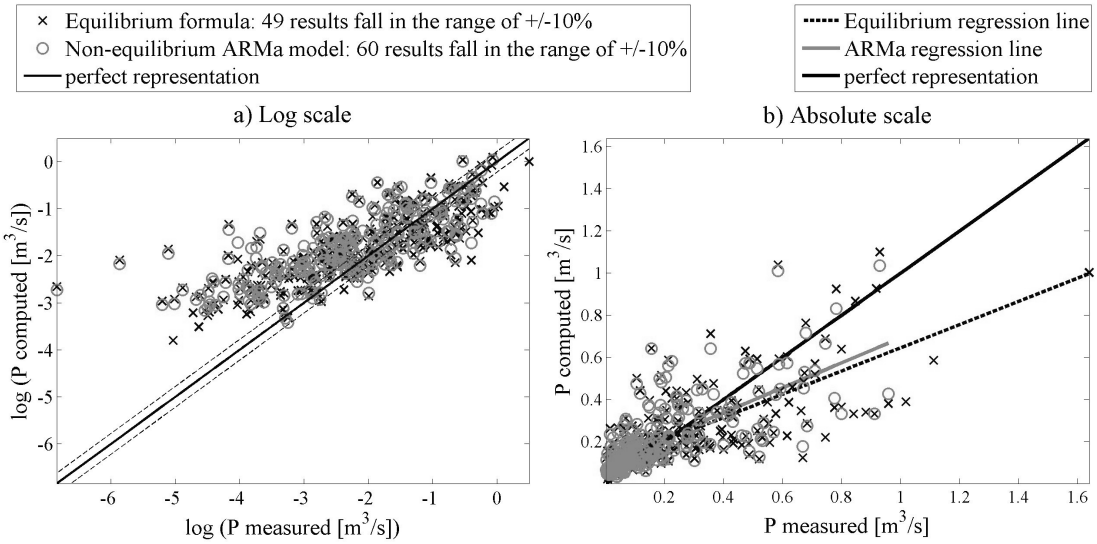

Figure 3.17: Suspended solid transport measured vs calculated (with equilibrium formula (crosses) and with the complete ARMA model (circles)) for the total period of **Pontelagoscuro** in the log-scale (a) and in the absolute scale (b). In the log-scale graph (a) the dotted lines identify a range of $+/-10\%$ with respect to the perfect representation.

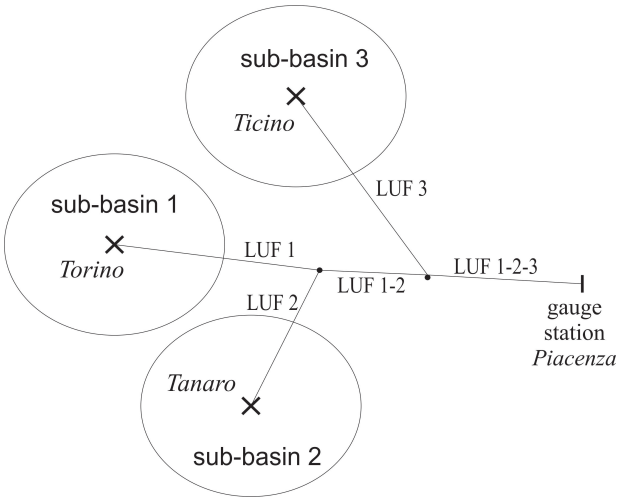

Figure 3.18: Subdivision of the basin of the river Po. They are identified also in the map of the basin in the Figure 3.13.

3.9 Numerical applications to the Venice Lagoon catchment area

We have collaborated with a research program established between CORILA (Consortium for the management of the center for coordination of research activities inherent the Venice Lagunar system) and the Veneto Region oriented to the acquisition of new information about the Venice Lagoon, its watershed area and its opposite see, the Adriatic see. In this context we tried to apply the long-term equilibrium model to this particular case, very dissimilar from the previous two. The Venice Lagoon is located in northern Adriatic Sea (Gulf of Venice, Italy). The coastline of this region is affected by the inputs of 11 main rivers of variable size and discharge.

The drainage basin investigated in this section is the territory whose surface supplies water discharge to the Venice Lagoon during normal flow conditions [Autoritá di Bacino dell'Adige e dell'Alto Adriatico, 2010]. The entire basin surface is nearly 2040 km^2 and the drainage network, with a total length of about 3780 km. It comprises some natural waterways (Dese, Zero, Marzenego-Osellino, Lusore, Muson Vecchio, Tergola, Scolo Soresina, Scolo Fiumazzo, Canale Montalbano), streams with controlled or partially controlled flow, in the central and southern areas (Naviglio Brenta, Canale di Mirano, Taglio Nuovissimo), canals with full mechanical drainage in the low-lying areas at south and a dense network of outfall drain. The drainage basin also includes part of the area of the resurgence waters (resurgent area) that does not drain superficially but, through the groundwater, feeds the streams northernmost.

Furthermore the small river sub-basins are interconnected each other and exchange substantial amounts of water (by pumping stations) with the large rivers which are not flowing into the lagoon, like Brenta, Sile and Bacchiglione, especially in flood conditions.

The contributions of this total drainage basin flow into the lagoon of Venice in 27 distinct injection points. The drainage network has a total number of 27 outlets in the the Venice Lagoon [Autoritá di Bacino dell'Adige e dell'Alto Adriatico, 2010] distributed along perimeter of the lagoon. However, a predominant fraction (97% according to Zuliani et al., 2005) of the total runoff is conveyed by the 12 main tributary

sub-basins represented in the Figure 3.19.

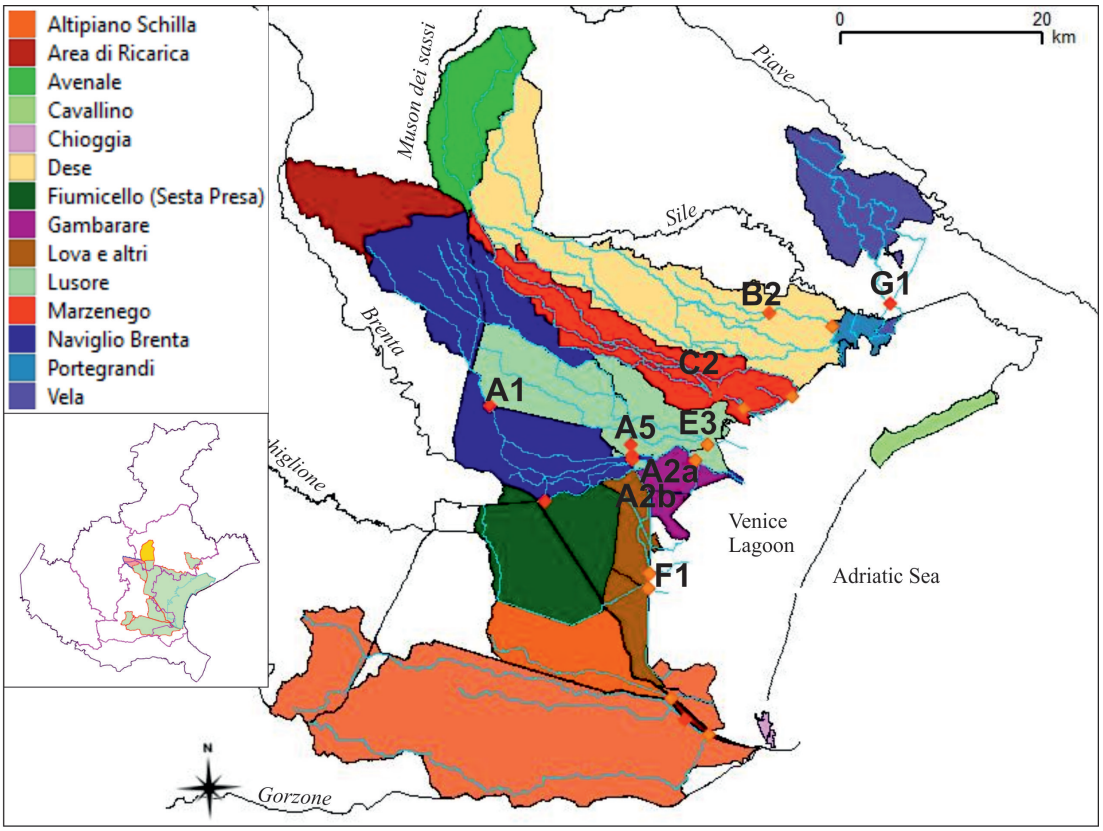

Figure 3.19: The catchment area to the Venice Lagoon: in different colours are represented the main sub-basins (this subdivision is valid in normal flow-conditions). With the dots are represented the automatic network of gauging station: the codes visualized identify the gauge stations used for the calibration of the model.

Obviously the model will not be applied to the entire catchment area, but it has to be applied to each singular sub-basins identified in Figure 3.19, since the application need to recognize the main course and the discharge of a river.

In this case the basins and the rivers investigated are much smaller with respect to the previous two cases (Adige and Po rivers), and they are characterized by relatively uniform territory. The small lowland watercourses, with relatively uniform arable watershed, transport finer material and the concentration of sediments does not have a large variability as in the large mountain basins, dominated by the presence of landslides and debris flows. By contrast, sporadic exceptional storms can produce deviations from equilibrium, also related to the growth of the vegetation.

3.9.1 Geomorphological data and calibration

The principal water courses of the basin are monitored through automatic gauging stations, some managed by ARPAV (Agenzia Regionale per la Prevenzione e la Protezione Ambientale del Veneto, namely the Regional Environmental Agency) and others by CVN (Magistrato alle Acque - Consorzio Venezia Nuova, namely the Venetian Water Authority). The gauging stations measure at time intervals of one hour both the hydrology and the quality parameters of the flow, among which the turbidity.

The liquid discharge is calculated on the basis of current measurements with the methodology governed by ISO 6416.

Only for the river Zero (B2) the liquid discharge is calculated from data of the water level through a rating curve calibrated in the 2007.

The turbidity is a parameter that quantifies the reduction of the transparency of the water due to the presence of particles in suspension and is expressed in FTU (Formazine Turbidity Units). For each station systematic samples of water are manually collected in order to determine the suspended sediment concentration (SSC $[mg/l]$). Specific correction and calibration procedures between the records of turbidity and the SSC samples are made in order to transform the turbidity data in SSC data. Then the usual conversion (3.15) explained in the section 3.7.1 was applied to achieve the measured volumetric solid discharge $P(t)$.

Moreover, for the period 1996-2011 data of temperature and daily precipitation measured by several gauging stations from the regional network managed by the Meteorological Center of ARPAV are available.

Finally is important to note that some gauging stations, which are near to the outlet of the river, are strongly influenced by the tidal excursion on the Lagoon. For certain rivers, with very low values of liquid flow, negative discharges are sometime recorded. It is physically more useful, beside easier to treat with, evaluate and deal with the daily average values of the measured data. We can assume that the liquid discharge in the rivers and the tide are independent of each other and so we can do the daily average of the hourly records of the measures of the liquid discharge and of the data of the solid discharge.

A lot of records are not continuous, but some of them have also very long periods during which the gauging station did not worked. In the Table 3.9 there is the list of the rivers with appreciable continuous records of measures that we analyzed with the long-term equilibrium model. The code of the corresponding gauging stations are represented in the Figure 3.19.

3.9.1.1 Grain-size composition

During the research project samples of the bottom sediments have been collected to determine the grain-size distribution at each gauging station. The procedure was not simple because the extremely fine sediment involved and the frequently presence of thick vegetation on the bottom. However some results have been extrapolated, showing a moderate variability with regard to the different grain-size fractions. We do not observe a trend of the size fractions in relation to the location of stations. The diameters used as representative for the two characteristic classes of grain-size are listed in the Table 3.9.

Its somehow surprising the fact that the level of uniformity of the bottom $d = d_{16}/d_{84}$ results lower with respect to the value calculated both for the Adige and the Po rivers. This is probably due, although the Adige and Po rivers have a part of the main course of mountain characteristics, by the consideration of an average grain-size distribution curve for the entire river, that lead to a probability distribution with long tails (representing the finer and the coarser sediments) beyond the 16% and the 84% respectively.

3.9.2 Results

A preliminary analysis of the records of data shows that their behaviour is less seasonal than the previous two cases. Through a Fourier analysis we found that is possible to recognize an annual principal sinusoidal wave only for the liquid discharge, but it is not always the first. For the solid discharge most of the records present huge peaks above a quasi-uniform signal that do not have a relevant characteristic period.

The minimum periods $min[T_w]$ of the boundary conditions necessary for the ap-

Table 3.9: List of the rivers of the catchment area in the Lagoon of Venice to which the long-term equilibrium model has been applied.

Alias	**River**	d_{16} $[\mu m]$	d_{84} $[\mu m]$
A2a	r. Serraglio	8.32	309.00
A2b	s. Tergolino	2.12	278.00
B2	r. Zero	4.23	209.00
C2	f. Marzenego	5.21	393.00
A5	c. Taglio di Mirano	2.37	52.00
A1	f. Tergola	3.73	171.00
E3	s. Lusore	3.29	75.10
G1	c. Vela	4.10	304.00
F1	s. Fiumazzo	1.61	77.94

plication of the LUF hypothesis (see section 2.6.2) are shown in the Table 3.10: for almost all the rivers we can consider T_w equal both to $1 year$ and to $6 months$. Only the river Marzenego has a minimum T_w greater than $1 year$: we admit to apply the model, namely using the hypothesis LUF, accepting a reasonable error due to a corresponding value of $\bar{\epsilon} = 8,1$, which is however $\gg 1$. Below some results of the calibration of the model are presented maintaining the characteristic period of the boundary conditions T_w equal to $1 year$.

In this case the data available are daily mean values instead of the monthly mean values. Even if this fact means that we can have theoretically a greater number of data, the series are in any case short. In fact, considering that we have recognize the characteristic period of the boundary condition equal to $1 year$, series of at most 5 years are (statistically) too much short in order to recognize the chronological dependence of the solid discharge $P(t)$ from preceding values of the equivalent liquid discharge $Q^m(t-k)$, especially because indeed the records are further reduced by the delay k.

In order to avoid to further reduce the series with the delay k and the accumulation period p, a simple hydrological model (briefly exposed in Appendix C) has been developed to reconstruct the liquid discharge passing through the cross-section of the gauge stations before 2006. We use the meteorological data starting from the 1996 and some primary information from the land reclamation authority about the flow regulation management.

3.9.2.1 Calibration of the equilibrium formula

In the Table 3.10 there are the results of the calibration of the equilibrium formula, its corresponding NSE, the resulting delay k and attenuation coefficient α_{att}.

From the Table 3.10 we see that the rivers Tergolino (A2b), Tergola (A1) and Fiumazzo (F1) are the smallest three channel between the analyzed. In particular for Tergola and Fiumazzo we have a really low values for the NSE of the equilibrium.

Tergola (A1) has a huge peak during the March of the 2011 that considerably reduce the value of the NSE even if the results are good. This river naturally flow into the Serraglio, then measured at the gauging station A2a. The great values for the March of 2011 is not recorded, however another huge peak is measured during May of the 2010. Also for the river Lusore (E3) a peak turns out for the same period. Apparently, correspondingly to these phenomena, there are not extraordinary high values of the liquid discharge of the rivers.

3.9.2.2 ARMA calibration of the non-equilibrium perturbations

Preliminarily we tried to apply the usual formulation of the model to define the dimensionless perturbation of the morphological characteristics $m_c(t)$, namely using the equation (3.6). Then we used the (3.7) in order to better represent the surface erosion as the main mechanism of sediment production.

If with the (3.6) formulation the delay p represent the characteristic time required to fill the slopes and activate a landslide, in this case, with the (3.7), the delay p should represent the time required to the sediments and water to cover the dense network of irrigation ditch, in addition to the role played by the different vegetation cover.

Below the Figures for the rivers Serraglio (A2a), Marzenego (C2), Taglio Mirano (A5) and Vela (V1) are presented as example only through the graphs that compare the measured data with the calculated results.

First version for the dimensionless perturbation of the morphological characteristics: $m_c(t)$. The first trial application of the combined ARMA-recursive procedure kipping the delay k equal to the value resulting from the calibration of the

Table 3.10: Results of the calibrationof the equilibrium formula for rivers flowing into the Lagoon of Venice.

	Serraglio (A2a)	**Tergolino (A2b)**	**Zero (B2)**	**Marzenego (C2)**	**Tergola (A1)**	**Taglio Mirano (A5)**	**Lusore (E3)**	**Fiumazzo (F1)**	**Vela (G1)**
$L\ [km]$	48	15	27	$32,5$	24	33	32	25	25
m	1.6	1.6	2.1	2.6	1.0	2.0	1.5	1.4	1.7
M	1.16 x 10^{-5}	2.52 x 10^{-5}	4.72 x 10^{-6}	4.89 x 10^{-6}	1.40 x 10^{-5}	8.96 x 10^{-6}	1.98 x 10^{-5}	3.16 x 10^{-5}	4.69 x 10^{-6}
NSE of the calibrated equilibrium formula	24.25 %	58.31 %	58.86 %	81.18 %	4.43 %	70.19 %	55.13 %	12.24 %	83.41 %
$\bar{P}\ [m^3/s]$	1.26 x 10^{-4}	2.08 x 10^{-5}	1.07 x 10^{-4}	5.50 x 10^{-5}	3.30 x 10^{-5}	7.40 x 10^{-5}	1.23 x 10^{-4}	1.48 x 10^{-4}	5.39 x 10^{-5}
$\overline{Q^m}\ [m^3/s]$	9.85	0.74	24.31	11.39	2.40	8.10	6.45	4.63	11.30
$\bar{Y}$	0.88	0.40	0.68	0.55	0.53	0.30	0.98	1.00	0.53
$\bar{U}$	1.58	0.97	1.57	0.66	1.67	0.96	1.51	1.12	1.28
$min[T_w]\ [d]$	118	87	67	446	67	28	329	108	78
α_{EH}	1.10 x 10^{-4}	2.37 x 10^{-4}	1.94 x 10^{-7}	1.32 x 10^{-7}	1.50 x 10^{-2}	1.43 x 10^{-6}	6.32 x 10^{-4}	3.93 x 10^{-3}	4.14 x 10^{-6}
$c_{f_1}[\backslash]$	0.00066	0.00071	0.00051	0.00057	0.00028	0.00076	0.00092	0.00121	0.00031
$c_{f_1}\bar{U}\ [km/y]$	33	22	25	12	15	23	44	43	13
$k\ [d]$	536	253	393	1003	603	525	267	215	717
$L_{f_1}[\backslash]$	2.0 x 10^5	3.8 x 10^5	3.5 x 10^5	3.0 x 10^4	2.8 x 10^5	1.7 x 10^6	9.4 x 10^4	2.4 x 10^5	1.9 x 10^5
$L_{f_1}\bar{U}\ [km]$	179	149	236	16	152	522	92	242	103
α_{att}	0.684	0.852	0.836	0.225	0.786	0.902	0.626	0.849	0.705

equilibrium formula (see Table 3.10) found positive ARMA parameters a_1^* and a_2^* only for two rivers: Serraglio (A2a) and Tergolino (A2b). The results are reported in the Tables 3.11.

Table 3.11: Preliminary results of the ARMA procedure for the rivers Serraglio (A2a) and Tergolino (A2b) using the original formulation (3.6) for the evaluation of the boundary condition $m_c(t)$ (also the NSE and the RSR of the equilibrium results are reported for simplicity of comparison).

	Serraglio (A2a)	Tergolino (A2b)
k $[d]$	536	253
p $[d]$	413	581
E_u	1.7	0.5
a_1^*	0.6671	0.0035
a_2^*	0.0059	0.0007
NSE	36.54 %	59.97 %
equilibrium NSE	24.25 %	58.31 %
RSR	0.488	0.676
equilibrium RSR	0.373	0.658

The results obtained by the model with the recursive procedure applyed also on the value of the delay k are shown in the Tables 3.12. In the Figures 3.20, 3.21, 3.22 and 3.23 there are the graphs of the results for the river Serraglio, Marzenego, Taglio Mirano and Vela respectively. These Figures show the comparison between the measured data with the results obtained both with the equilibrium formula and with the complete model: on the left a) compares the results in the log scale and shows the number of data included in an certain interval; on the right b) compares the results in the absolute scale, with the interpolation line of both the results.

Alternative version for the dimensionless perturbation of the morphological characteristics: $m_c(t)$. As for the previous case, the first trial application of the combined ARMA-recursive procedure kipping the delay k equal to the value resulting from the calibration of the equilibrium formula (see Table 3.10) found positive ARMA parameters a_1^* and a_2^* only for the two rivers Serraglio (A2a) and Tergolino (A2b). The results are reported in the Table 3.13.

The results obtained by the model with the recursive procedure applyed also on the

Table 3.12: Results of the ARMA combined with recursive procedures for the rivers flowing in the Venice Lagoon using the original formulation (3.6) for the evaluation of the boundary condition $m_c(t)$ (also the NSE and the RSR of the equilibrium results are reported for simplicity of comparison).

	Serraglio (A2a)	**Tergolino (A2b)**	**Zero (B2)**	**Marzenego (C2)**	**Tergola (A1)**	**Taglio Mirano (A5)**	**Lusore (E3)**	**Fiumazzo (F1)**	**Vela (G1)**
k $[d]$	523	352	821	1984	1507	246	331	552	746
p $[d]$	924	98	105	322	168	35	203	406	77
E_u	1.6	2.5	2.5	2.5	2.5	2.5	2.5	0.1	0.1
a_1^*	0.8957	0.0320	0.0811	1.1125	1.4974	0.0061	0.0136	2.1877	0.0416
a_2^*	0.0035	0.0040	0.0046	0.0246	0.0009	0.0068	0.0033	0.0043	0.0058
NSE	41.99 %	65.09 %	67.68 %	88.64 %	6.67 %	76.97 %	57.85 %	39.55 %	91.29 %
equilibrium NSE	24.25 %	58.31 %	58.86 %	81.18 %	4.43 %	70.19 %	55.13 %	12.24 %	83.41 %
RSR	0.529	0.725	0.560	0.782	0.225	0.682	0.681	0.279	0.831
equilibrium RSR	0.373	0.658	0.508	0.686	0.181	0.622	0.699	0.173	0.778

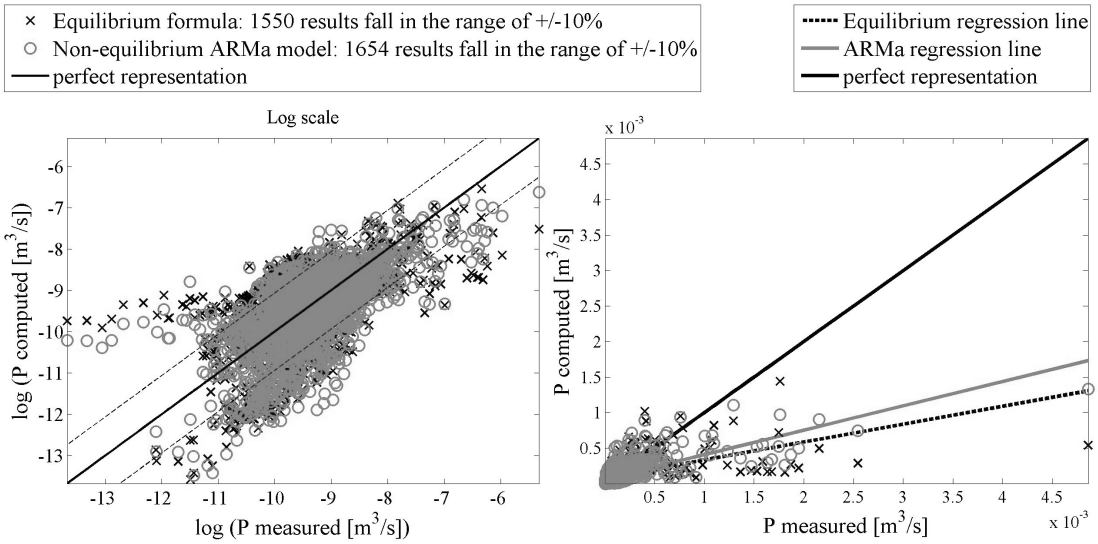

Figure 3.20: Suspended solid transport measured vs calculated (with equilibrium formula (crosses) and with the complete ARMA model (circles) using the original formulation (3.6)) for station **(A2a) Serraglio** in the log-scale (a) and in the absolute scale (b). In the log-scale graph (a) the dotted lines identify a range of $+/-10\%$ with respect to the perfect representation.

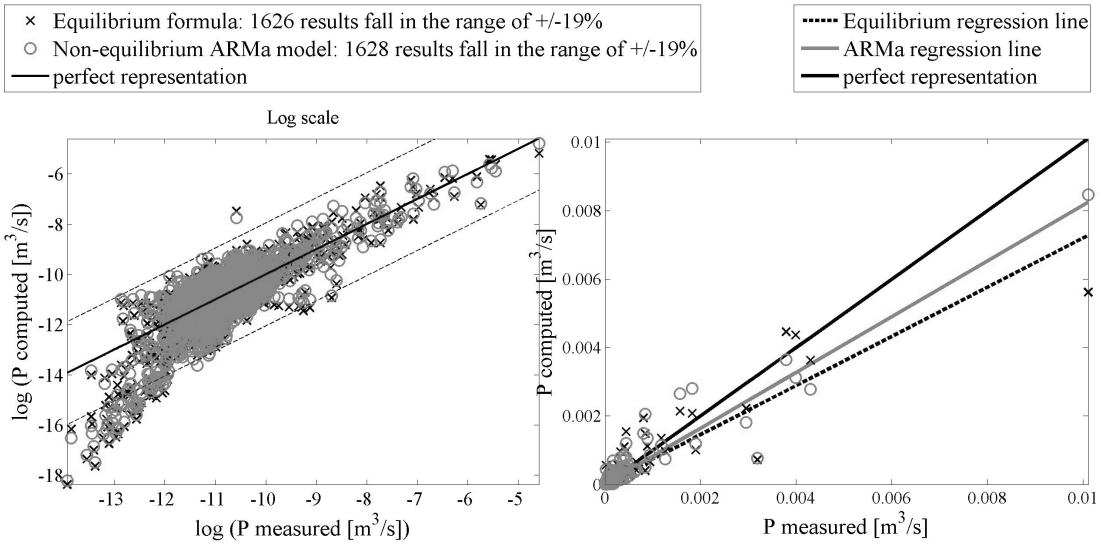

Figure 3.21: Suspended solid transport measured vs calculated (with equilibrium formula (crosses) and with the complete ARMA model (circles) using the original formulation (3.6)) for the total period of **(C2) Marzenego** in the log-scale (a) and in the absolute scale (b). In the log-scale graph (a) the dotted lines identify a range of $+/-10\%$ with respect to the perfect representation.

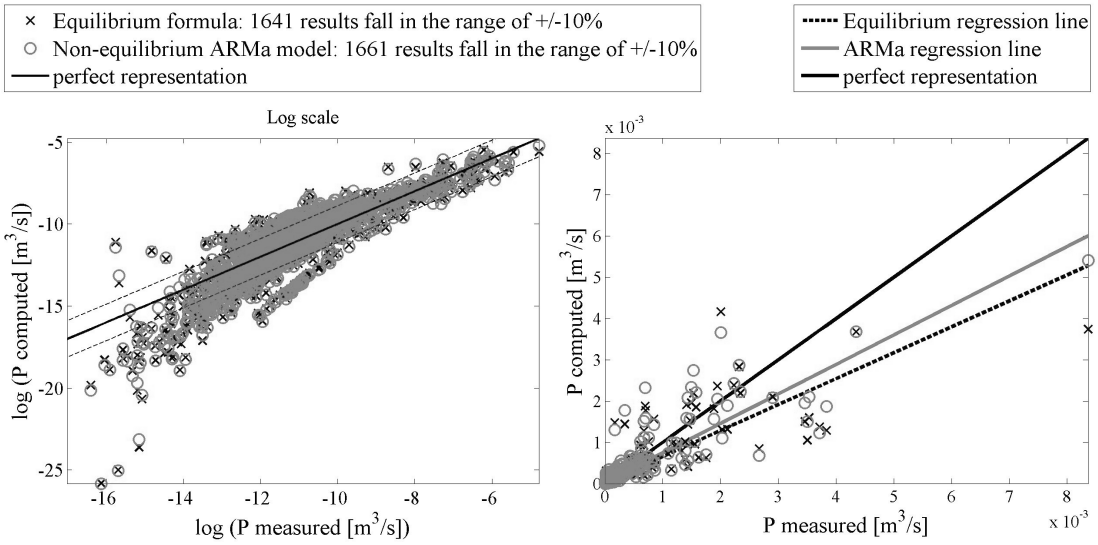

Figure 3.22: Suspended solid transport measured vs calculated (with equilibrium formula (crosses) and with the complete ARMA model (circles) using the original formulation (3.6)) for the total period of **(A5) Taglio Mirano** in the log-scale (a) and in the absolute scale (b). In the log-scale graph (a) the dotted lines identify a range of $+/-10\%$ with respect to the perfect representation.

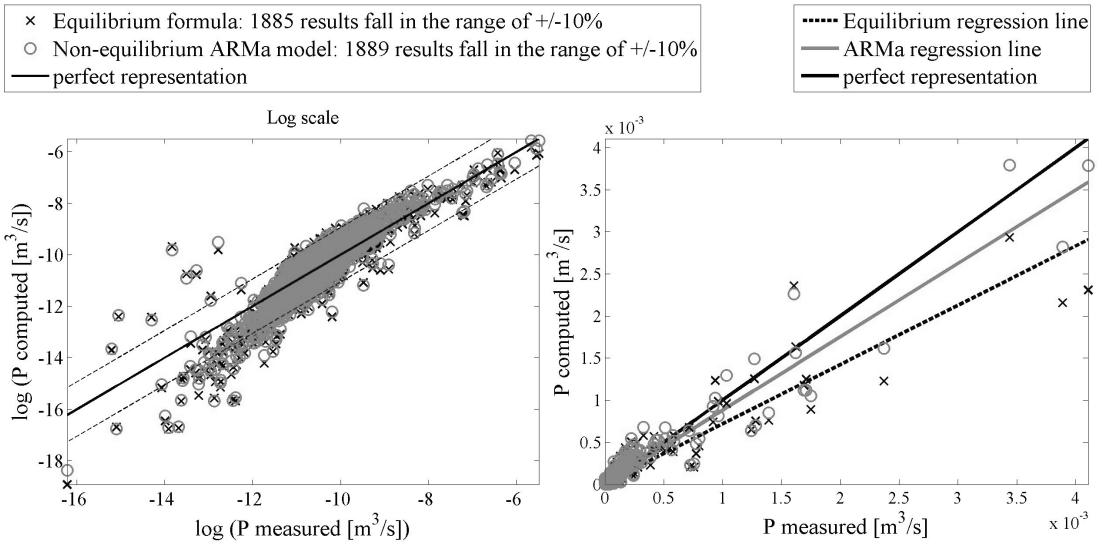

Figure 3.23: Suspended solid transport measured vs calculated (with equilibrium formula (crosses) and with the complete ARMA model (circles) using the original formulation (3.6)) for the total period of **(G1) Vela** in the log-scale (a) and in the absolute scale (b). In the log-scale graph (a) the dotted lines identify a range of $+/-10\%$ with respect to the perfect representation.

Table 3.13: Preliminary results of the ARMA procedure for the rivers flowing in the Venice Lagoon using the rainfall data (3.7) (also the NSE and the RSR of the equilibrium results are reported for simplicity of comparison).

	Serraglio (A2a)	**Tergolino (A2b)**
k $[d]$	536	253
p $[d]$	168	91
E_u	2.5	0.1
a_1^*	0.545	9.2 x 10^{-5}
a_2^*	5.4 x 10^{-5}	2.6 x 10^{-6}
NSE	31.61 %	58.35 %
equilibrium NSE	24.25 %	58.31 %
RSR	0.445	0.660
equilibrium RSR	0.373	0.658

value of the delay k are shown in the Tables 3.14. No results were found for the river Zero (B2). In the Figures 3.24, 3.25, 3.26 and 3.27 there are the graphs of the results for the river Serraglio, Marzenego, Taglio Mirano and Vela respectively. These Figures show the comparison between the measured data with the results obtained both with the equilibrium formula and with the complete model: on the left a) compares the results in the log scale and shows the number of data included in an certain interval; on the right b) compares the results in the absolute scale, with the interpolation line of both the results.

3.9.2.3 Sensitivity analysis and discussion

The evaluation of the celerity of the perturbation waves ((2.23) in section 2.6.2) is, although not obviously, directly proportional both to the grain-size and to the slope of the river through the factor γ, but inversely proportional to the relative thickness of the mixing layer. The celerity evaluated for the rivers flowing in the Venice Lagoon reported in Table 3.10 are lower than either those evaluated for the river Adige (Table 3.3) or for the river Po (Table 3.7). This fact can lead to conclude that the slope has a greater importance, but we have formerly corrected the values evaluated for the Adige and the Po rivers with the recursive procedure and found also very lower values (implicit in the resulting delay k).

Table 3.14: Results of the ARMA combined with recursive procedures for the rivers flowing in the Venice Lagoon using the rainfall data (3.7) (also the NSE and the RSR of the equilibrium results are reported for simplicity of comparison).

	Serraglio (A2a)	**Tergolino (A2b)**	**Marzenego (C2)**	**Tergola (A1)**	**Taglio Mirano (A5)**	**Lusore (E3)**	**Fiumazzo (F1)**	**Vela (G1)**
k $[d]$	887	149	234	1542	575	226	986	802
p $[d]$	7	14	112	28	7	35	14	28
E_u	2.5	2.5	2.5	2.5	1.2	2.5	2.5	2.5
a_1^*	1.745	0.039	0.103	1.217	0.345	0.004	2.275	0.116
a_2^*	5.09×10^{-5}	2.74×10^{-5}	1.68×10^{-5}	5.96×10^{-5}	3.78×10^{-6}	3.76×10^{-5}	9.83×10^{-4}	4.32×10^{-5}
NSE	30.12 %	69.64 %	49.48 %	6.22 %	65.22 %	62.69 %	24.33 %	81.95 %
equilibrium NSE	24.25 %	58.31 %	81.18 %	4.43 %	70.19 %	55.13 %	12.24 %	83.41 %
RSR	0.443	0.729	0.164	0.210	0.652	0.743	0.220	0.663
equilibrium RSR	0.373	0.653	0.686	0.181	0.622	0.699	0.173	0.778

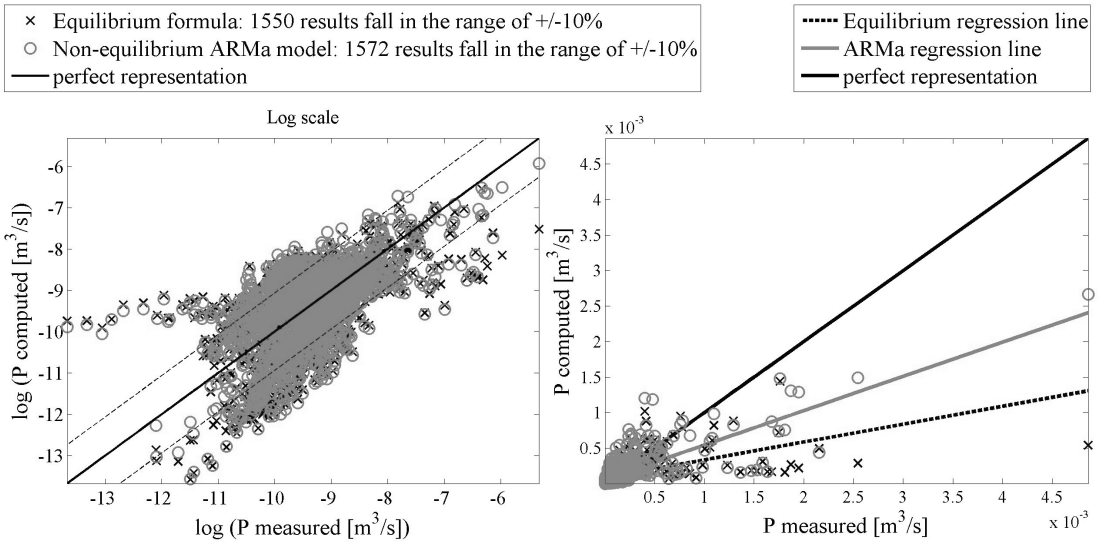

Figure 3.24: Suspended solid transport measured vs calculated (with equilibrium formula (crosses) and with the complete ARMA model (circles) using the rainfall data (3.7)) for station **(A2a) Serraglio** in the log-scale (a) and in the absolute scale (b). In the log-scale graph (a) the dotted lines identify a range of $+/-10\%$ with respect to the perfect representation.

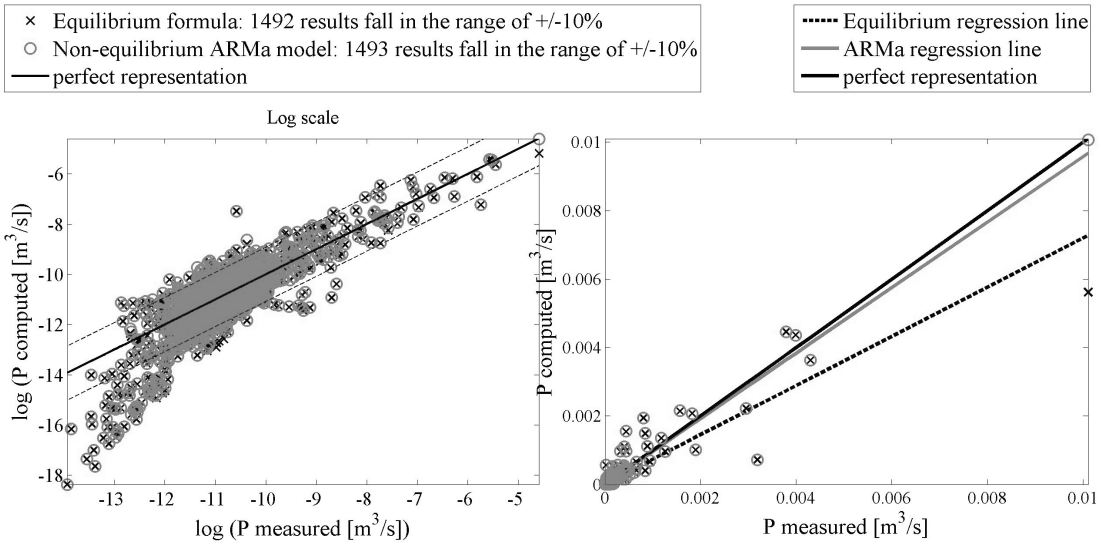

Figure 3.25: Suspended solid transport measured vs calculated (with equilibrium formula (crosses) and with the complete ARMA model (circles) using the rainfall data (3.7)) for the total period of **(C2) Marzenego** in the log-scale (a) and in the absolute scale (b). In the log-scale graph (a) the dotted lines identify a range of $+/-10\%$ with respect to the perfect representation.

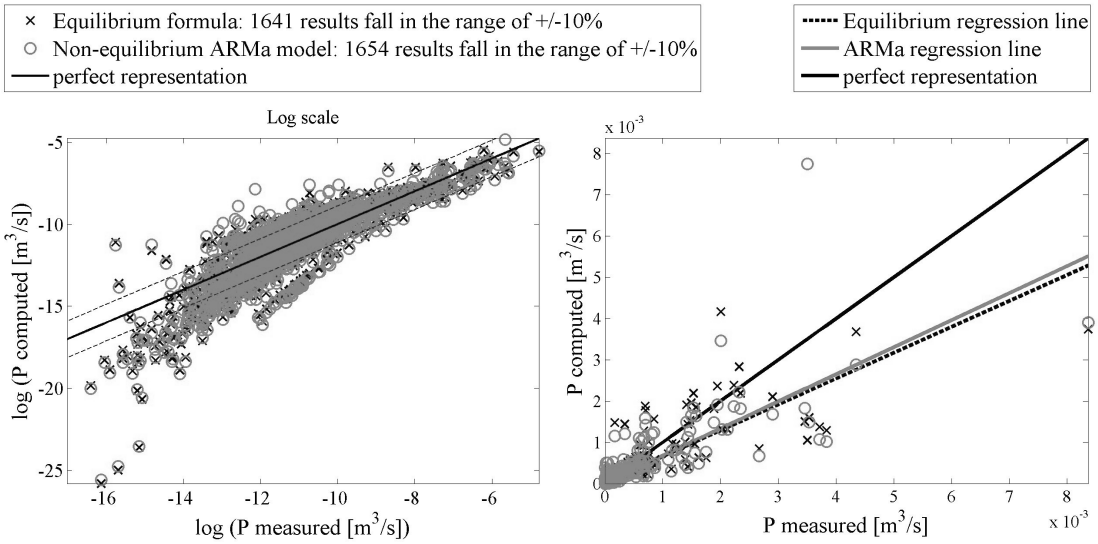

Figure 3.26: Suspended solid transport measured vs calculated (with equilibrium formula (crosses) and with the complete ARMA model (circles) using the rainfall data (3.7)) for the total period of **(A5) Taglio Mirano** in the log-scale (a) and in the absolute scale (b). In the log-scale graph (a) the dotted lines identify a range of $+/-10\%$ with respect to the perfect representation.

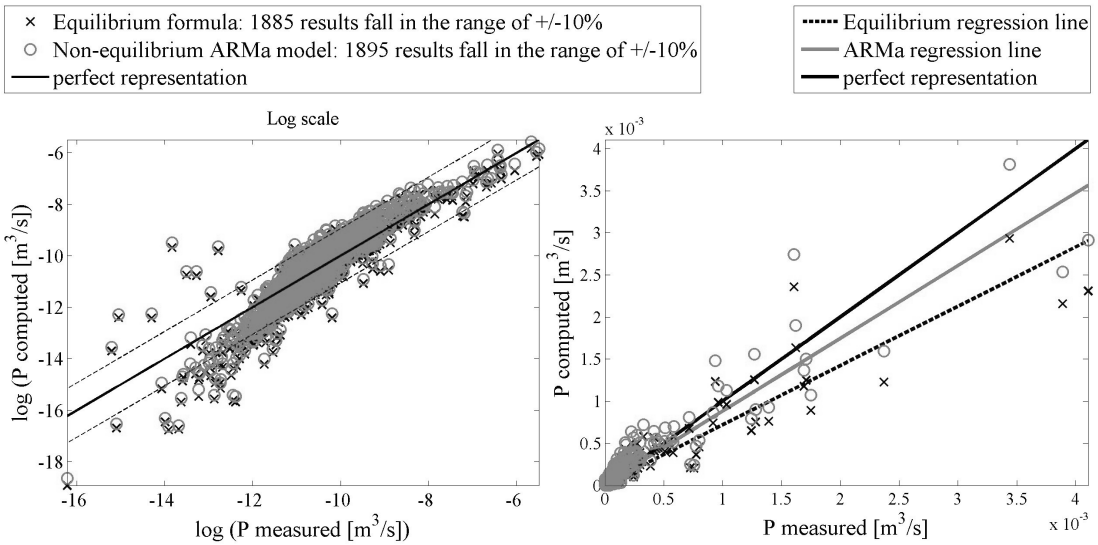

Figure 3.27: Suspended solid transport measured vs calculated (with equilibrium formula (crosses) and with the complete ARMA model (circles) using the rainfall data (3.7)) for the total period of **(G1) Vela** in the log-scale (a) and in the absolute scale (b). In the log-scale graph (a) the dotted lines identify a range of $+/-10\%$ with respect to the perfect representation.

The results found with the new formulation (3.7) seem less precise with respect to the corresponding values of the NSE, lower than the values evaluated for the original formulation (3.6). But the same results are characterized by values of RSR better (namely lower) for the new formulation.

Also in this case with the sensitivity analysis we found a generally periodic behaviour of the values of the delay k found as providing the best results.

On the contrary the model have not found a great importance for the cumulative delay p. Probably the dense network of irrigation ditch over the watershed surface is divided in area with different and various behaviour from a season to another and from a zone to another. For this reason is difficult to identify a characteristic value for the entire surface and the results are so variable.

This is not true for the rivers Serreglio (A2a) and Marzenego (C2), for which results deeply depend on the value of p. These two are rivers with a resourgive contribution.

On the other hand there are some rivers, like Fiumazzo (F1), which present a relevant dependence on the value of the parameter E_u. But this dependence seem to in its turn depend on the value of k. However, in general, the value of E_u is indifferent, except if equal to 0, for which no result has been found.

Finally the model is far to be a general method to evaluate the sediment input in the Lagoon from its watershed. For this goal now the unique valid method is to continue to use the gauging network. The model, instead, can be a valid procedure to complete series of data measured by gauge that do not work correctly for all the time but that gives records with many missed data. The model will complete these series in a better way than the typical substitution of the missing data with the average value.

Chapter 4

Long-term non-equilibrium model

In this chapter we investigate an intermediate temporal scale in order to improve the evaluation of the solid transport of a river in the present day.

4.1 Renouncing to the long-term equilibrium

We renounce to the hypothesis of the existence of a long-term equilibrium, and consider a slowly evolving river configuration at multiannual scale τ, above which a short-term perturbation at scale t propagate as in the previous Chapter 3 (see Figure 4.2). Namely we assume that, integrated at scale τ, the averaged small perturbations ($P'(x,t)$ in (3.2)) are null by definition, while the morphological parameter M (as well as its component I and d_{eq} in equation (2.16)) are changing till an equilibrium long-term configuration is eventually reached at $\tau \to \infty$. Note that the "perturbation" $P'(x,\tau)$ will reamain also when the long-term equilibrium configuration is reached; at $t \to \infty$, by contrast, the τ-averaged values of the parameters will be constant and the long-term solid input will be equal to the long-term output.
We will identify the τ averaged values with a *tilde* ($\tilde{}$).

In this Chapter we will maintain the LUF hypothesis with the sediment and water input concentrated at the upstream end of the channel.

At the short-time scale t we have:

$$P(t,\tau) = \tilde{P}(\tau) + P'(t) \tag{4.1}$$

where the short-term perturbations $P'(t)$ are computed by the same procedure described in the previous Chapter 3, while the τ-averaged transport $\tilde{P}(\tau)$ is given by the usual transport formula

$$\tilde{P}(\tau) = M(\tau)\widetilde{Q^m}(\tau) \tag{4.2}$$

Differently from the preceding Chapter, we have now a τ-scale evolving morphodynamic parameter $M(\tau)$.

The time-depending value of $M(\tau)$ depend in principle on the evolution of each morphological parameter (slope, width of the bed and its grain-size composition) entering the formulation of the Engelund-Hansen type (see equation (2.13)). The complete formulation of $M(\tau)$, assuming two representative grain-size classes, is the equation (2.17), recalled here below:

$$M(\tau) = \alpha_{EH}\frac{\tilde{I}(\tau)^n}{B^p(\tau)}\frac{\tilde{\beta}(\tau)((1/d)^{q-s}-1)+1}{d_c^q(\tilde{\beta}(\tau)(d-1)+1)^s} = \alpha_{EH}\frac{\tilde{I}(\tau)^n\ c_1(\tilde{\beta}(\tau))}{B^p(\tau)d_c^q} \tag{4.3}$$

where d_c is the diameter of the coarser class, β is the bottom composition of the finer class, B and I are the width and the mean slope of the channel respectively and c_1 is an implicit function of $\beta(\tau)$ (and $d = d_f/d_c$) as reported in the equation (2.18) and recalled here below:

$$c_1(\beta(t)) = \left(\frac{d_c}{d_{eq}(\beta(t))}\right)^q = \frac{\beta(t)((1/d)^{q-s}-1)+1}{(\beta(t)(d-1)+1)^s} \tag{4.4}$$

Some other studies have been done about the long-term morphological response of a river due to a change of boundary conditions; for example Tealdi et al. [2011] have found an analytical solution to study the morphological changes of a river after

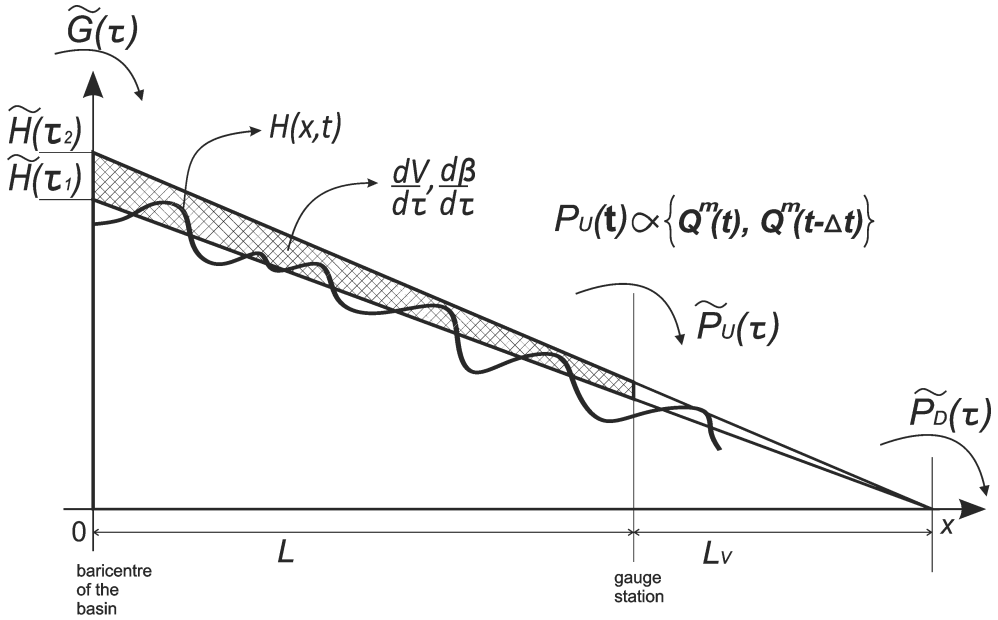

Figure 4.1: scheme of the LUF channel without a long-term equilibrium, but evolving in τ-scale.

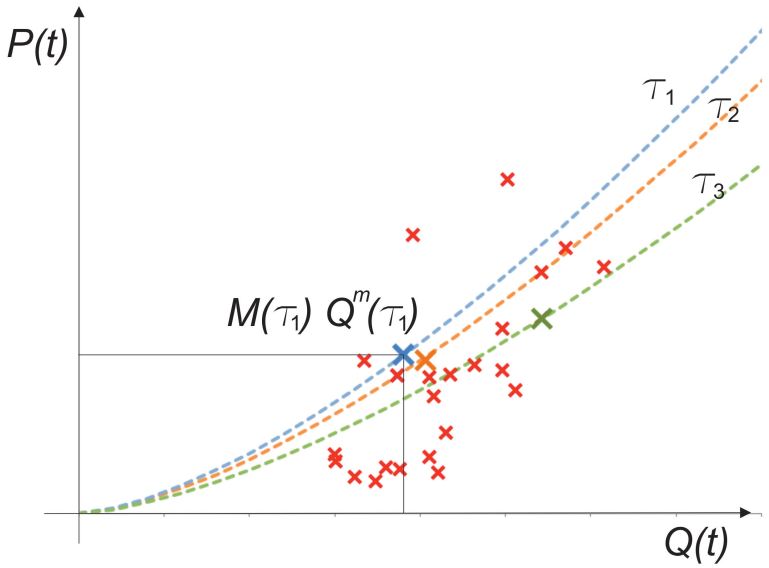

Figure 4.2: Example of the τ-scale rating curve on the graph $P(t)$ *vs* $Q(t)$ graph: the crosses are the t-scale data while the curve are derived by averaging in τ-scale.

stepwise perturbations on either the liquid or the solid input, but they consider a river with uniform grain-size and a variable width of the bed.

The variations on the mean river width assessed by Tealdi et al. [2011] are very small; in any case the relative importance of the width in the solid transport formula (see Table (2.1)) is less than the relative importance of the slope and of the bed composition. Moreover we want to preserve the LUF hypothesis with which we can integrate the equations to a zero-dimensional model. Thus we maintain a uniform and constant river width; this is compatible with the assumption of concentrated input and of relatively constant sediment and solid discharge.

The non-uniform grain-size sediment, by contrast, is crucial in the erosion and deposition processes at large spatial scales, as the grain-size distribution controls the downstream fining of the bed and the formation of its longitudinal profile, typically concave [Paola and Seal, 1995, Sinha and Parker, 1996].

Downstream fining and concave profile can be simulated by the 1-D model described in Chapter 2. Under the LUF hypothesis, moreover, we can take into account only the equations for the sediment continuity: namely the formal 1-D equation for the sediment continuity (Exner equation (4.5)) and the mass balance of each size fraction in the active layer (Hirano equation (4.6)):

$$B\frac{\partial(\tilde{H})}{\partial\tau} = -\sum_{k=1}^{2}\frac{\partial\widetilde{P_k}}{\partial x} \tag{4.5}$$

$$\delta B\frac{\partial(\widetilde{\beta_k}(x))}{\partial\tau} = -\frac{\partial\widetilde{P_k}}{\partial x} - \widetilde{\beta_k^*}(x)B\frac{\partial(\tilde{H})}{\partial\tau} \tag{4.6}$$

where B is the width of the river, P is the solid transport, H is the bed elevation above a reference and β_k is the percentage of the k-th fraction of the grain size composition.

To obtain an even simpler solution, concentrated on the closure section, the partial differential equations above will be preliminarily integrated to a zero-dimensional formulation.

4.2 Integration to a zero-dimensional model

We assume a zero-dimensional formulation as in Di Silvio and Nones [2013] (see Figure 4.1 or 5.2 in the section 5.2.1.1 in the next Chapter). Summarizing we assume LUF conditions, a constant (in time and space) width B and two characteristics grain size. Moreover we postulate a fixed point at the outlet of the river at mean sea level, so the horizontal length of the reach is constant. Thus we can integrate over x the equations (4.5) and (4.6) from $x = 0$, corresponding to the upstream end of our 0-D reach of the river, where the inputs of liquid and solid are concentrated, and $x = L$, the downstream end of the river:

$$\begin{cases} B\displaystyle\int_0^L \frac{\partial \tilde{H}}{\partial \tau} dx + \int_0^L \frac{\partial \tilde{P}}{\partial x} dx = 0 \\ \delta B \displaystyle\int_0^L \frac{\partial \tilde{\beta}(x)}{\partial \tau} dx + \int_0^L \frac{\partial \widetilde{P_k}}{\partial x} dx + B \int_0^L \tilde{\beta}(x) \frac{\partial \tilde{H}}{\partial \tau} dx = 0 \end{cases} \tag{4.7}$$

We identify the mean value over the length of the reach with the over line. Applying the divergence theorem we obtain:

$$\begin{cases} BL\dfrac{d\bar{\tilde{H}}}{d\tau} + (\tilde{P}(x = L, \tau) - \tilde{P}(x = 0, \tau)) = 0 \\ L\delta B\dfrac{d\bar{\tilde{\beta}}}{d\tau} + (\widetilde{P_k}(x = L, \tau) - \widetilde{P_k}(x = 0, \tau)) + BL\bar{\tilde{\beta}}\dfrac{d\bar{\tilde{H}}}{d\tau} = 0 \end{cases} \tag{4.8}$$

Practically we define our 0-D model as a LUF channel defined by a uniform slope equal to mean slope $\bar{\tilde{I}}(\tau)$ (see Figure 4.1), which is univocally related to the mean bed elevation $\bar{\tilde{H}}(\tau)$ ($\bar{\tilde{I}}(\tau) = \bar{\tilde{H}}(\tau)/\bar{L} = 2\bar{\tilde{H}}(\tau)/L$, having $\bar{L} = L/2$), where at the upstream end all the liquid and solid inputs from the watershed enter in the system while the values of the parameters at the downstream end are representative of all the entire reach. So we have that $\tilde{P}(x = 0, \tau) = \tilde{G}(\tau)$ and $\tilde{P}(x = L, \tau) = \tilde{P}(\tau)$. Let us note that in this case we have to know also the composition of the solid input $\widetilde{\alpha_G}(\tau)$ to define the term $\widetilde{P_k}(x = 0, \tau)$.

Recalling the (4.3) and the definition (2.15) of the composition of the solid transport

α, we get to the following complete system of ordinary differential equations:

$$\begin{cases} \dfrac{d\bar{\tilde{I}}}{d\tau} = \dfrac{2}{BL^2}(\tilde{G}(\tau) - \tilde{P}(\tau)) \\ \dfrac{d\bar{\tilde{\beta}}}{d\tau} = \dfrac{1}{\delta BL}[(\widetilde{\alpha_G}(\tau) - \bar{\tilde{\beta}}(\tau))\tilde{G}(\tau) - (\bar{\tilde{\alpha}}(\tau) - \bar{\tilde{\beta}}(\tau))\tilde{P}(\tau)] \\ \tilde{P}(\tau) = M(\tau)\widetilde{Q^m}(\tau) \\ M(\tau) = Cost\ \bar{\tilde{I}}(\tau)^n\ c_1(\bar{\tilde{\beta}}(\tau)) \end{cases} \tag{4.9}$$

Equations (4.9) describe the evolution of the long-term river profile and bottom composition represented by Figure 4.1. On the same figure are also indicated the short-term perturbations to be computed as shown in Chapter 3.

The boundary conditions of the system (4.9) are $\tilde{G}(\tau)$ and $\widetilde{\alpha_G}(\tau)$ at the upstream end and the elevation at the downstream end, as well as the input of the equivalent liquid discharge $\widetilde{Q^m}(\tau)$.

If the boundary conditions will remain constant, when $\tau \to \infty$ the system will reach an equilibrium condition fo which the solid flux (aligned with the liquid flow) is spatially constant; in this condition the sediment input and output of both grain-size classes become equal, namely: $\tilde{P}(\tau) = \tilde{G}(\tau)$ and $\tilde{\alpha}(\tau) = \widetilde{\alpha_G}(\tau)$.

As system (4.9) is implicit and non-linear, it is not possible to have an analytical solution and so we need a numerical evaluation. Later on some hypothesis will be introduced in order to analytically study this system and trying to apply it to the Adige river data in pluri-annual time-scale.

4.3 Toward an approximate analytical solution

In order to streamline the equations, from here on we will omit the bar to represent the mean 0-D value of the parameters.

The difference between the composition of the suspended transport of the input $\widetilde{\alpha_G}$ and the composition of the transport $\tilde{\alpha}$ will be ignored and we will consider a unique

value of $\tilde{\alpha}(\tau)$:

$$\tilde{\alpha}(\tau) \equiv \widetilde{\alpha_G} \tag{4.10}$$

In this way we can simplify the equations (4.9). We derive over the time τ the fourth equation of the system(4.9) and find a formulation of the evolution of the reach slope $\tilde{I}(\tau)$, the bottom composition $\tilde{\beta}(\tau)$ and the overall morphodynamic parameter $M(\tau)$:

$$\begin{cases} \dfrac{d\tilde{I}}{d\tau} = \dfrac{2}{BL^2}(\tilde{G}(\tau) - \tilde{P}(\tau)) \\ \dfrac{d\tilde{\beta}}{d\tau} = \dfrac{(\tilde{\alpha}(\tau) - \tilde{\beta}(\tau))}{L\delta B}\ (\tilde{G}(\tau) - \tilde{P}(\tau)) \\ \tilde{P}(\tau) = M(\tau)\widetilde{Q^m}(\tau) \\ \dfrac{dM}{d\tau} = M(\tau)\left[\dfrac{n}{\tilde{I}(\tau)}\dfrac{d\tilde{I}}{d\tau} + \dfrac{1}{c_1(\tilde{\beta}(\tau))}\dfrac{dc_1(\tilde{\beta}(\tau))}{d\tilde{\beta}}\dfrac{d\tilde{\beta}}{d\tau}\right] \end{cases} \tag{4.11}$$

In equations (4.11) we may recognize two characteristic volumes: $\widetilde{V_0}(\tau) = \tilde{I}(\tau)BL^2/2$, namely the triangular "filling" volume of the reach; while $V_m = L\delta B$ is the "filling" volume of the mixing layer of the reach.

We substitute the first two equations in the fourth; having simplified the second equation assuming the equivalence (4.10), we can collect the term $(\tilde{G}(\tau) - \tilde{P}(\tau))$ and obtain:

$$\frac{dM}{d\tau} = \frac{M(\tau)}{A(\tau)}(\tilde{G}(\tau) - \tilde{P}(\tau)) \tag{4.12}$$

where $A(\tau)$ is a characteristic volume which drives the morphodynamic evolution of the river:

$$\frac{1}{A(\tau)} = \frac{n}{\widetilde{V_0}(\tau)} + \frac{1}{c_1(\tilde{\beta}(\tau))}\frac{dc_1(\tilde{\beta}(\tau))}{d\tilde{\beta}}\frac{(\tilde{\alpha}(\tau) - \tilde{\beta}(\tau))}{V_m} \tag{4.13}$$

4.4 Analyzing the characteristic volume $A(\tau)$

Recalling the expression of the term $c_1(\tilde{\beta}(\tau))$ reported in the equation (4.4)) and the equation (2.15)) with which the transport composition $\tilde{\alpha}(\tau)$ is written in terms of bed composition $\tilde{\beta}(\tau)$, we can get to:

$$\begin{cases} \dfrac{1}{c_1(\tilde{\beta}(\tau))}\dfrac{dc_1(\tilde{\beta}(\tau))}{d\tilde{\beta}} = \dfrac{((\frac{1}{d})^{q-s}-1)}{\tilde{\beta}(\tau)((\frac{1}{d})^{q-s}-1)+1} - \dfrac{s(d-1)}{\tilde{\beta}(\tau)(d-1)+1} \\ \tilde{\alpha}(\tau) - \tilde{\beta}(\tau) = \dfrac{\tilde{\beta}(\tau)(1-\tilde{\beta}(\tau))((\frac{1}{d})^{q-s}-1)}{\tilde{\beta}(\tau)((\frac{1}{d})^{q-s}-1)+1} \end{cases} \tag{4.14}$$

Thus we obtain the complete formulation of $A(\tau)$:

$$\begin{cases} \dfrac{1}{A(\tau)} = \dfrac{n}{\tilde{V}_0(\tau)} + \\ \quad + \dfrac{1}{V_m}\left[\dfrac{((\frac{1}{d})^{q-s}-1)}{\tilde{\beta}(\tau)((\frac{1}{d})^{q-s}-1)+1} - \dfrac{s(d-1)}{\tilde{\beta}(\tau)(d-1)+1}\right]\dfrac{\tilde{\beta}(\tau)(1-\tilde{\beta}(\tau))((\frac{1}{d})^{q-s}-1)}{\tilde{\beta}(\tau)((\frac{1}{d})^{q-s}-1)+1} = \\ \quad = \dfrac{1}{\tilde{V}_0(\tau)} f_1(i(\tau)) + \dfrac{1}{V_m} f_2(\tilde{\beta}(\tau), d) \end{cases} \tag{4.15}$$

The behaviour of the transport composition α, of the function $c_1(\beta)$ and of the different terms that appear in the previous equation (4.15) with respect to the bed composition β is shown in the graphs of appendix D. In a typical river with a non-null slope is always verified that $V_0 \gg V_m$ (as it is possible to verify from the synthetic Table 4.1 about the volumes of Adige river); for this reason it is possible to ignore the first addend in the denominator of the $A(\tau)$ formualation (4.15), and say that:

$$A(\tau) \approx \frac{V_m \; c_1(\tilde{\beta}(\tau))}{\frac{dc_1(\tilde{\beta}(\tau))}{d\tilde{\beta}}(\tilde{\alpha}(\tau) - \tilde{\beta}(\tau))} = \frac{V_m}{f_2(\tilde{\beta}(\tau), d)} \tag{4.16}$$

where $f_2(\tilde{\beta}(\tau), d)$ is a particular function of the river that evolves with $\tilde{\beta}(\tau)$. From

the graph in the figure D.5 of the Appendix D is possible to verify that the value of the function $f_2(\tilde{\beta}(\tau), d)$ does not remarkably change when $\tilde{\beta}(\tau)$ ranges between $0,4$ and 1 (i.e. $0,4 \lesssim \beta < 1$). Let us also remember the hypothesis that the composition of the input does not change during the analyzed period. Moreover we know from our daily experience (and confirmed by the results of the next Chapter 5) that the mean slope of the river changes slowly enough to be considered constant during the analyzed period. Thus we may approximately consider also the bed composition constant and conclude that the volume A is a characteristic parameter of the river in the period analyzed.

4.5 Logistic curve expressing the analytical evolution of $M(\tau)$

With a constant value of the characteristic volume A it is possible to analytically study the evolution of $M(\tau)$ during the analyzed period considering that the input of solid and liquid in the system are represented by the long-term τ-averaged values. In fact, if we substitute $\tilde{P}(\tau)$ with $M(\tau)\overline{Q^m}$, the relation (4.12) can be read as the logistic curve, solution of the Verhulst model [Gaeta, 2007]. In this model M is the growing "population", $\bar{G}/A$ is the proportional increase of the "population" M in one unit of time and $\bar{G}/\overline{Q^m}$ is the equilibrium value of the "population" toward to M tends asymptotically because the antagonistic effect (called "bottleneck"). We can assume that this value is the value of M at $(\tau \to \infty)$, called M_∞.

$$\frac{dM}{d\tau} = \frac{M(\tau)}{A}(\bar{G} - \tilde{P}(\tau)) = M(\tau)\frac{\bar{G}}{A}\left(1 - \frac{M(\tau)}{\bar{G}/\overline{Q^m}}\right)$$

$$\rightarrow \quad \frac{dM}{d\tau} = M(\tau)\frac{\bar{G}}{A}\left(1 - \frac{M(\tau)}{M_\infty}\right) \tag{4.17}$$

By integrating equation (4.17), we find:

$$M(\tau) = \frac{M_\infty}{1 + \left(\frac{M_\infty}{M(\tau_0)} - 1\right) e^{-\frac{\bar{G}}{A}(\tau - \tau_0)}} \tag{4.18}$$

This equation has a typical S shape (see figure 4.3), called logistic curve.

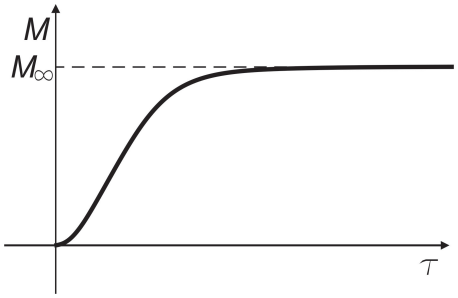

Figure 4.3: typical shape of the logistic curve.

The time τ_{p_1} required to reach the percentage p_1 of M_∞ starting from a $M(\tau_0)$ equal to a percentage p_0 of M_∞ is:

$$\tau_{p_1} = -\frac{A}{\bar{G}}\, ln\left(\frac{p_0(1-p_1)}{p_1(1-p_0)}\right) + \tau_{p_0}$$

Considering the Adige data that will be presented in the next section (see section 4.6) the time required to arrive to 90 % M_∞ starting from a 10 % M_∞ is only about 15 years.

We intuitively recognize that such a value of the "reaction time" is definitely too short for the Adige river. In the following paragraph 4.8 a discussion will be made. For this moment, however, we will maintain equation (4.18) to estimate a constant value of $\tilde{G}$, in order to have a sort of measure of the solid input from the basin. In fact, if we have the measurements of the liquid and solid discharge, we also have a measure of the morphodynamic parameter $M(\tau)$ from the equation (4.2) and so a measure of its evolutions. Thus, by equation (4.12) we get:

$$\bar{G}(\tau) = \frac{A}{M(\tau)}\frac{dM}{dt} + P(\tau) \tag{4.19}$$

which provides the amount of sediment entering the river at time τ.

4.6 Numerical application to Adige river

In this section we want to verify the model just exposed to the measurements of the Adige river (the available data are described in the section 3.7).

Assuming that τ is equal to one year, is possible to evaluate the annual average values of the solid and the m-power liquid discharges (equivalent discherges) and then calculate the $M(\tau)$. The graphs of these three quantity are shown in Figures 4.4, 4.5 and 4.6. The values of the volumes V_0 and V_m and the value of the characteristic volume A are shown in the Table 4.1.

Table 4.1: Characteristic volumes for the river Adige.

δ [\]	10% Y	5% Y
V_m $[m^3]$	7.63 x 10^5	1.35 x 10^6
V_0 $[m^3]$	1.31 x 10^9	3.31 x 10^9
A $[m^3]$	2.97 x 10^5	9.86 x 10^5

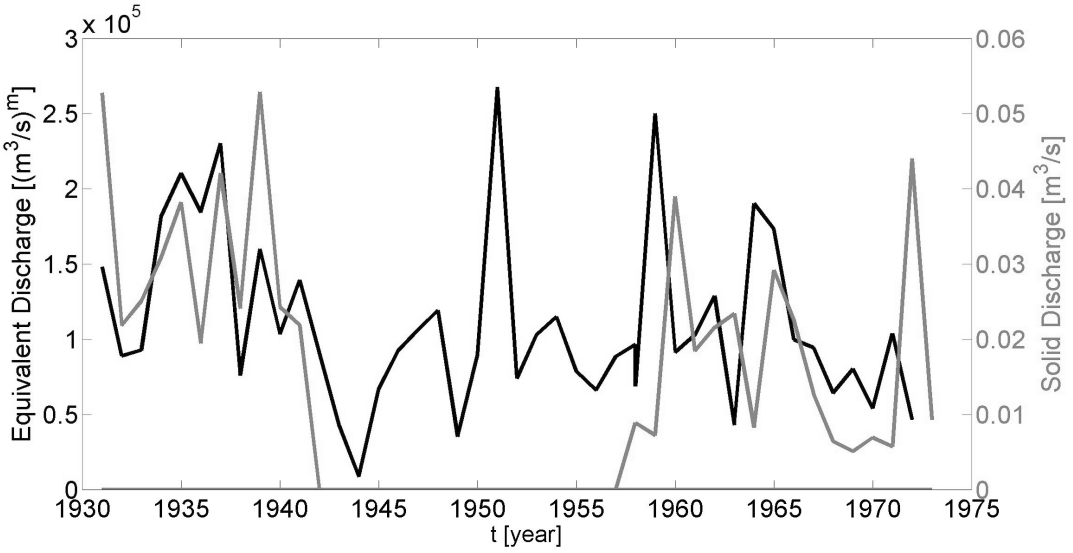

Figure 4.4: Comparison between the annual average solid discharge (in grey, with the axes on the right) and the equivalent discharge (in black, with the axes on the left) in Trento.

The resulting $M(\tau)$ for the Adige river in the two distinct gauge station is very different.

Thus we can calculate the hypothetical sediment input from the basin $\tilde{G}(\tau)$ with

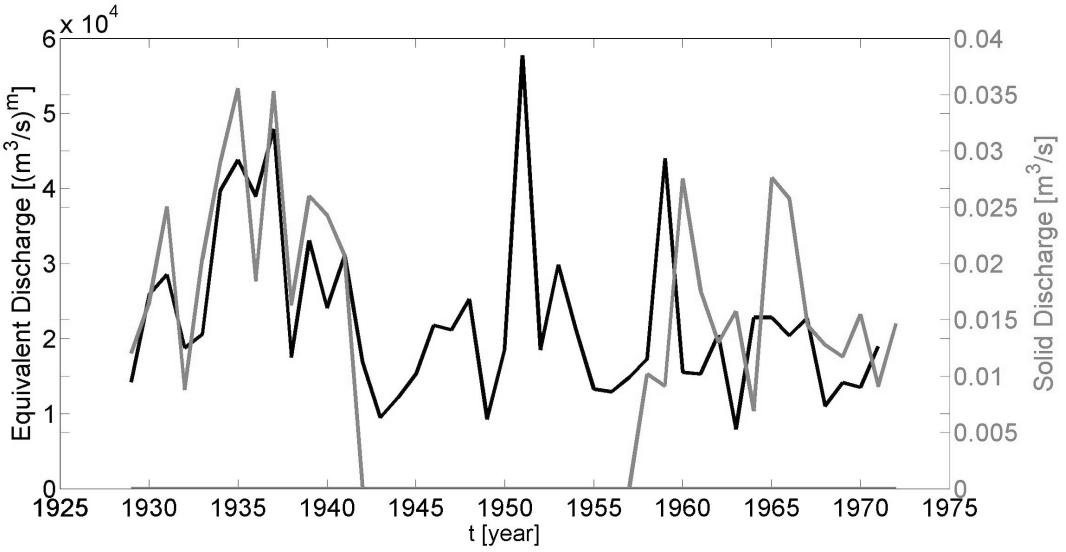

Figure 4.5: Comparison between the annual average solid discharge (in grey, with the axes on the right) and the equivalent discharge (in black, with the axes on the left) in Boara Pisani.

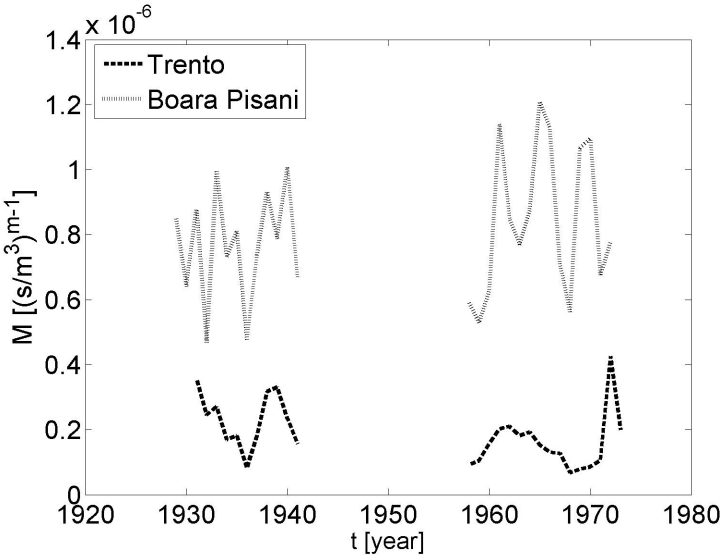

Figure 4.6: The annual morphodynamic parameter $M(\tau)$ evaluated for the river Adige.

the equation (4.19), evaluating the derivative term of $M(\tau)$ as a central difference:

$$\frac{dM}{dt} \approx \frac{M(\tau+1) - M(\tau-1)}{2\tau} \tag{4.20}$$

The results are shown in the Figures 4.7 and 4.8. It seems that the river closing in Trento is almost in equilibrium showing a great concordance between the input and the output of sediment, i.e. the term $\frac{A}{M(\tau)}\frac{dM}{dt}$ is very small. The river closing in Boara is still evolving, showing a greater differences between the input and the output of sediments.

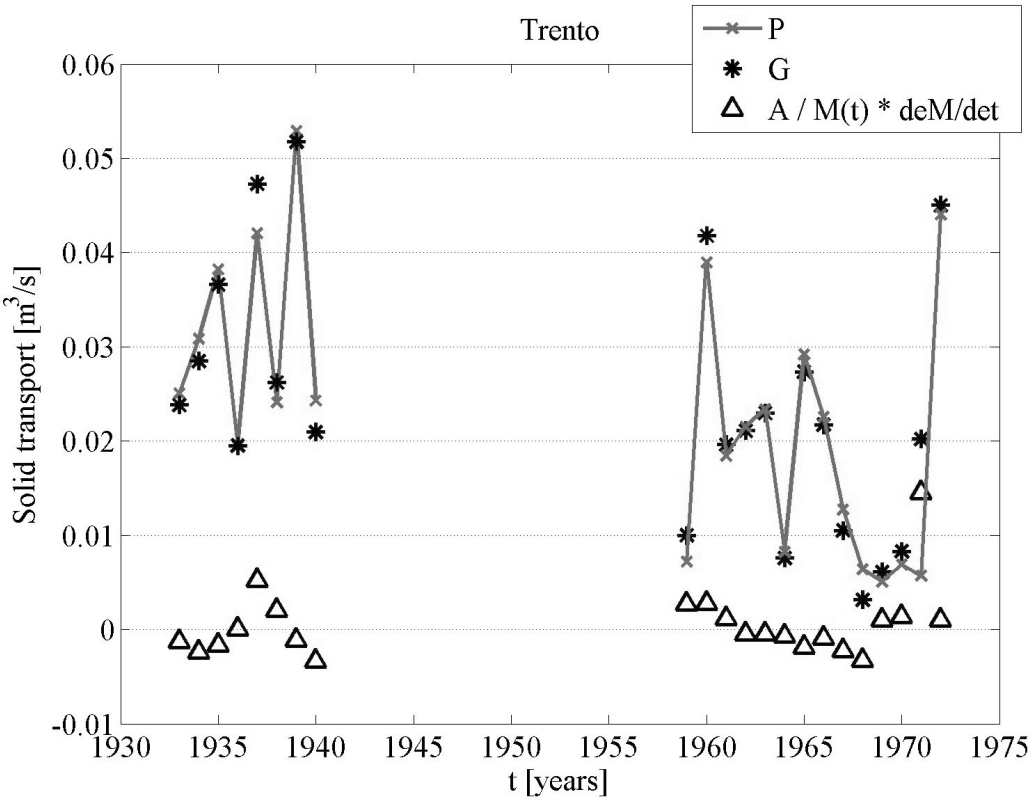

Figure 4.7: Comparison between the annual solid transport measured in Trento, the evaluated solid input calculated with the equation (4.19) and their difference.

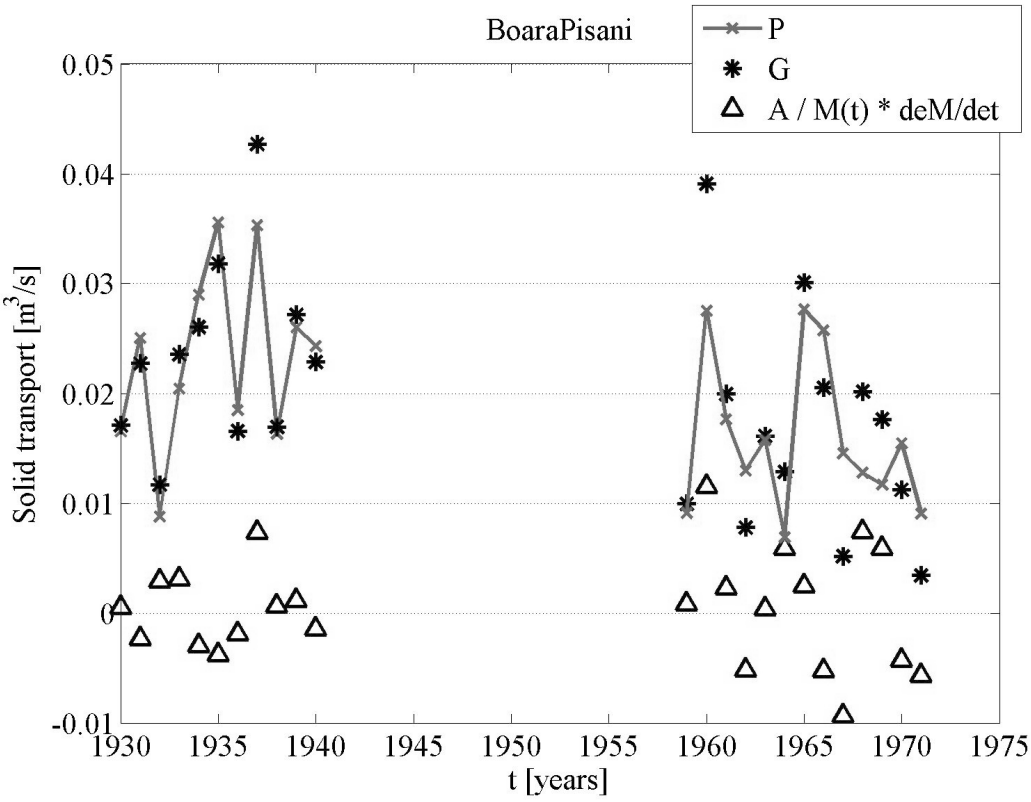

Figure 4.8: Comparison between the annual solid transport measured in Boara Pisani, the evaluated solid input calculated with the equation (4.19) and their difference.

4.6.1 Evaluation of the human intervention on the basin

Is important now to recognize that the basin is far to be natural: the human intervention is instead great, especially with regard to the second period of measuring (after 1958) for the Adige river. In fact during the '50 in Italy there was a great rate of construction of reservoirs, as well as a substantial intervention on the slope for the erosion control and mines of material directly from the bed of the rivers. Indeed, from the graph of the liquid and sediment discharge for the river Adige a reduction of the these values from the first period to the second is clear.

For the basin of the Adige river we have collected a series of data about the main reservoirs, the interventions for the erosion control and the mines, but its really difficult to know with precision all the anthropogenic interventions made on this great surface. Especially for the mine, which was regulated only after 1990.

In sake of simplicity the effects of the reservoirs and of the interventions for the erosion control are taken into account as a reduction of the sediment input proportional to the portion of the surface of the basin involved, thus we can evaluate the natural input as follows:

$$\tilde{G}(\tau) = \widetilde{G_{nat}}(\tau) + \Delta G_{antr}(\tau) = \widetilde{G_{nat}}(\tau)\left[1 - \gamma_r \frac{\Delta S_r}{S} - \gamma_e \frac{\Delta S_e}{S}\right] - \gamma_m \Delta G_m(\tau)$$

$$\rightarrow \widetilde{G_{nat}}(\tau) = \frac{\tilde{G}(\tau) + \gamma_m \Delta G_m(\tau)}{1 - \gamma_r \frac{\Delta S_r}{S} - \gamma_e \frac{\Delta S_e}{S}} \tag{4.21}$$

where G_{nat} is the natural input, ΔG_{antr} is the sediment input removed by the anthropogenic interventions, ΔS_r, ΔS_e and S are respectively the surface affected by the reservoirs, the surface affected by the erosion control intervention and the total surface of the basin, $\Delta G_m(\tau)$ is the quantity of sediment extracted from the bed of the rivers by mining operations and γ_r, γ_e and γ_m are the proportionality coefficients.

The data about the portion of surface of the basin interested by reservoirs and interventions on the soil erosion and about the mining from the bed of the river were col-

lected from various data-base from the web-site of the Veneto Region [Veneto, b,a], the independent Province of Trento [di Trento], from the independent Province of Bolzano [di Bolzano], from the web-site of the commercial companies managing the reservoirs (e Edison). The data collected are reported on the graph in the figure 4.9.

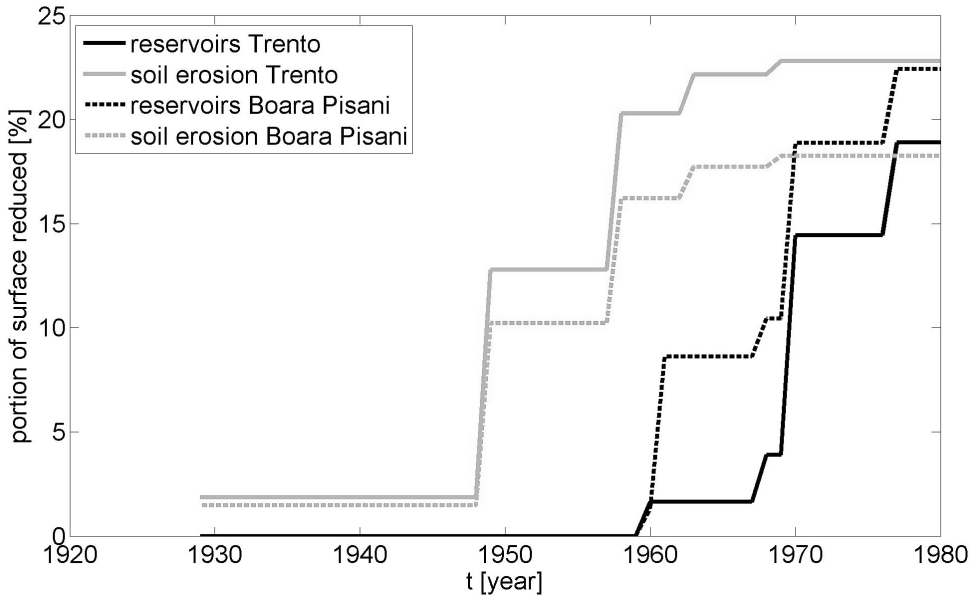

Figure 4.9: Portion of surface of the total basin year by year affected by the construction of new reservoirs or by interventions of soil erosion

Assuming that the information about the anthropogenic intervention we have are sufficiently complete, we consider that there is not a significant change on climatic condition, and that the average natural input can be considered constant. Thus, in order to calibrate this equation, we apply an ARMA procedure (see Appendix B). The results lead to no possible γ_e values (negative calibration values). It is probably due by the fact that the intervention of erosion control are underestimated and not taken into account in the correct manner. It is very difficult to classify all these type of intervention, and they are really very numerous. As we are using an empirical model we can think that their contribution is still included in the other two terms.
The results of the calibration is reported in the Table 4.2.

Table 4.2: Values of the parameter of the equation (4.21) calibrated for the river Adige.

γ_r	γ_m	γ_e
63.96 %	1.28 %	0.00 %

4.7 Numerical application to Po river

In this section we briefly show some results obtained with the measurements of the Po river (the available data are described in the section 3.8).

In the Table 4.3 the characteristic volumes described in the previous section 4.3 are reported. The Figures 4.10, 4.11 and 4.12 represent the solid and the equivalent discharge every year for each station, Piacenza, Boretto and Pontelagoscuro respectively. The Figure 4.13 represent the subsequent "measured" morphodynamic parameter from the evaluation $M(\tau) = \tilde{P}(\tau)/\overline{Q^m}$. Then the Figures 4.10, 4.11 and 4.12 represent the comparison between the measured annual solid transport, the evaluated solid input $\tilde{G}(\tau)$ calculated with the equation (4.19) and their difference $\frac{A}{M(\tau)}\frac{dM}{dt}$. In this case the value of the difference is greater.

Table 4.3: Characteristic volumes for the river Po.

	Piacenza	Boretto	Pontelagoscuro
δ [\]	5% Y	5% Y	5% Y
V_m $[m^3]$	5.7481 x 10^6	1.17 x 10^7	2.03 x 10^7
V_0 $[m^3]$	4.9027 x 10^9	1.09 x $10^1$0	1.98 x $10^1$0
A $[m^3]$	2.94 x 10^6	4.73 x 10^7	5.97 x 10^7

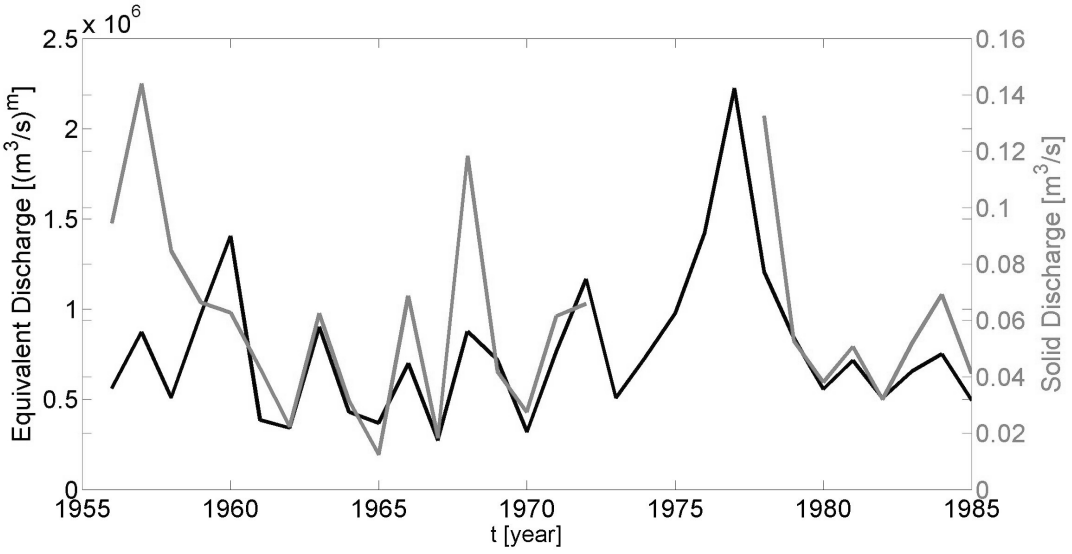

Figure 4.10: Comparison between the annual average solid discharge (in grey, with the axes on the right) and the equivalent discharge (in black, with the axes on the left) in Piacenza.

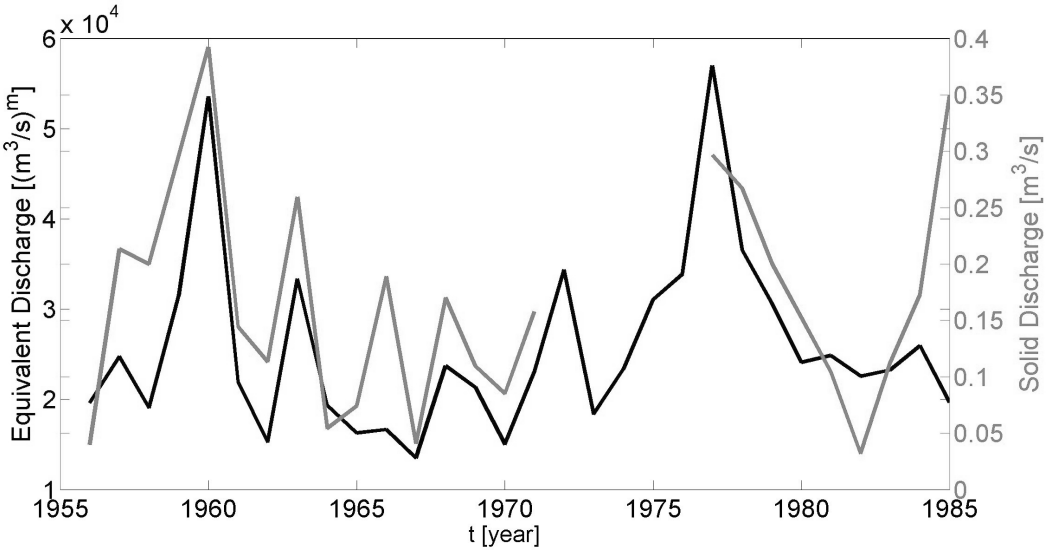

Figure 4.11: Comparison between the annual average solid discharge (in grey, with the axes on the right) and the equivalent discharge (in black, with the axes on the left) in Boretto.

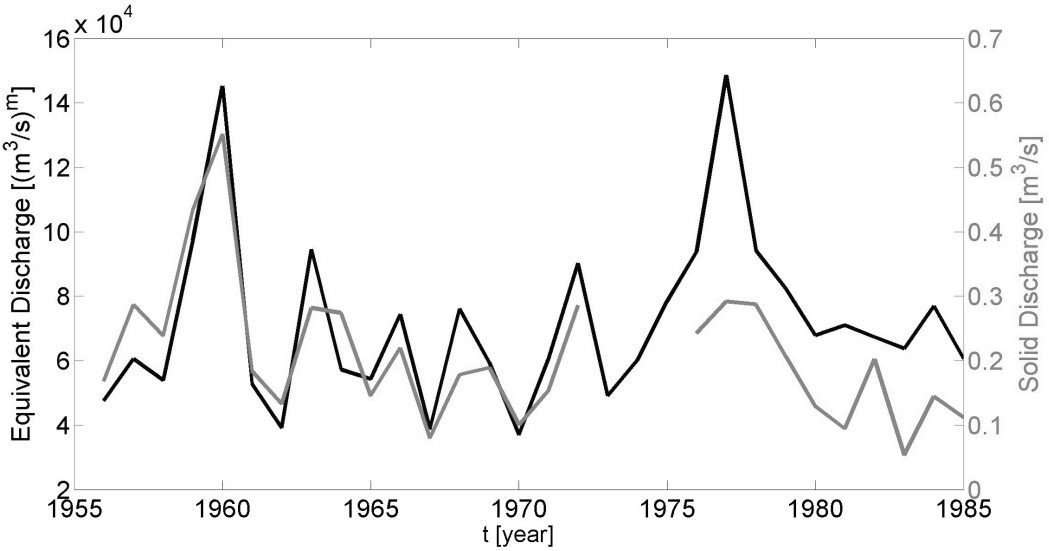

Figure 4.12: Comparison between the annual average solid discharge (in grey, with the axes on the right) and the equivalent discharge (in black, with the axes on the left) in Pontelagoscuro.

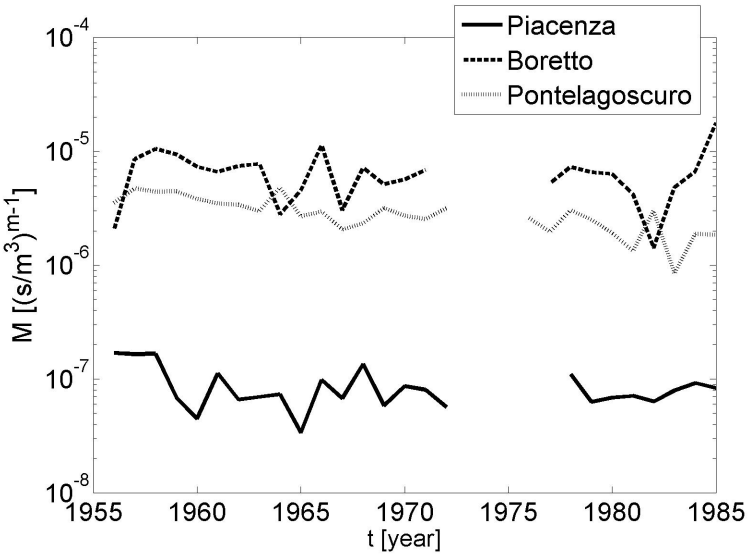

Figure 4.13: The annual morphodynamic parameter $M(\tau)$ evaluated for the river for the river Po.

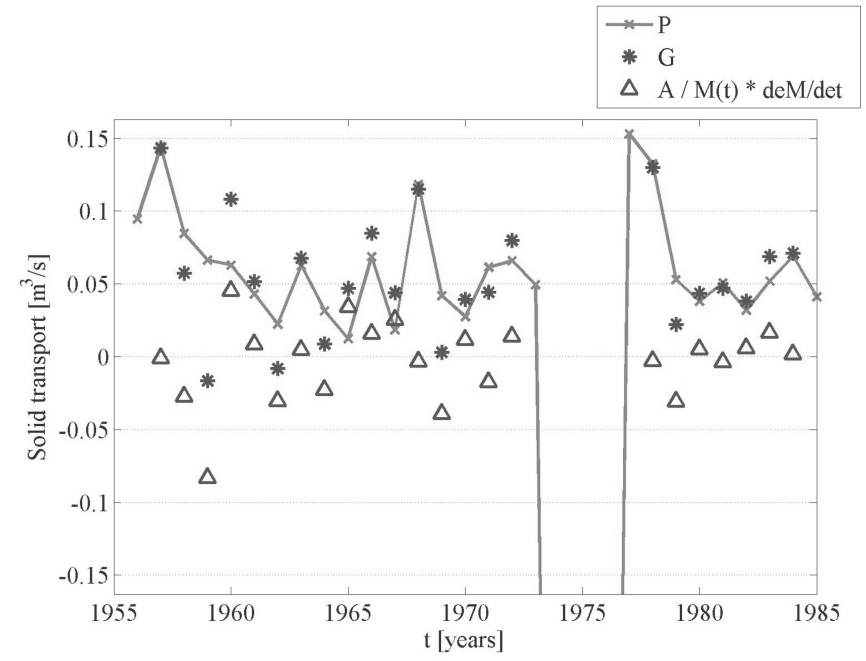

Figure 4.14: Comparison between the annual solid transport measured in Piacenza, the evaluated solid input calculated with the equation (4.19) and their difference.

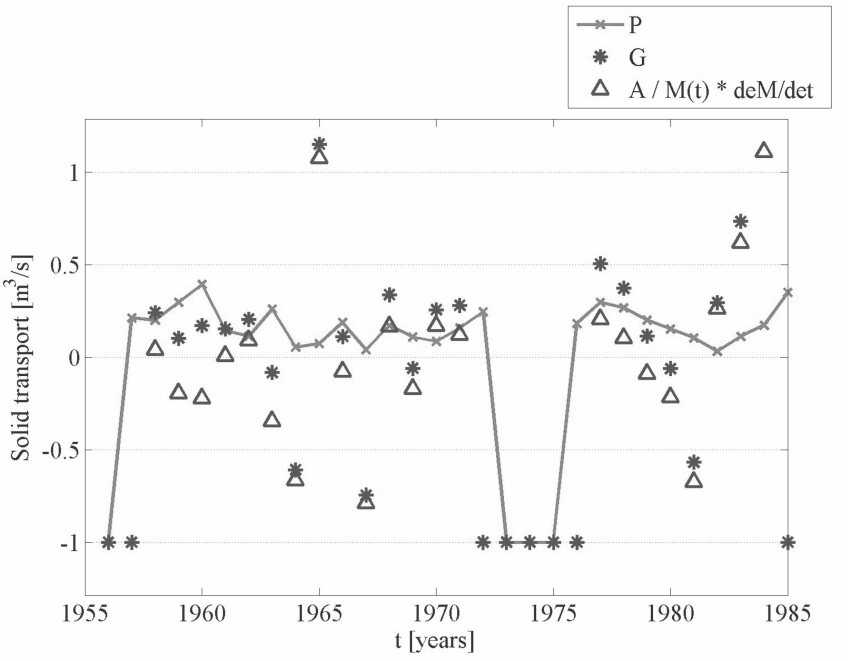

Figure 4.15: Comparison between the annual solid transport measured in Boretto, the evaluated solid input calculated with the equation (4.19) and their difference.

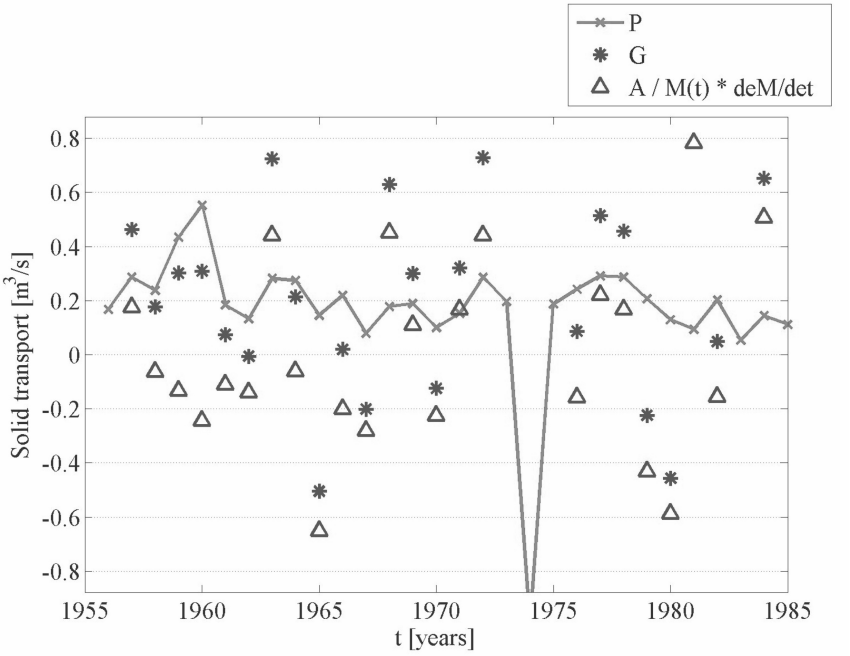

Figure 4.16: Comparison between the annual solid transport measured in Pontelagoscuro, the evaluated solid input calculated with the equation (4.19) and their difference.

4.8 Discussion on the numerical value of A

In the preceding applications to Adige and Po rivers (respectively paragraphs 4.6 and 4.7) we have observed that the *characteristic volume* A (provided by equation (4.16)) has invariably an extremely small value; consequently the sediment input G from the watershed slopes results to be -every year- practically equal to the sediment output P (sediment transport trough the closure section), as indicated by the equation (4.19). Indeed, although in principle the value of A depend on both the "filling volume" V_0 of the profile and the "filling volume" V_m of the mixing layer, it is practically coincident with V_m (being $V_m \ll V_0$). In other words the 0-D model described by equations (4.11) and Figure 4.1 seems to depend exclusively on the adaptation process of the grain-size composition (almost instantaneous) and not on the adaptation process of the river profile (very much slower). This outcome is valid only if we consider again (as in the long-term equilibrium model described in the Chapter 3) that the system is not so far from the equilibrium conditions, namely the slope is very similar to the equilibrium slope. In other words this analytic solution can not be used for a generic river. The reasons for this inefficiency is in principle due to different causes: 1) the linearization process applied to the equations (4.9); 2) the assumption in the second equation of the system (4.9) that $\alpha_G = \alpha$ and 3) the 0-D schematization of the watercourse, based on *one single reach*. The last assumption implies that the typical concavity of the profile (necessarily connected to the fining of the bottom grain-size) has totally disappeared when we moved from the complete 1-D model towards a 0-D approach. While neglecting the profile concavity may be possible in presence of a uniform grain-size, this is not acceptable anymore when we want to deal with two interactive different particle diameters.

For this reason in the next Chapter 5, the 0-D schematization has been reconsidered by renouncing the simplification 1) and 2) (and so numerically solving the complete system (4.9)) and also by assuming two different 0-D reaches in series (simplification 3)).

Chapter 5

Morphological reaction of rivers at geological scale

In this chapter we investigate the morphological reaction of a schematic river and its long-term evolution analyzed with a zero-dimensional model.
In order to streamline the equations, in this Chapter we will use the generic t to indicate in this case the time in a geological temporal scale and omit any over symbol to indicate temporal averaged values of the variables involved.

We have resumed here the complete mathematical formulation developed in the previous Chapter 4 (see equation (4.9))but, in order to keep trace of the concave profile of the river, the preliminary integration to a zero-dimensional model made in the section 4.2 has been made over two subsequent reaches connected in series.

We assume all the simplifications used till now by the other 0-D model. In particular we have LUF conditions and two representative grain-size classes. The sediment and water input are concentrated at the upstream end. As discussed in the previous chapter (see section 4.1) we will consider a uniform river width B but evolving slope I and bed composition β for each reach. Moreover we postulate for the downstream reach a fixed point at the outlet of the river at mean sea level: the longitudinal length of each reach are constant and equal, respectively, to the extension of the highland and the lowland part of the river basin.

Moreover we assume that there are not neither substantial variations in the climatic

conditions or substantial anthropogenic interventions. Thus we can consider that the typical flow duration curve of the river is constant, and take into account only the equations for the sediment continuity: the formal 1-D equation for the sediment continuity (Exner equation (4.5)), and the mass balance per each size fraction of the active layer (Hirano equation (4.6)).

Finally we evaluate the solid discharge per each size fraction passing through a section of a river with the usual rating curve as the (4.2).

If the boundary conditions will remain constant, for a $t \to \infty$ the system can reach an equilibrium condition when the solid flux, aligned with the liquid flow, is spatially constant, i.e. when the input and the output become equal. At this point the slopes and the gran-size compositions of the two reaches will be the same and stationary (equilibrium state).

In this Chapter we investigate the following questions: How and in how much time the river gets to this equilibrium state?

With all these assumption we get to a system (see equation (5.1) in section 5.1) which is implicit and non-linear and it is not possible to have an analytical solution of it: we need a numerical evaluation. Nevertheless, solving it is extremely simpler and faster than a 1-D model before investigated, for example by Tealdi et al. [2011].

5.1 Subdivision in two reaches

Without adding much complication to the 0-D model, we can divide the river in two different reaches. In typical middle-large rivers one can distinguish a mountain part, with higher slopes and coarser grain size, from an alluvial course, flatter and finer. If we divide the schematic river in two reaches we can verify if the model can simulate the typical concave profile of the natural rivers, at least before reaching the (eventual) equilibrium state mentioned above.

The zero-dimensional, two-reaches model is represented in the Figure 5.1, where the subscripts U and D are imposed to the parameters regarding respectively the upstream and the downstream reach.

The 1-D model is preliminarily integrated in a 0-D model as described in the section

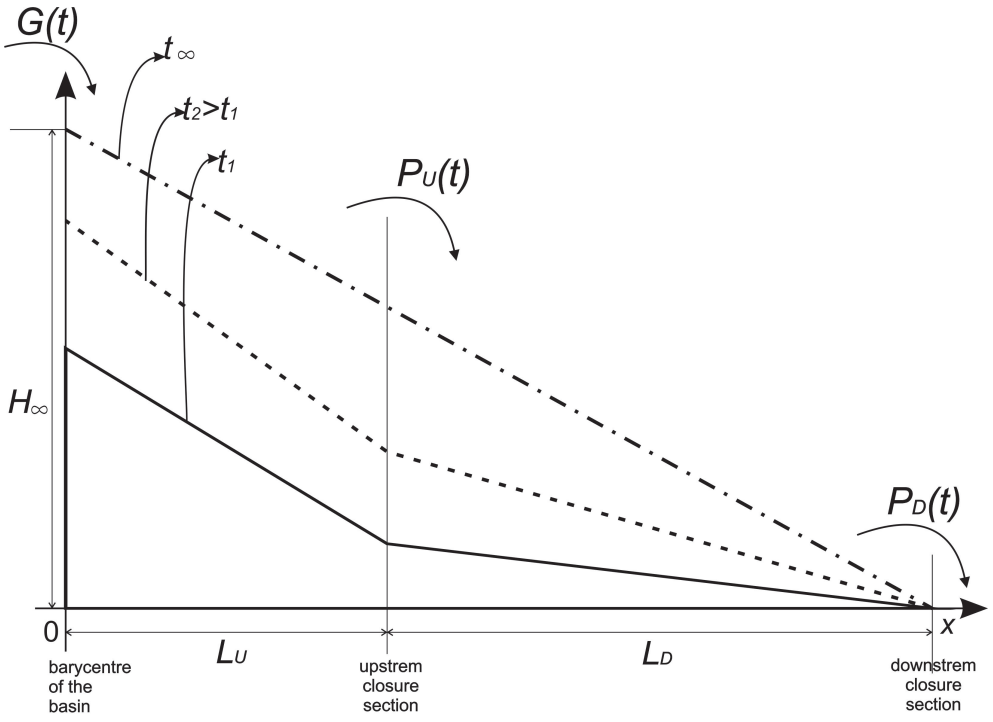

Figure 5.1: Scheme of the zero-dimensional, two-reaches model

4.2, but for both the reaches (the upstream reach from $x = 0$ to $x = L_U$, the downstram reach from $x = L_U$ to $x = L_U + L_D$).In this case we get to a system of eight equations (the overline indicate the space average of the parameter), similar to the four equations

of the system (4.9), but four for each reach:

$$\begin{cases} \dfrac{d\overline{I_U}}{dt} = \dfrac{2}{\bar{B}L_U^2}\left(G(t) - P_U(t)\right) - \dfrac{2L_U}{L_D}\left(P_U(t) - P_D(t)\right) \\ \dfrac{d\overline{\beta_U}}{dt} = \dfrac{1}{L_U\bar{\delta}\bar{B}}\left[\left(\alpha_G(t) - \overline{\beta_U}(t)\right)G(t) - \left(\overline{\alpha_U}(t) - \overline{\beta_U}(t)\right)P_U(t)\right] \\ P_U(t) = M_U(t)Q^m(t) \\ M_U(t) = Cost\ \overline{I_U}(t)^n\ c_1(\overline{\beta_U}(t)) \\ \dfrac{d\overline{I_D}}{dt} = \dfrac{2}{\bar{B}L_D^2}\left(G(t) - P(t)\right) \\ \dfrac{d\overline{\beta_D}}{dt} = \dfrac{1}{L_D\bar{\delta}\bar{B}}\left[\left(\overline{\alpha_U}(t) - \overline{\beta_D}(t)\right)_U P(t) - \left(\overline{\alpha_D}(t) - \overline{\beta_D}(t)\right)P_D(t)\right] \\ P_D(t) = M_D(t)Q^m(t) \\ M_D(t) = Cost\ \overline{I_D}(t)^n\ c_1(\overline{\beta_D}(t)) \end{cases} \tag{5.1}$$

We recognize that the term $\bar{B}L_U^2/2$ is the triangular "filling" volume of the upstream reach $V_{0,U}$ (from the elevation of the barycenter in $x = 0$ to the elevation in $x = L_U$) divided by the slope $\overline{I_U}(t)$. Similarly $\bar{B}L_D^2/2$ is the triangular "filling" volume of the downstream reach $V_{0,D}$ divided by the slope $\overline{I_D}(t)$. In the same way one can recognize that the terms $L_U\bar{\delta}\bar{B} = V_{m,U}$ and $L_D\bar{\delta}\bar{B} = V_{m,D}$ are the "filling" volumes of the mixing layer of the upstream reach and of the downstream reach respectively.

If we derive over time the fourth and the eighth expression of the system (5.1) we express the evolution of the morphodynamic of the river directly through the evolution of the morphodynamic parameter M:

$$\frac{dM}{dt} = M(t)\left[\frac{n}{\bar{I}(t)}\frac{d\bar{I}}{dt} + \frac{1}{c_1(\bar{\beta}(t))}\frac{dc_1(\bar{\beta}(t))}{d\bar{\beta}}\frac{d\bar{\beta}}{dt}\right] \tag{5.2}$$

The previous equation is valid for both the upstream reach and the downstream reach respectively. Let us call $c_3(\bar{\beta}(t)) = \frac{1}{c_1(\bar{\beta}(t))}\frac{dc_1(\bar{\beta}(t))}{d\bar{\beta}}$, namely the first equation of the system (4.14), where c_1 is expressed by the equation (4.4).

5.1.1 A non-dimensional formulation of the 0-D model

Let us introduce the dimensionless parameters reported in the Table 5.1 and defined as the relative deviation from the equilibrium ($t \to \infty$) value. The slopes I and the grain-size compositions α and β are in and of itself dimensionless parameters, nevertheless we study the evolution of their relative deviations from the equilibrium value.

If we consider the Figure 5.1, we may write:

$$\begin{cases} i_U(t) = \dfrac{L_U + L_D}{L} h_U(t) - \dfrac{L_D}{L_U} h_D(t) \\ i_D(t) = h_D(t) \end{cases} \tag{5.3}$$

Table 5.1: List of the dimensional and dimensionless parameter

Dimensional parameter	Dimensionless parameter
$\overline{H_U}$, $\overline{H_D}$	h_U, h_D
L_U, L_D	l_U, l_D
$\overline{I_U}$, $\overline{I_D}$	i_U, i_D
P_U, P_D	p_U, p_D
G	g
Q^m	q^m
M_U, M_D	$m_{orph,U}$, $m_{orph,D}$
$\overline{\beta_U}$, $\overline{\beta_D}$	b_U, b_D
α_G, $\overline{\alpha_U}$, $\overline{\alpha_D}$	a_G, a_U, a_D

Moreover we know that the equilibrium values of the three sediment discharges $G(t \to \infty)$, $P_U(t \to \infty)$ and $P_D(t \to \infty)$ coincide, as well as their grain-size composition, namely $\alpha_G(t \to \infty) = \overline{\alpha_U}(t \to \infty) = \overline{\alpha_D}(t \to \infty)$. If we call these values G_∞ and α_∞ ,

the system (5.1), written in non-dimensional terms, becomes:

$$\begin{cases} \dfrac{di_U}{dt} = \dfrac{G_\infty}{V_{0,U}} \left[(g(t) - p_U(t)) - \dfrac{2L_U}{L_D} (p_U(t) - p_D(t)) \right] \\ \dfrac{db_U}{dt} = \dfrac{G_\infty}{\beta_\infty V_{m,U}} \left[(\alpha_G(t) - \beta_U(t)) (g(t) + 1) - \right. \\ \qquad \left. - (\alpha_U(t) - \beta_U(t)) (p_U(t) + 1) \right] \\ (p_U(t) + 1) = (m_{orph,U}(t) + 1) (q^m(t) + 1) \\ (m_{orph,U}(t) + 1) = (i_U(t) + 1)^n \ \dfrac{c_1(b_U(t))}{c_1(\beta_\infty)} \\ \dfrac{di_D}{dt} = \dfrac{G_\infty}{V_{0,D}} (p_U(t) - p_D(t)) \\ \dfrac{db_D}{dt} = \dfrac{G_\infty}{\beta_\infty V_{m,D}} \left[(\alpha_U(t) - \beta_D(t)) (p_U(t) + 1) - \right. \\ \qquad \left. - (\alpha_D(t) - \beta_D(t)) (p_D(t) + 1) \right] \\ (p_D(t) + 1) = (m_{orph,D}(t) + 1) (q^m(t) + 1) \\ (m_{orph,D}(t) + 1) = (i_D(t) + 1)^n \ \dfrac{c_1(b_D(t))}{c_1(\beta_\infty)} \end{cases} \tag{5.4}$$

In the dimensionless version of the equations all the characteristic "filling" volumes identified in the previous section are divided for the equilibrium value of the sediment input G_∞. Thus one can recognize four characteristic time of the evolution of the slopes and of the bed composition:

- $\frac{V_{0,U}}{G_\infty} = T_{0,U}$: the "filling" time of the triangular volume of the upstream reach;
- $\frac{V_{0,D}}{G_\infty} = T_{0,D}$: the "filling" time of the triangular volume of the downstream reach;
- $\frac{\beta_\infty V_{m,U}}{G_\infty} = T_{mob,U}$: the "filling" time which refer to the volume of the mixing layer of the upstream reach;
- $\frac{\beta_\infty V_{m,D}}{G_\infty} = T_{mob,D}$: the "filling" time which refer to the volume of the mixing layer of the downstream reach;

As well as the triangular volume of the entire slope is very much greater then the volume of the mixing layer, the evolution of the bed composition is faster than the

evolution of the slope of the reach.

For sake of simplicity we assume that the equivalent water discharge Q^m is constant, meaning that there are not significant climatic changes or anthropogenic intervention and that the dimensionless parameter $q^m(t)$ (in the considered temporal scale) is null. In this way it is easy to find out that $m_{orph,U}(t) = p_U(t)$ and $m_{orph,D}(t) = p_D(t)$, namely the non-dimensional perturbation of the morphodynamic parameter is equal to the non-dimensional perturbations of the transport. Thus is possible to substitute those terms in the system (5.4), omit the third and the seventh equations which are simple equivalences, and derive over time the fourth and the eighth expressions also for the non-dimensional version of the model in order to express the evolution of the morphodynamic of the river directly through the evolution of the perturbation of the morphodynamic parameter m_{orph} (remember that $c_3(b(t)) = \frac{1}{c_1(b(t))}\frac{dc_1(b(t))}{db}$):

$$\begin{cases} \dfrac{di_U}{dt} = \dfrac{1}{T_{0,U}}\left[g(t) - m_{orph,U}(t) - \dfrac{2L_U}{L_D}\left(m_{orph,U}(t) - m_{orph,D}(t)\right)\right] \\ \dfrac{db_U}{dt} = \dfrac{1}{T_{mob,U}}\left[\left(\alpha_G(t) - \beta_U(t)\right)\left(g(t)+1\right) - \right. \\ \qquad \left. - \left(\alpha_U(t) - \beta_U(t)\right)\left(m_{orph,U}(t)+1\right)\right] \\ \dfrac{dm_{orph,U}}{dt} = \left(m_{orph,U}(t)+1\right)\left[\dfrac{n}{i_U(t)+1}\dfrac{di_U}{dt} + c_3(b_U(t))\dfrac{db_U}{dt}\right] \\ \dfrac{di_D}{dt} = \dfrac{1}{T_{0,D}}\left(m_{orph,U}(t) - m_{orph,D}(t)\right) \\ \dfrac{db_D}{dt} = \dfrac{1}{T_{mob,D}}\left[\left(\alpha_U(t) - \beta_D(t)\right)\left(m_{orph,U}(t)+1\right) - \right. \\ \qquad \left. - \left(\alpha_D(t) - \beta_D(t)\right)\left(m_{orph,D}(t)+1\right)\right] \\ \dfrac{dm_{orph,D}}{dt} = \left(m_{orph,D}(t)+1\right)\left[\dfrac{n}{i_D(t)+1}\dfrac{di_D}{dt} + c_3(b_D(t))\dfrac{db_D}{dt}\right] \end{cases} \tag{5.5}$$

5.2 River reaction to perturbations of the boundary conditions

In this section some results of the reaction of the river schematized by the 0-D, two reaches model just described to different variations of the boundary conditions, starting from an equilibrium condition, are exposed.

In order to find an analytical solution, we may linearize the system (5.4) assuming that there are only little perturbations with respect to the equilibrium configuration ($t \to \infty$) and so approximating the non linear terms as follow:

$$\begin{cases} \dfrac{\overline{I_U}^n(t)}{I_\infty^n} = (1+i_U(t))^n \approx (1+n\ i_U(t)) = \\ \qquad\qquad\qquad\qquad \approx \left[1+n\left(\dfrac{L_U+L_D}{L_U}h_U(t) - \dfrac{L_D}{L_U}h_D(t)\right)\right] \\ \dfrac{\overline{I_D}^n(t)}{I_\infty^n} = (1+i_D(t))^n \approx (1+n\ i_D(t)) = (1+n\ h_D(t)) \\ c_1(b_U(t)) \approx c_1(\beta_\infty)\left(1+\beta_\infty \dfrac{1}{c_1(\beta_\infty)}\ \dfrac{dc_1(b_u(t))}{db_U}\Big|_{b_U(t)=\beta_\infty} b_U(t)\right) \\ c_1(b_D(t)) \approx c_1(\beta_\infty)\left(1+\beta_\infty \dfrac{1}{c_1(\beta_\infty)}\ \dfrac{dc_1(b_D(t))}{db_D}\Big|_{b_D(t)=\beta_\infty} b_D(t)\right) \end{cases} \tag{5.6}$$

Substituting the previous equations (5.6) in the definition of the perturbation of the morphodynamic parameter m_{orph} (namely the fourth and the eighth equations of the (5.4)), we find the following expression valid for both the upstream and the downstream reach:

$(m_{orph}(t)+1) = \ (1+ni(t))\ (1+\beta_\infty c_3(\beta_\infty)b(t))$

where $c_3(\beta_\infty) = \frac{1}{c_1(\beta_\infty)}\ \frac{dc_1(b(t))}{db}\Big|_{b(t)=\beta_\infty}$.

However, the non-linearity remain in the mixed product $(i(t)\cdot b(t))$. (Unluckily this term is not explicit, but is inside the complicated formulation of $i(t)\cdot c_3(b(t))$, and is not possible to reduce it writing $i(t)b(t) \approx i_\infty b_\infty + i'(t)b_\infty + i_\infty b(t))$.

So, it is not possible to find an analytical solution of the problem and we need numerical evaluation. In particular we use a predictor-corrector scheme using an explicit Eulero prediction of the values of the variables in the $(t+\Delta t)$, then cyclically corrected with a Cranck-Nicholson algorithm until convergence.

The variations of the boundary conditions investigated are of two types: stepwise and sinusoidal.

Stepwise perturbation From equilibrium conditions we impose a stepwise perturbation of a boundary condition (for example the sediment input $G(t)$) of the type:

$$g(t) = 0 \quad \text{per } t \leq 0$$
$$g(t) = g_0 \quad \text{per } t > 0$$

In this case, the dimensionless value g_0 correspond to a constant perturbation that lead the system to a new equilibrium condition controlled by the new sediment input $G_1 = G(t > 0)$:

$$g_0 = \frac{G_1 - G_0}{G_0}$$

Sinusoidal perturbation In this case we impose, for example, a sinusoidal sediment input:

$$g(t) = 0 \quad \text{per } t \leq 0$$
$$g(t) = g_0 \, sin(\omega t) \quad \text{per } t > 0$$

where g_0 is the amplitude of the periodical input $g(t)$ and $\omega = 2\pi/T_w$ is the angular frequency linked to the forcing period T_w of the perturbation $g(t)$. In this case the quasi equilibrium conditions, reached after the transitory stage, will be periodical.

5.2.1 Particular cases of the model

Before numerically solving the system (5.5) we will analyze different particular cases beginning from the simpler one: one single reach and a constant grain size composition. Then we will sum these two complications one a time: firstly we will divide the river in two reaches with constant grain-size, then we consider a time-variability of the grain size composition and finally we expose the results of the complete model.

We generally impose that $m = n = 2$.

5.2.1.1 One reach, constant grain size model

With the scheme adopted by Di Silvio and Nones [2013], this approach schematizes the river as a unique reach with a uniform slope from the basin barycenter (where the inputs of sediment and water enter in the system) to the downstream end, which is supposed at a fixed elevation. Moreover this model assumes that the size of the bottom sediments is constant, so that the only time-dependent variable is the slope. In order to maintain the same terminology for the variables, we simply consider the model of the Figure 5.1 but with $\overline{I_U} = \overline{I_D}$ (or conveniently setting $L_D = 0$). The zero-dimensional, one-reaches model is represented in Figure 5.2

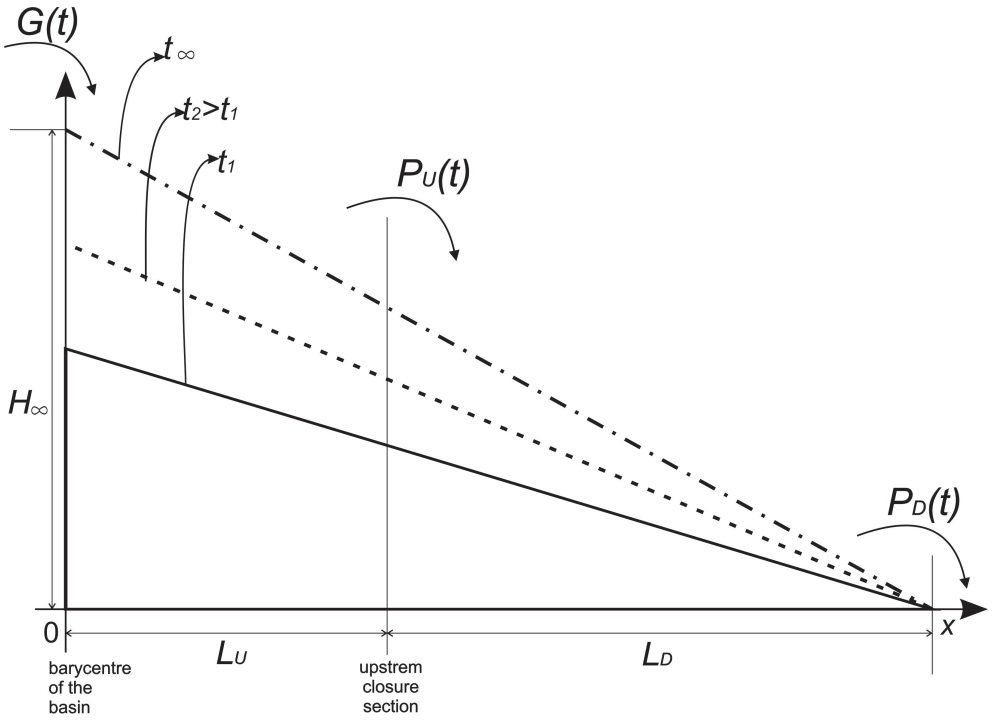

Figure 5.2: Scheme of the zero-dimensional, one-reach (namely one slope) model. The nomenclature of the Figure 5.1 is maintained, but formally here we have $P_U(t) = P_D(t)$

In this case we have that $P_U(t) = Cost_1\overline{I_U}(t)^n = Cost_1\overline{I_D}(t)^n = P_D(t)$. The non-dimensional terms $i_U(t)$ and $i_D(t)$ coincide, and coincide also with $h_U(t) = h_D(t)$. Having $m = n = 2$, if we linearize the problem through $(1 + i_U(t))^n = (1 + i_U(t))^2 \approx (1 + 2\ i_U(t)) = (1 + 2\ h_U(t))$, we have that $p_U(t) = 2h_U(t)$ and get to the following simple ordinary differential equation describing the morphological evolution of the

model:

$$\frac{dh_U}{dt} = \frac{1}{T_{0,U}} \left(g(t) - 2h_U(t) \right) \tag{5.7}$$

The characteristic filling time of this model is referred to the trapezoidal volume that has to be filled with respect to the position of the gauging station: $T_{0,U} = \frac{2G_0}{H_0 L_U B(2 - L_U/(L_U+L_D))}$.

Stepwise perturbation (see page 122) Imposing the initial condition that $h_U(t = 0) = 0$, the solution of the integration of the equation (5.7) is

$$h_U(t) = \frac{g_0}{2}(1 - e^{2t/T_{0,U}})$$

Having $h_U(t) = 2p_U(t)$, this means that

$$p_U(t) = g_0(1 - e^{2t/T_{0,U}})$$

so $p_U(t \to \infty) = g_0$ and the solid transport $P_U(t \to \infty)$ tends to the new value G_1.

In the Figure 5.3 there is the representation of an example of the evolution for a river with a perturbation g_0 equal to the 20 %. In the legend of the Figure some step of the evolution are specified with the indication of both the level of the evolution for the dimensionless morphodynamic parameter and for the slope.

Sinusoidal perturbation (see page 123) In this case the new equilibrium conditions reached after a transient interval will be periodical. We assume again the initial condition $h_U(t = 0) = 0$, then the solution of the integration of the linearized equation (5.7) is:

$$h_U(t) = \frac{g_0}{4+\omega^2 T_{0,U}^2}\left(T_{0,U}\omega e^{-2t/T_{0,U}} + 2sin(\omega t) - T_{0,U}\omega cos(\omega t)\right)$$

The transitory term is the exponential, which will tend to 0 for $t \to \infty$, and the dimensionless solid transport perturbation will be dumped with respect to g_0 as follows:

$$p_U(t \to \infty) = \frac{2}{4+\omega^2 T_{0,U}^2}\left(2g(t) - T_{0,U}\frac{dg}{dt}\right) = \frac{2g_0}{4+\omega^2 T_{0,U}^2}\left(2sin(\omega t) - T_{0,U}\omega cos(\omega t)\right)$$

5.2.1.2 Two-reaches, constant grain size model

Now, we want to extent the previous model dividing the channel in two different zero-dimensional reaches with different slopes $I_U(t) \neq I_D(t)$. The inputs of sediment and water are entering again in the system at the upstream end of the river and the downstream end is supposed at a fixed elevation; but now there is a discontinuity of the slope, where, however, the mass balance has to be verified (Figure 5.1).

The system is the (5.5) but with a constant bed composition ($\bar{\beta}(t) = \bar{\beta}_\infty$, $b(t) = 0$ and $c_1(\bar{\beta}(t)) = c_1(b(t)) = 1$), so we have $db_U/bt = db_D/dt = 0$ and the second and the fifth equations become two identities. Then we have that $m_{orph}(t) + 1 = (i(t) + 1)^n$. Substituting the first and the fourth equations respectively in the third and in the sixth, we can obtain the following non-linear and implicit system with the equations of the evolution of the morphodynamic parameters of the two reaches:

$$\begin{cases} \dfrac{dm_{orph,U}}{dt} = \dfrac{n}{T_{0,U}}(m_{orph,U}(t)+1)^{1-1/n}\cdot \\ \qquad\qquad \cdot\left[(g(t) - m_{orph,U}(t)) - \dfrac{2L_U}{L_D}\left(m_{orph,U}(t) - m_{orph,D}(t)\right)\right] \\ \dfrac{dm_{orph,D}}{dt} = \dfrac{n}{T_{0,D}}(m_{orph,D}(t)+1)^{1-1/n}\left(m_{orph,U}(t) - m_{orph,D}(t)\right) \end{cases} \tag{5.8}$$

In this case we have two distinct characteristic filling time: $T_{0,U}$ referred to the triangular upstream volume and $T_{0,D}$ referred to the triangular downstream volume.

With $m = n = 2$, we can linearize the system (5.8) assuming the first two simplifications of the system (5.6), namely:

$$\begin{cases} (i_U(t)+1)^n = (m_{orph,U}(t)+1) \approx (1+n\ i_U(t)) = \\ \qquad\qquad \approx \left[1+n\left(\dfrac{L_U+L_D}{L_U}h_U(t) - \dfrac{L_D}{L_U}h_D(t)\right)\right] \\ (i_D(t)+1)^n = (m_{orph,D}(t)+1) \approx (1+n\ i_D(t)) = (1+n\ h_D(t)) \end{cases}$$

and find that

$$\frac{dm_{orph}}{dt} \approx n\frac{di}{dt}$$

The resulting following system describes the evolution of the morphodynamic of the river with two reaches and a constant bed composition:

$$\begin{cases} \dfrac{dm_{orph,U}}{dt} = \dfrac{n}{T_{0,U}}\left[g(t) - m_{orph,U}(t) - \dfrac{2L_U}{L_D}(m_{orph,U}(t) - m_{orph,D}(t))\right] \\ \dfrac{dm_{orph,D}}{dt} = \dfrac{n}{T_{0V}}(m_{orph,U}(t) - m_{orph,D}(t)) \end{cases} \tag{5.9}$$

Stepwise perturbation (see page 122) Substituting g_0 to $g(t)$ in the linearized system (5.9) we had integrated the system with the software *Wolfram Mathematica* and found the explicit solutions for $m_{orph,U}(t)$ and $m_{orph,D}(t)$. These solutions are two exponential expressions which are very long and they will be not presented here. Both $m_{orph,U}(t \to \infty)$ and $m_{orph,D}(t \to \infty)$ tend to g_0 as we expected, but analyzing their behaviour we find some instability when the speed of the convergence relaxes.

This expressions are not invertible, so we can not explicit the evaluation of the time that the system takes to reach the new equilibrium conditions. From the graphs we can see three cases:

1. when $L \approx L_D$ for $t \approx 4T_{0,U}$ we have $m_{orph,U}(t) \approx 90\% g_0$ and $m_{orph,D}(t) \approx 80\% g_0$;

2. when $L >> L_D$ we find great instability very soon;

3. when $L << L_D$ we find a rapid convergence of the value $m_{orph,U}(t)$ to g_0 (since $t \approx 0,2\%\, T_{0,D}$) and the instability occurs for $t \approx 17\%\, T_{0,D}$, when $m_{orph,D}(t) \approx 2\%\, g_0$.

Then we solved numerically the systems, both the exact (5.8) and the linearized (5.9). The linearized model is much slower then the exact one as a confirm of the scarce reliability of the linearization. An example of the results of the exact solution obtained for a river with $L_U = 0.2\, L_D$ and $g_0 = 0.5$ are shown in the Figure 5.4. In this Figure the horizontal axes is limited to low values in order to highlight the shape of the function, that is similar to a classical logistic curve, with a certain delay of the evolution of the downstream reach that depend on the relative length of the reaches.

Sinusoidal perturbation (see page 123) In this case we study the problem (both exact solution (5.8) and linearized (5.9)) only numerically. If the period T_w of oscillation of the boundary conditions is enough lower than the time required to reach the new equilibrium configuration, the resulting curve of the evolution of the morphology are similar to those found with the stepwise perturbations, but the curve are now periodical around that solution. Otherwise the evolution can be more complicated. A larger discussion about this argument will be done later with the complete solution (see 5.2.2) .

Also in this case we find a faster convergence to the new state of equilibrium for the exact solution.

5.2.1.3 One reach, variable grain-size model

Now we consider again a reach with a unique slope but with a variable bottom composition $\beta(t)$. This model correspond to the system (4.9) found in the previous Chapter (see section 4.2).

Using the present notation and the dimensionless parameters, as for the section

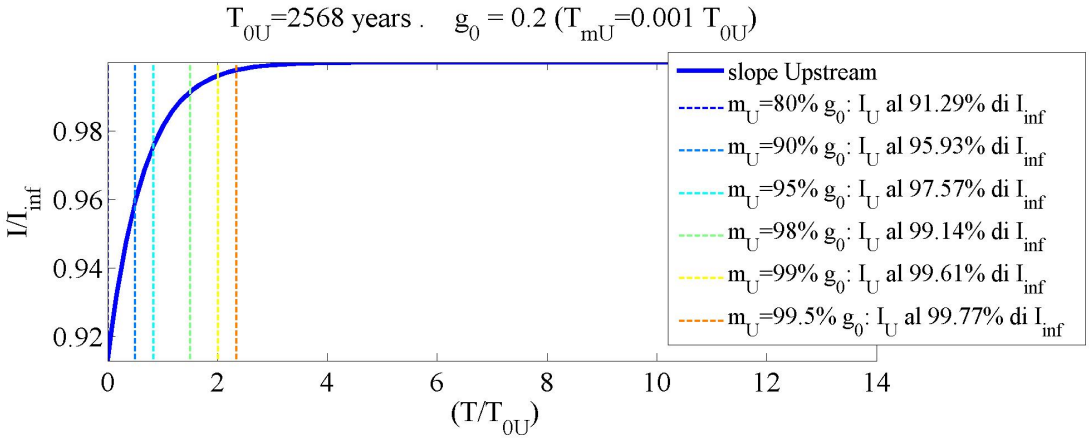

Figure 5.3: One reach, constant grain size model: example of the evolution of the slope of a river from an initial equilibrium state applying a stepwise perturbation g_0 equal to the 20 %. In the legend some step of the evolution of the morphodynamic parameter are compared with the correspondent step of the evolution of the slope.

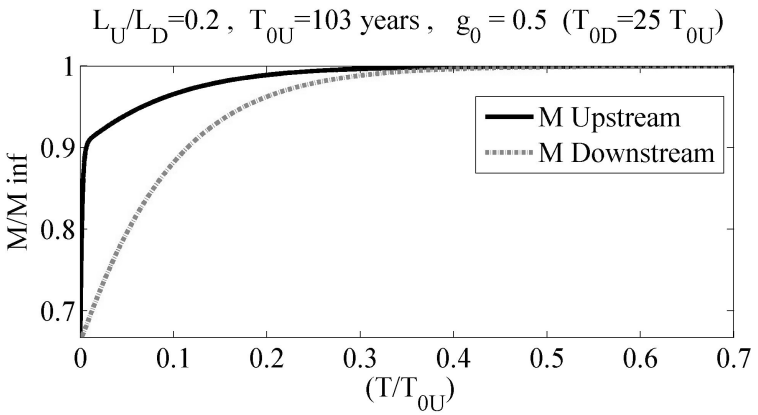

Figure 5.4: Two-reaches, constant grain size model: example of the evolution of a river from an initial equilibrium state applying a stepwise perturbation g_0 equal to the 50 %. Numerical results for the integration of the systems (5.8) and (5.9) for $L = 0.2L_D$.

5.2.1.1, we have $m_{orph,U}(t) = m_{orph,D}(t)$.

$$\begin{cases} \dfrac{di_U}{dt} = \dfrac{dh_U}{dt} = \dfrac{1}{T_{0,U}} \left[g(t) - m_{orph,U}(t) \right] \\ \dfrac{db_U}{dt} = \dfrac{1}{T_{mob,U}} \left[\left(\alpha_G(t) - \beta_U(t) \right) \left(g(t) + 1 \right) - \right. \\ \qquad \left. - \left(\alpha_U(t) - \beta_U(t) \right) \left(m_{orph,U}(t) + 1 \right) \right] \\ \dfrac{dm_{orph,U}}{dt} = \left(m_{orph,U}(t) + 1 \right) \left[\dfrac{n}{i_U(t) + 1} \dfrac{di_U}{dt} + c_3(b_U(t)) \dfrac{db_U}{dt} \right] \end{cases} \tag{5.10}$$

As usual $m = n = 2$. If we linearize the previous system (5.10) with the first and the third approximations of the system (5.6), we obtain that $(m_{orph,U}(t) + 1) = (1 + nh_U(t))\ (1 + \beta_\infty c_3(\beta_\infty) b_U(t))$.

Thus, the linearized form of the third equation of the system (5.10) is:

$$\frac{dm_{orph,U}}{dt} = \left(m_{orph,U}(t) + 1 \right) \left[\frac{n}{1 + nh_U(t)} \frac{dh_U}{dt} + \frac{\beta_\infty c_3(\beta_\infty)}{1 + \beta_\infty c_3(\beta_\infty) b_U(t)} \frac{db_U}{dt} \right] \tag{5.11}$$

In this case we have one more unknown and one more equation with respect to the model without a variable bottom composition in the section 5.2.1.1. If we substitute the equations of the system (5.10) in the (5.11), we obtain an implicit equation not only dependent on $m_{orph,U}(t)$, but also dependent by the terms $h(t)$ and $b(t)$, which in turn are dependent by themselves and by $m_{orph,U}(t)$. A numerical evaluation is necessary. This fact happens also for the linearized form of the model.

A large discussion about the results of the model that involves the variability of the bottom composition is directly postponed to the next section 5.2.2.

5.2.2 General case: two-reaches and variable grain-size model

Now we analyze the complete model described before in the section 5.1 and represented by the systems (5.1) and (5.4). If we know the boundary conditions $\overline{Q^m}$, $\bar{G}$ and

$\overline{\alpha_G} = \alpha_\infty$, we can evaluate the equilibrium conditions as:

$$\begin{cases} M_\infty = \dfrac{\bar{G}}{\overline{Q^m}} \\ \beta_\infty = \dfrac{\alpha_\infty}{(1/d)^{q-s}\ (1-\alpha_\infty) + \alpha_\infty} \\ I_\infty = \left(\dfrac{M_\infty}{Cost} c_1(\beta_\infty) \right)^{1/n} \end{cases} \tag{5.12}$$

Below we will take into consideration a perturbation of a different boundary condition at a time.

5.2.2.1 Perturbations of the amount of sediment input

In this section we are going to analyze the reaction of the river, initially in equilibrium conditions, in response to a perturbation of the sediment input $G(t)$.

Stepwise perturbations From equilibrium conditions we impose a stepwise perturbation g_0 that correspond to a constant perturbation that lead the system to a new equilibrium condition controlled by the new sediment input $G_1 = G(t > 0) = G_0$ as described in the section 5.2 at page 122.

The results depend upon the length of the upstream reach with respect to the length of the downstream reach. The results obtained for a schematic river with $L_U = 0.2\, L_D$ and a perturbation $g_0 = 0.2$ are shown in the Figure 5.5. After a stepwise increase of the solid input firstly we have a rapid fining of the bottom composition $\beta(t)$ that lead to a rapid increase of the morphodynamic parameter $M(t)$, then there is a slower phase during which the slope $I(t)$ increase and the bottom composition decrease to the equilibrium value, equal to the initial one.

As we increase the length of the upstream reach, the speed of its evolution decrease and the curves of the evolution of the two reaches tend to coincide. In the Figure 5.6 are shown the results obtained for a schematic river similar to the river used for the example presented in the section 5.2.1.1 with the model with a single reach and with a constant bottom composition (see Figure 5.3). Namely we have a negligible length for

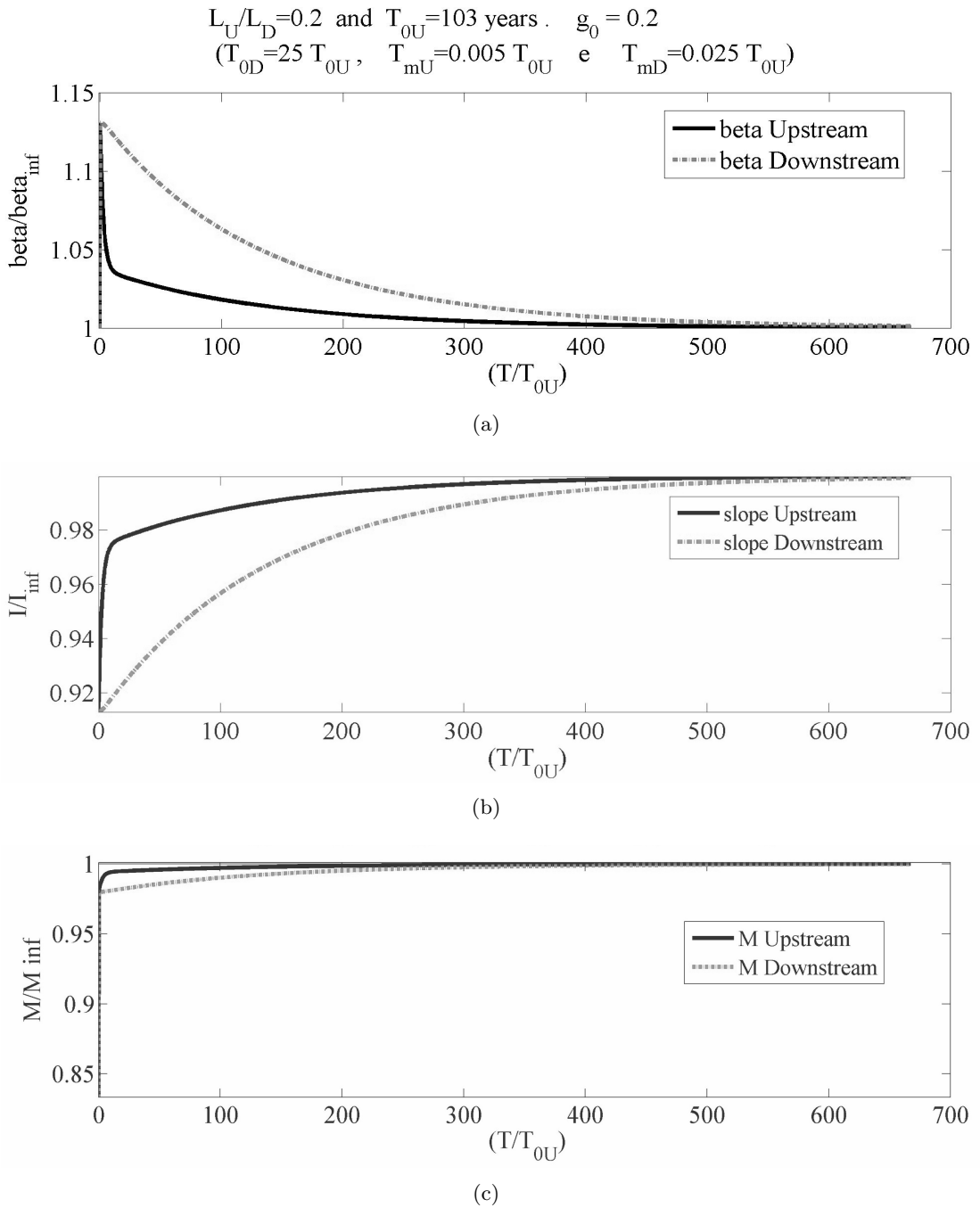

Figure 5.5: Two-reaches, variable grain-size model: example of the evolution of a river with $L = 0.2L_D$ from an initial equilibrium state applying a stepwise perturbation g_0 equal to the 20 %. 5.5(a) describe the evolution of the bottom composition $\beta(t)$ with respect to its equilibrium value β_∞ (that is the same before and after the perturbation g_0 as is possible to verify from the equation 5.12); 5.5(b) describe the evolution of the slope $I(t)$ of the river with respect to its new equilibrium value I_∞; 5.5(c) describe the evolution of the morphodynamic parameter $M(t)$ with respect to its new equilibrium value M_∞.

the downstream reach ($L_U = 5\ L_D$) and so the solutions for the downstream reach are almost equal to the solutions for the upstream reach (as we were taking into account only one reach). From the comparison of the Figures we can see that the evolution in the present section, with the exact solution developed numerically, is slower than the results obtained with the linearized solution developed by Di Silvio and Nones [2013].

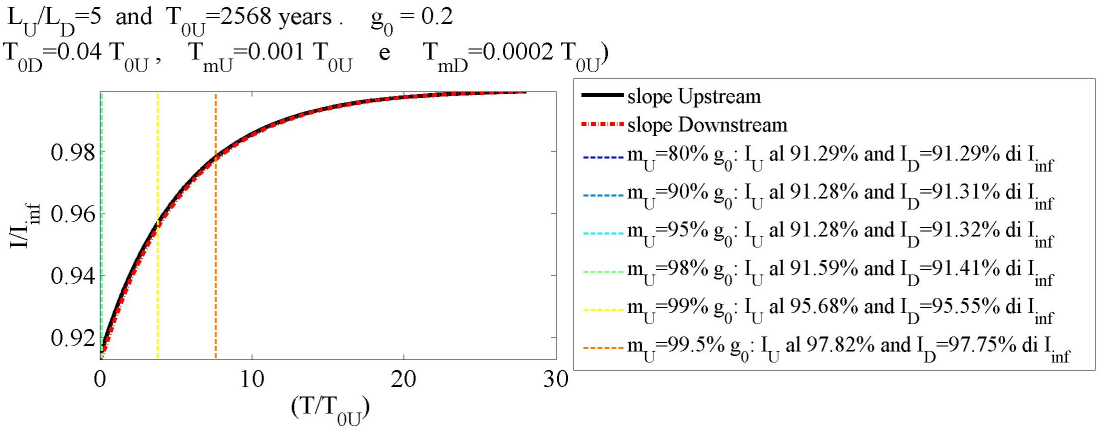

Figure 5.6: Two-reaches, variable grain-size model: example of the evolution of a river with $L_U = 5\ L_D$ and a stepwise perturbation of the sediment input $g_0 = 0.2$ that can be compared with the Figure 5.3 that show the result for the same river calculated with the model with a single reach and with a constant bottom composition (section 5.2.1.1). In the legend some step of the evolution of the morphodynamic parameter are compared with the correspondent step of the evolution of the slope.

Sinusoidal perturbations The perturbation of the sediment input $g(t)$ is now sinusoidally variable in time as described in the section 5.2 at page 123.

The new equilibrium conditions have to be defined by average values over a longer time, namely the forcing period T_w.

Also in this case the results are different taking different values of L_U/L_D. When there is an important length of the downstream reach the solution for the two reaches sensibly differ. Increasing the T_w we find that there is a limit for which the perturbation is more similar to a step-wise type, because the time required to reach the new equilibrium conditions are less than $T_w/4$ (note that it is the same result for the T_{win} found by Fasolato et al. [2011] exposed in the section 2.6.2).

5.2.2.2 Perturbations of the composition of the sediment input

In this section we analyze the effect of a stepwise (dimensionless) perturbation $a_{G,0}$ of the composition of the sediment input $\alpha_G(t)$:

$$\begin{aligned} a_G(t) &= 0 \quad \text{per } t \leq 0 \\ a_G(t) &= a_{G,0} \quad \text{per } t > 0 \end{aligned} \tag{5.13}$$

With the numerical results we find out that the perturbation of the composition of the sediment input can substantially modify the slope of the river, as shown in the Figure 5.7, which shows an example of the evolution of a river when the sediment input become finer with a stepwise perturbation of the sediment input composition $a_G(t < 0) = 0.5\,\%$. In fact, although the equilibrium ($t \to \infty$) morphodynamic coefficient $M_\infty = G_\infty/Q^m$ remain the same, the equilibrium bed composition is finer, thus the equilibrium slope decrease. There is an initial rapid fining of the bottom, followed by a very long period required to reach the new equilibrium. The slope change only very slowly, while the morphodynamic parameter respond to the rapid fining increasing, and then it will slowly decrease till the initial (and final) equilibrium value. In the Figure 5.7 the results shown are concentrated in the initial period of evolution with $t < T_{0,U}$ showing the rapid fining of the bottom.

5.2.2.3 Subsidence and sea-level rise

The mean-sea level is changing in geological time. The only proved reason for this phenomenon is the glacial cycles, but it can be influenced also by the tectonics. There are many authors that estimats the local or the global changing of the sea level in the history, often offering conflicting opinions. Watts and Torné [1992] reported that in the last 8 millions of years the subsidence of the Valencia through (Western Mediterranean sea) is of about 1000 m. It means that we can consider a mean subsidence of about $1.25 * 10^{-2}$ mm/yr.

As one can guess, this type of simulations are maybe too long-term and the results go beyond our engineering interests on the phenomenon we are studying.

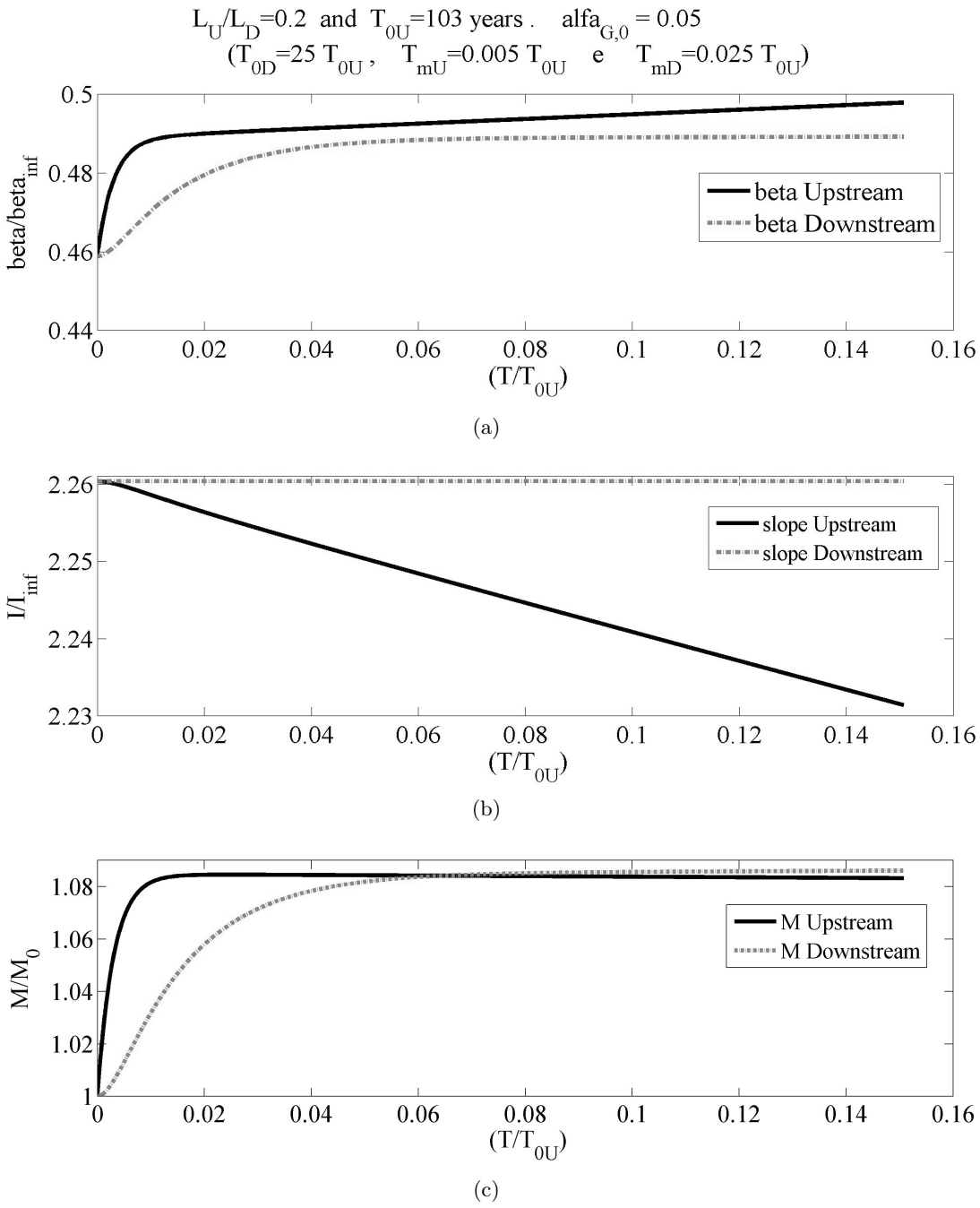

Figure 5.7: Two-reaches, variable grain-size model: example of the evolution of a river with $L = 0.2L_D$ from an initial equilibrium state applying a stepwise perturbation $a_{G,0}$ equal to the 0.5 %. 5.7(a) describe the evolution of the bottom composition $\beta(t)$ with respect to its equilibrium value β_∞; 5.7(b) describe the evolution of the slope $I(t)$ of the river with respect to its new equilibrium value I_∞; 5.7(c) describe the evolution of the morphodynamic parameter $M(t)$ with respect to its new equilibrium value M_∞ (that is the same before and after the perturbation $a_{G,0}$ as is possible to verify from the equation 5.12).

5.2.2.4 Perturbation on the input of the liquid discharge

In this section we analyze the effects generated by a perturbation on the liquid discharge. We have initially supposed that there was not substantial variation of this value, in order to simplify the equations, finding that the perturbation on the solid discharge correspond to the perturbation of the morphodynamic parameter, i.e. $p(t) = m_{orph,U}(t)$. Now we consider that exist a perturbation $q^m(t)$ of the equivalent liquid discharge of the river. It means that there is a variation of the duration curve but, in these temporal and spatial scales, we maintain the LUF hypothesis. Thus the only parameter that should change in the equation of the evolution of the morphology is the thickness of the mixing layer δ. This value is extremely arbitrary, sometimes supposed to be a percentage of the mean water depth, sometimes the diameter of the d_{90}. For this reason we neglect the influence of the change of the liquid discharge in the river and consider only the influence of the equivalent liquid discharge directly on the equilibrium formula. Now we have that the perturbation parameter of the solid discharge is evaluated as:

$$p(t) = (m_{orph,U}(t) + 1)(q^m(t) + 1) - 1 \tag{5.14}$$

A study of a series of perturbations of the duration curve of the liquid discharge, characterized by a sinusoidal behaviour with different period, can represent the natural changing of the climatic conditions. In the Figure 5.8 a comparison of the evolution of the morphodynamic parameter $M(t)$ with different characteristic period T_w. For limited temporal simulations the results obtained for a T_w equal to 10, 100 and 1000 $T_{0,U}$ are shown.

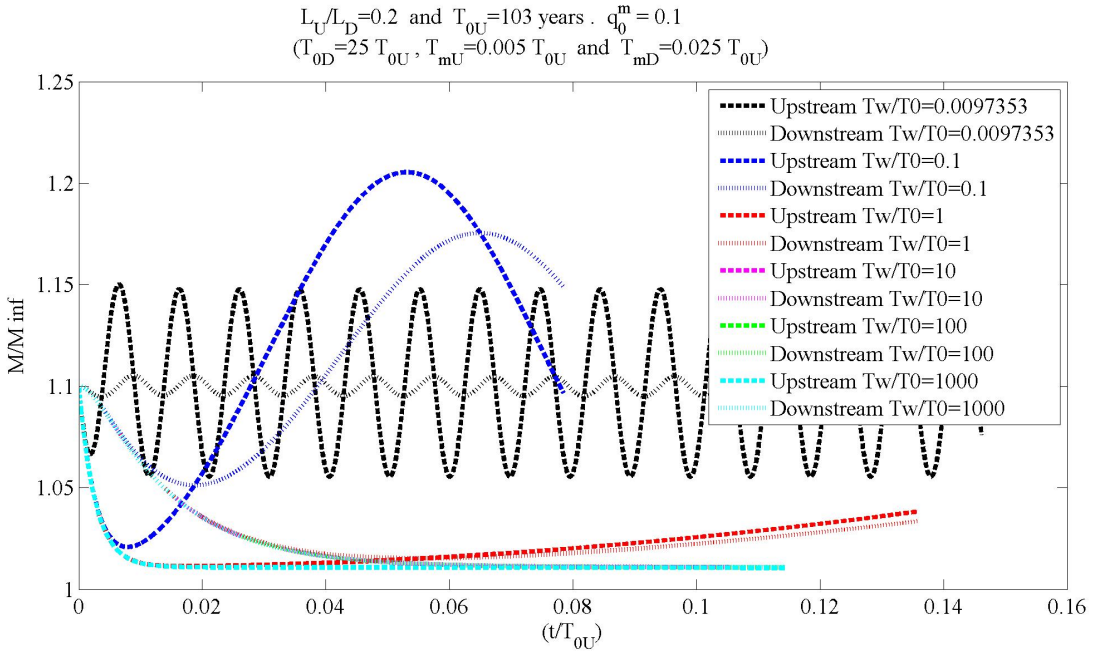

Figure 5.8: Two-reaches, variable grain-size model: comparison between the numerical results of the system (5.4) and of the linearized version (obtained with the assumptions (5.6)) for $L_U = 0.2\ L_D$ and a sinusoidal perturbation of the equivalent discharge input $q^m(t > 0) = q^m_{G,0} sin(\omega t)$ with $q^m_{G,0} = 0.1$ and for different period of oscillation T_w. Graphs of the evolution in time of the morphodynamic parameter $M(t)$

5.3 River evolution with $t \to \infty$

In this section we analyze the evolution for $t \to \infty$ of the river with constant boundary conditions if we begin the simulation from an arbitrary state of the river.

It seems that for every type of initial conditions, the variables swing in order to arrive always at the same layout, from which then the river evolves toward the equilibrium conditions. This typical layout always verified has a bed composition of both the two reaches finer then the equilibrium composition and a smaller slope of the equilibrium slope. Moreover it maintain the observed natural characteristics of concave profile and downstream fining [Sinha and Parker, 1996], i.e. the downstream reach has smaller slope and finer bed composition than the upstream bed.

This analysis can maybe represent a sort of a laboratory experiment about the filling of a basin, given the boundary conditions. It is far from the natural conditions because in this so long temporal scale the boundary conditions are far to be constant, but a lot of processes take place, as climatic changing or degradation of the basin itself, because the mountains are not an infinite source of sediments or because of humans intervention [Park and Jain, 1987].

Indeed, if we start from any initial conditions, even if convex and with a uniform bed composition, the morphology of the river evolves to a concave profile with downstream fining before finally reach the equilibrium conditions, both considering an upstream reach shorter and longer than the downstream reach, as is possible to see in the Figures 5.9 and 5.12. In the Figure 5.10 the evolution of the three parameters bottom slope $\beta(t)$, slope $I(t)$ and morphodynamic parameter $M(t)$ are shown for the case with an upstream reach shorter than the downstream reach. In the Figure 5.11 there is a zoom of the graph of the evolution of the bottom composition. From this zoom is possible to verify that, starting form a bed composition formerly equal to the equilibrium value, the sediment rapidly become finer and then start a slow evolution to the coarser equilibrium value, always respecting the downstream fining characteristic.

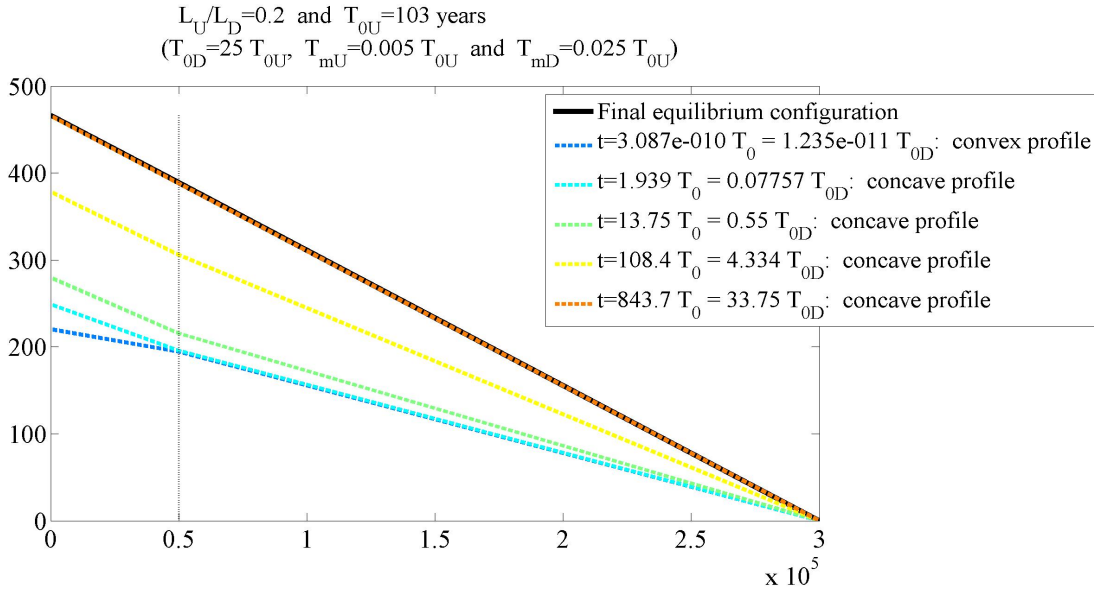

Figure 5.9: Evolving longitudinal profile of a schematic river with $L_U = 0.2\, L_D$ starting from a condition of a convex longitudinal profile.

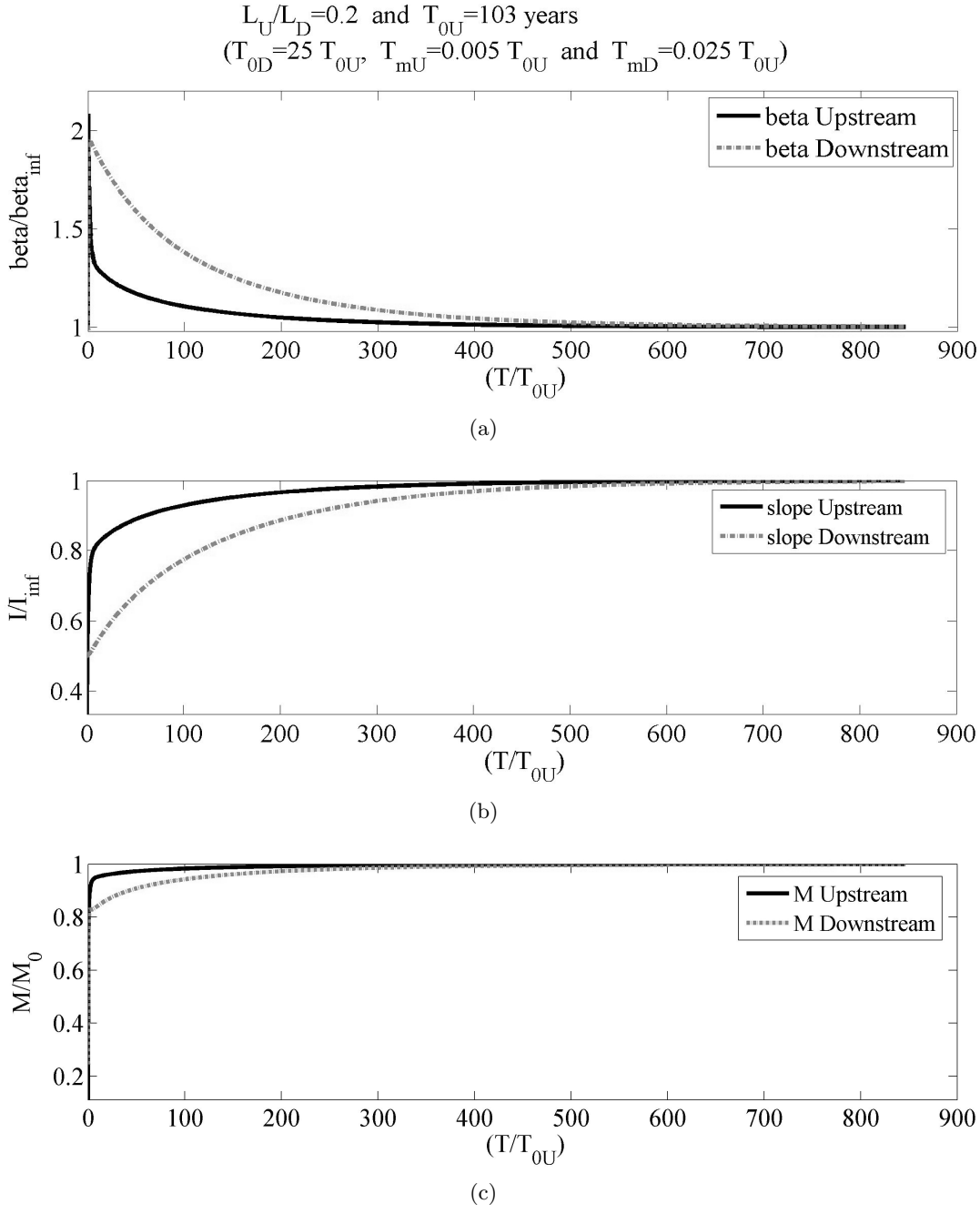

Figure 5.10: Evolution of a schematic river with $L_U = 0.2\, L_D$ starting from a condition of a convex longitudinal profile and a bottom composition formerly equal to the equilibrium value. 5.10(a) describe the evolution of the bottom composition $\beta(t)$ with respect to its equilibrium value β_∞; 5.10(b) describe the evolution of the slope $I(t)$ of the river with respect to its new equilibrium value I_∞; 5.10(c) describe the evolution of the morphodynamic parameter $M(t)$ with respect to its new equilibrium value M_∞.

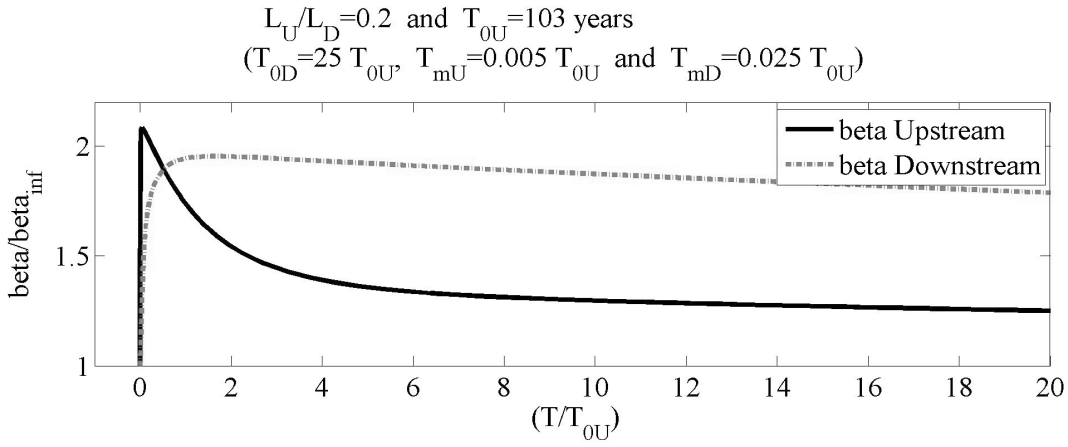

Figure 5.11: Zoom to the initial period of the graph 5.10(a) that describe the evolution of the bottom composition $\beta(t)$ with respect to its equilibrium value β_∞ for a schematic river with $L_U = 0.2\, L_D$ starting from a condition of a convex longitudinal profile.

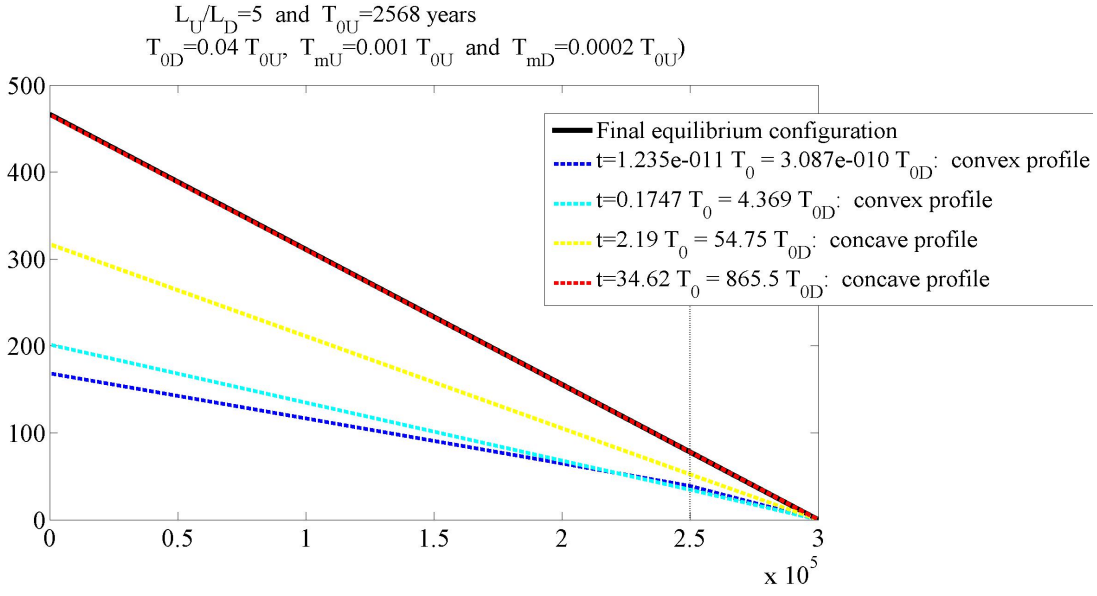

Figure 5.12: Evolving longitudinal profile of a schematic river with $L_U = 5\, L_D$ starting from a condition of a convex longitudinal profile.

Chapter 6

Conclusive remarks and perspectives

In the present thesis a number of mathematical models have been developed with the purpose to predict the amount of sediments (**sediment yield**) conveyed through a certain cross section of a river.

The models are to be applied, separately or in combination, taking into account the space- and the time-scale under consideration. The general idea is to utilize at their best the hydrological, morphological and grain-size data at our disposal, as well as the available measurements regarding sediment transport (solid discharge, concentration, filling process of a reservoir, etc...), no matter how numerous and continuous they can be.

Most of the models developed in this work are physically based, namely based on the typical "conservation equation" of the physics (even if more or less simplified). This class of models differs from other two classes of models applied for the simulation of the sediment yield of a basin: the empirical models and the conceptual models. This classification, mentioned also in the Chapter 1, is widely discussed by Merritt et al. [2003]. While the physically based models are mainly applied to simulate the sediment transport along the river network, the other two types are principally used to simulate the sediment production from the basin surface. As explained in the Section 2.2, our purpose is to find basin-scale models able to evaluate the amount of sediments

coming from a watershed area with no need of a sediment production model. Indeed a reliable sediment production model should be necessarily very detailed and complicated, needing many information and long computational time. In a physically based model, by contrast, the sediment production from the basin surface is obtained indirectly from the sediment transport data.

Theoretically the parameters used by physically based models are measurable, but in practice also these types of models need to be calibrated against observed data, because of the large number of parameters involved and the heterogeneity of their values (the more so we are considering a basin scale).

A typical set of data to be utilized by the models of this work is formed by a continuous record of water flow through a given cross-section and some basin-scale averaged morphological (as river slope, width and length) and grain-size information. If we have also a continuous record of the solid transport, contemporary to the water flow record, is possible to calibrate the models.

All the models presented here refer to the classical rating curve of Engelund and Hansen type (see equation (2.4)), a monomial power relation between the solid and the liquid discharge (that always needs to be calibrated against a certain set of measures of liquid discharge and solid transport at a cross-section of a river). We postulate that this type of relation identifies a stationary condition of the system under consideration, related to a specific space- and time-scale of the processes involved, called "equilibrium" condition. In this equilibrium formula of Engelund-Hansen type (see equation (2.4)) the proportionality parameter, that links the solid discharge with the m-power liquid discharge (equivalent discharge, see section 3.2), is called morphodynamic parameter and incorporates all the morphological and grain-size information.

Moreover all the models are based on the fundamental hypothesis of the Local Uniform Flow (LUF), which implies a univocal relation between the solid transport and the averaged bottom slope (slowly variable with the "morphological" time) instead of the energy slope (quickly variable, in principle, with the "hydraulic" time). This assumption (necessary consequence of working at basin-scale, see section 2.6.2) permits in practice to carry out very long-term simulations on very large rivers. Indeed all the

models proposed consider the basin-scale as the space-scale.

Finally all the models work with a non-uniform grain-size composition, identified as a basic assumption in order to better represent the morphological behaviour of the river. For sake of simplicity, we have considered only two representative diameter of the sediments, representing the fine and the coarse fraction respectively. Two classes have proved to be sufficient to show the typical behaviour of a river with a non-uniform sediment composition.

The models developed permit to evaluate the deviations of the real solid transport $P(t)$ from the value calculated with the "equilibrium" formula $\bar{P}[Q(t)]$. The deviations $P'(t)$ and $P'(\tau)$ depend on the time-scale considered:

$$P(t) = \bar{P}[Q(t)] + P'(t) + P'(\tau)$$

In particular we have developed three models, valid in three different time-scales.

Long-term equilibrium model with short-term perturbations (Chapter 3): with this model we consider a short time-scale (daily or monthly), assuming the existence of a basic configuration (equilibrium condition) at a longer time-scale. In order to evaluate the short-term deviations from this basic state, we have used the information provided by the chronological behaviour of the liquid discharge. In other words, with the support of the 1-D deterministic analytical solution described in the Chapter 2, we link the present deviation of the solid transport recorded downstream with the perturbation of the liquid discharge, happened upstream at a previous time.

Some numerical application of the model have been made with the chronological series of data for the Adige river (see section 3.7) and for the Po river (see section 3.8). Unluckily the morphological data available were not contemporary with the records of the solid transport and of the liquid discharge. For this reason also some parameters, theoretically measurable, had to be calibrated in order to be coherent with the solid transport data. Moreover, in a context of a collaboration with CoRiLa and Veneto Region, we tried to apply the long-term equilibrium

model to the rivers flowing in the Venice Lagoon (see section 3.9), a particular case very dissimilar from the previous two. The calibrated model was used to complete lacking series of data for the evaluation of the long-term solid input from the watershed area draining in the Lagoon. The numerical application show that the model can improve the results obtain with the simple rating curve, but the prediction could be further enhanced by considering the large watershed ares subdivided in smaller and more uniform sub-basin, each one collecting a different LUF channel (see section 3.6). This subdivision obviously needs the morphological information (averaged at sub-basin scale) for each sub-basin.

Long-term non-equilibrium model (Chapter 4): with this model we investigate an intermediate time-scale (pluri-annual). On the basis of the previous model, we assume that the short-term perturbation averaged on this new time-scale are null, but we renounce to the constant basic state of equilibrium. So there are now long-term perturbations to be evaluated. With this purpose, the one-dimensional model is integrated to a zero-dimensional model, enough representative for the space- (basin scale) and for the time-scale considered. As we have not a basic constant state, the morphodynamic parameter is evolving: in particular we consider a constant river width and variable bottom composition and slope of the LUF channel. The mathematical system found is implicit and non-linear. In order to find an analytical solution for the morphological evolution of the river we assume a series of simplifications finally leading to admit that the river is not so far from the equilibrium conditions, namely that the present slope and grain-size are very similar to their asymptotic values: the evolution depends on the adaptation process of the grain-size (almost instantaneous) and not on the adaptation process of the river profile (very much slower). Such a solution is in fact hardling realistic; nevertheless the model has been applied to the records of Adige river and Po river, inverting the formulation and finding a rapid and simple estimation of the sediment production from the watershed area. As expected, the resulting difference between the input and the output of sediment in and from the river is very small, consistently with the (discutible) solution that we are not so far from

the equilibrium condition.

Morphological reactions rivers at geological scale (Chapter 5): in this Chapter we consider a geological time-scale, by renouncing from the previous integrated 0-D model many of the assumed simplifications.

With the assumption of a non-uniform grain-size bottom composition (that is crucial in the erosion and deposition processes) and by splitting the LUF reach in two LUF reaches representing the highland and the lowland part of the river basin, we verified that the morphological evolution results to be (realistically) much slower and that the model can simulate both the typical natural phenomena of the downstream fining and of the concave longitudinal profile.

Moreover we find a strict intercorrelation between the slope and the bottom composition. A perturbation on a generic boundary condition generally cause a rapid reaction of the river with the fining of the bed, followed by a very slow reaction of both the slope and the bottom composition itself. The river will tend to the new equilibrium condition, unless there is another perturbation.

The mathematical system is implicit and non-linear and it is not possible to find an analytical solution; we used a numerical evaluation based on a Predictor-Corrector scheme. Nevertheless, solving it is extremely simpler and faster than solving a 1-D model.

It would be interesting apply this model also to shorter but more realistic perturbations, also of anthropogenic origin. For example estimating the response of a river after its damming, by considering both the sediment interception by the reservoir and the regulation of the liquid discharge for irrigation or potable purpose. In particular the attention could be addressed to the Asian rivers, where very large rivers are continuously monitored, both for the liquid discharge and the sediment flux, also by more than fifty years. During the monitored periods there are evident decreasing or increasing trend, generally due by human activities. For example the Pearl River, the second larger river in China (in terms of mean annual water discharge), is monitored till the 50s by three gauging stations

placed in its three main tributaries. Different response of this river to different kind of human interventions happened in the observed period have been already observed [Zhang et al., 2011].

Appendix A

Principal notation

Table A.1: List of the principal notation used in this thesis.

Symbol	Definition	Units
Q	water discharge of the LUF channel	m^3/s
Y	water depth of the LUF channel	m
U	velocity of the current of the LUF channel	m/s
I	bottom slope of the LUF channel	-
J	energy slope of the LUF channel	-
B	width of the LUF channel	m
H	bottom level of the LUF channel	m
L	Length of the LUF channel	m
d_{eq}	equivalent diameter of the sediment	m
d_c	diameter of the coarser class	m
d_f	diameter of the finer class	m
α	percentage presence of the finer diameter in the current	-
β	percentage presence of the finer diameter in the bottom	-
δ	mixing layer thickness	m
V_0	characteristic triangular volume of the LUF channel	m^3
V_m	characteristic volume of the mixing layer of the LUF channel	m^3
P	output solid discharge	m^3/s
G	input solid discharge	m^3/s
M	morphodynamic parameter of the LUF channel	$(s/m^3)^{m-1}$
m	exponent of the transport formula	-
n	exponent of the transport formula	-
p	exponent of the transport formula	-
q	exponent of the transport formula	-
α_{EH}	calibration coefficient of the Engelund-Hansen transport formula	-

Appendix B

ARMA procedure

A thorough description of the **A**uto-**R**egressive **M**oving-**A**verage model (ARMA) may be found in Choi [2012]. We synthesize herein the main features of this procedure.

To describe the output $y(t)$ from a "'black-box" by means of a discrete-time model (necessary from the computational point of view) we may express the analyzed variable $y(t)$ as a function of the n past values of the output itself and by the n values of the input x:

$$\begin{aligned} y(t) &= a_1 y(t-1) + ... + a_n y(t-n) + b_0 u(t) + b_1 u(t-1) + ... + b_n u(t-n) + \epsilon(t) = \\ &= \sum_{i=1}^{n} (a_i y(t-i)) + \sum_{i=0}^{n} (b_i x(t-i)) + \epsilon(t) \end{aligned} \tag{B.1}$$

Equation (B.1)may be seen as a discrete formulation of the ordinary differential equation that describe the evaluation of the quantity $y(t)$ through the physical system represented by the black-box. If we have a set of measures of the output y and of the input x, we can calibrate this model against the measured data finding the values for the coefficients a_i and b_i. The solution is found through the minimization of the term $\epsilon(t)$.

As for finding the interpolation line of records of data, if we have a total of N measures, the problem is the minimization of the mean square errors from the measured

data:

$$MIN_{a_i,b_i} \sum_{t=n}^{N} \epsilon^2(t)$$

where n is the order of the model. We call θ the vector which element are the $(2n+1)$ unknowing a_i, b_i, while $\phi(t)$ is the vector which element are the set of data: $\phi(t) = [y(t-1)y(t-2)...y(t-n)u(t)u(t-1)...u(t-n)]^T$. In the case of $n = 1$ we have:

$$\phi(t) = \begin{bmatrix} y(t-1) \\ u(t) \\ u(t-1) \end{bmatrix}$$

Thus, if we write $\epsilon(t)$ form the (B.1) in vectorial form we have:

$$\epsilon(t) = y(t) - \theta^T \phi(t) = y(t) - \phi^T(t)\theta$$

We aim to minimize, in function of θ, the quantity:

$$J_n(\theta) = \sum_{t=n}^{N} \epsilon^2(t) = \sum_{t=n}^{N} [y(t) - \theta^T \phi(t)]^2 \tag{B.2}$$

We can recognize that $\epsilon^2(t)$ is a quadratic form:

$$\begin{aligned} \epsilon^2(t) &= [y(t) - \theta^T \phi(t)]^2 = \\ &= \begin{bmatrix} 1 & -\theta^T \end{bmatrix} \begin{bmatrix} y^2(t) & y(t)\phi^T(t) \\ \phi(t)y(t) & \phi(t)\phi^T(t)] \end{bmatrix} \begin{bmatrix} 1 \\ -\theta^T \end{bmatrix} = \\ &= \begin{bmatrix} 1 & -\theta^T \end{bmatrix} M(t) \begin{bmatrix} 1 \\ -\theta^T \end{bmatrix} \end{aligned}$$

namely $\epsilon^2(t) \geq 0$, so the matrix $M(t)$ is at least a semi-defined positive matrix,

namely $M(t) \geq 0$. Moreover we can see that the $M(t)$ matrices can be parted in four matrix, which are in their turn semi-defined positive:

$$M(t) = \begin{bmatrix} m_1(t) & m_2^T(t) \\ m_2(t) & m_3(t) \end{bmatrix}$$

Substituting this last result in the expression (B.2) of $J_n(\theta)$ we have:

$$\begin{aligned} J_n(\theta) &= \left[1 - \theta^T\right] \sum_{t=n}^{N} M(t) \begin{bmatrix} 1 \\ -\theta^T \end{bmatrix} = \\ &= \left[1 - \theta^T\right] \sum_{t=n}^{N} \begin{bmatrix} \sum_{t=n}^{N} y^2(t) & \sum_{t=n}^{N} [y(t)\phi^T(t)] \\ \sum_{t=n}^{N} [\phi(t)y(t)] & \sum_{t=n}^{N} [\phi(t)\phi^T(t)] \end{bmatrix} \begin{bmatrix} 1 \\ -\theta^T \end{bmatrix} = \\ &= \left[1 - \theta^T\right] M(N) \begin{bmatrix} 1 \\ -\theta^T \end{bmatrix} \end{aligned}$$

If we define the matrices $r(N) = \sum_{t=n}^{N} y^2(t)$, $s(N) = \sum_{t=n}^{N} [\phi(t)y(t)]$ and $Q(N) = \sum_{t=n}^{N} [\phi(t)\phi^T(t)]$, we can say that:

$$J_n(\theta) = r(N) - \theta^T s(N) - s^T(N)\theta + \theta^T Q(N)\theta$$

Because $M(N) \geq 0$, is possible to demonstrate that the equation $Q(N)\,\theta = s(N)$ always has at least one solution, in particular, if $Q(N) > 0$ (i.e. strictly defined positive), exists a unique solution: $\theta = Q^{-1}(N)\,s(N)$.

We want to demonstrate that θ_0 is a solution of the problem $MIN_\theta J_n(\theta)$ if and only if $Q(N)\,\theta_0 = s(N)$.

1. $Q(N)\,\theta_0 = s(N) \Rightarrow \theta_0 = MIN_\theta J_n(\theta)$

   Any θ can be written as $\theta = \theta_0 + \theta_1$.

$$\begin{aligned} J_n(\theta_0+\theta_1) =& r(N) - (\theta_0+\theta_1)^T s(N) - s^T(N)(\theta_0+\theta_1) + \\ &+ (\theta_0+\theta_1)^T Q(N)(\theta_0+\theta_1) = \\ =& r(N) - \theta_0^T s(N) - s^T(N)\theta_0 + \theta_0^T Q(N)\theta_0 - \theta_1^T s(N) - s^T(N)\theta_1 + \\ &+ \theta_1^T Q(N)\theta_1 + \theta_0^T Q(N)\theta_1 + \theta_1^T Q(N)\theta_0 \end{aligned}$$

The hypothesis are that $Q(N)\theta_0 = s(N)$, so we have that $\theta_1^T Q(N)\,\theta_0 = \theta_1^T s(N) = s^T(N)\,\theta_1 = \theta_0^T Q(N)\,\theta_1$. Then:

$$\begin{aligned} J_n(\theta_0+\theta_1) =& r(N) - \theta_0^T s(N) - s^T(N)\theta_0 + \theta_0^T Q(N)\theta_0 + \theta_1^T Q(N)\theta_1 = \\ =& J_n(\theta_0) + \theta_1^T Q(N)\theta_1 \geq J_n(\theta_0) \end{aligned}$$

because $Q(N) \geq 0$.

2. $\theta_0 = MIN_\theta J_n(\theta) \Rightarrow Q(N)\theta_0 = s(N)$

   If $J_n(\theta_0) \leq J_n(\theta) = J_n(\theta_0+\theta_1)$, from the previous calculations we have that $J_n(\theta_0) = J_n(\theta)$ if and only if $\theta_1^T Q(N)\theta_1 = 0$. But, if $Q(N) \geq 0$, we have also that $Q(N)\theta_1 = 0$. In particular we have:

$$Q(N)\theta = Q(N)(\theta_0+\theta_1) = Q(N)\theta_0 + Q(N)\theta_1 = Q(N)\theta_0) = s(N)$$

Appendix C

Hydrological model

A simple hydrological model has been developed to reconstruct the liquid discharge passing through the cross-section of the gauge stations of rivers flowing into the Venice Lagoon before 2006 (see section 3.9). We use the meteorological data of rainfall and temperature starting from the 1996 and some primary information from the land reclamation authority about the flow regulation management. In particular we have reconstruct the general network of the interconnections between the different sub-basins and channels and we have the average monthly values of the artificial discharge diverted from each one of them. The exact value of the diverted discharge moved every day is impossible to know because the channel are regulated by hand and often according to the opinion of the farmers.

The territory is quietly uniform, so we can interpolate the values of the meteorological stations with the method of Thiessen polygons. We calculate the monthly mean evapotranspiration with the Thornthwaite formula (C.1), and then extrapolate the daily value (Pareira et al., 2004).

$$ET(t) = K \left[1.62 \left(\frac{10\, T(t)}{I} \right)^{a} \right] \tag{C.1}$$

where ET is the monthly evapotranspiration ($[cm]$); K is the latitude correlation coefficient of the ith month, equal to the quotient between the daytime hours and the half of the daily hours (= 12); $T(t)$ is the monthly mean air temperature ([℃]); a is a factor

dependent on I and I is the annual index of heat.

For the entire area of the watershed of the Venice Lagoon we assume a mean runoff coefficient φ (the ratio between the water volume which crosses the closing section of the basin and the rainfall input over the related surface) equal to 70 % and that the subsequent infiltration goes to an underground reservoir that will give back the water Q_{inf} to the river with a linear law.

Therefore we perform a smooth hydrological model based on the mass balance of input and output of water in every single sub-basin system. We have to calibrate the following schematic relationship:

$$Q(t) = [a_1\varphi R(t-d_1) - a_2 ET(t-d_1) + a_3 Q_{inf}(t-d_2)] + Q_{IN}(t) - Q_{OUT}(t)$$

Where $Q(t)$ is the liquid discharge measured at the gauge station, $R(t)$ is the rainfall, so $\varphi R(T)$ is the runoff (input), $ET(t)$ is the evapotranspiration (output), Q_{inf} is the contribute from the underground reservoir of the rainfall infiltrated (equal to $(1-\varphi)R$), Q_{IN} and Q_{OUT} are the artificial input and output at the basin. Both the runof and the evapotranspiration are relative to a previous time that has to be determined on the bases of the time of concentration of the basin d_1 (that is the time that a liquid particle fallen in farthest point of the basin require to reach the closing section). The process of infiltration followed by the linear empty of the underground reservoir implies a different delay d_2 associated to Q_{inf}. The coefficient a_1, a_2 and a_3 are the site-specific calibration parameter determined by an ARMA procedure.

Notice that the real runoff coefficient, the ratio between the water volume which crosses the closing section of the basin and the rainfall input over the related surface, is influenced by the strong human activities, that deviate the natural flow of the water, as we can see from the results of the DRAIN project published in Zuliani et al. [2005], where they found also some values of φ greater than 1. Nevertheless the assumption of the value of the runoff coefficient is negligible, because its value (or the correction of the value chose) can be incorporated inside the calibration parameter.

The artificial regulations done by the land reclamation authority typically works

through channel deviations by exceeding of a threshold, but there is no recording of this work, and often the thresholds are manually modified case by case. As mentioned before, we know only some principal values of the monthly average artificial input and output from the different sub-basins. We extrapolate the daily regulation thinking that the inputs have to be proportional to the evapotranspiration $Q_{IN}(t) \propto ET(t)$, i.e. the need of water by the cultivations, and the output can occur when there are flood conditions $Q_{OUT}(t) \propto R(t)$.

The model incorporates also a representation of the snow melting based on the daily average temperature as explained in the section 3.6, but it has not a great importance at this latitude and altitude.

The ARMA calibration of the model is combined with a recursive model in order to find the values of the time of concentration d_1, the characteristics delay of the underground reservoir d_2 and its initial condition (the volume of the reservoir at the begin of the simulation) that best represent the record of data available. Although the anthropic interventions are taken into account with some reasonable law, sometimes the calculated liquid discharge can be evaluated as negative. We assume that the contribution of the underground reservoir can compensate the lack of specific information.

Appendix D

Trend of the components of the characteristic volume $A(\tau)$

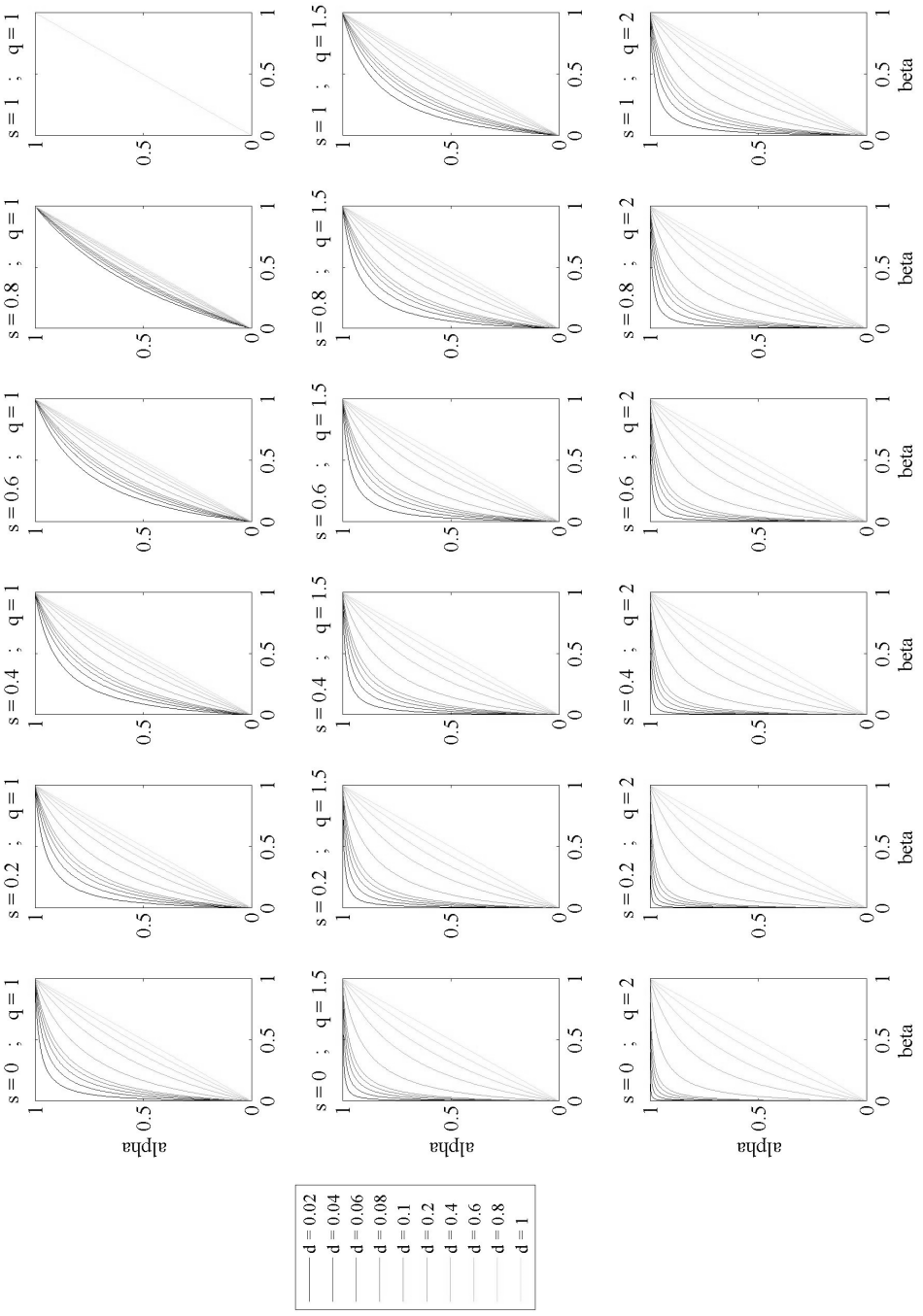

Figure D.1: Trend of the transport composition α with respect to the bed composition β varying the exponents s and q (and so m).

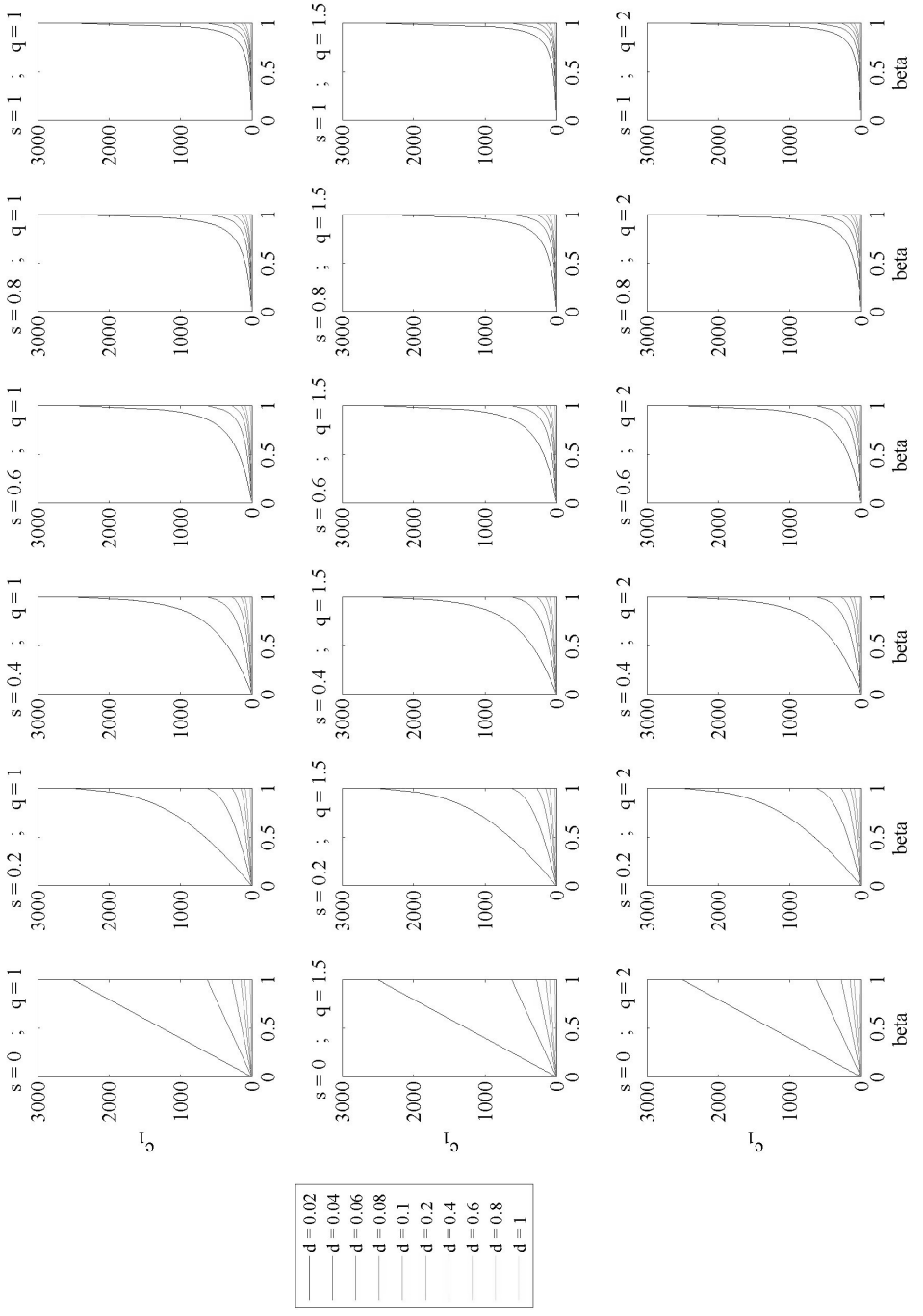

Figure D.2: Trend of the function $c_1(\beta)$ with respect to the bed composition β varying the exponents s and q (and so m).

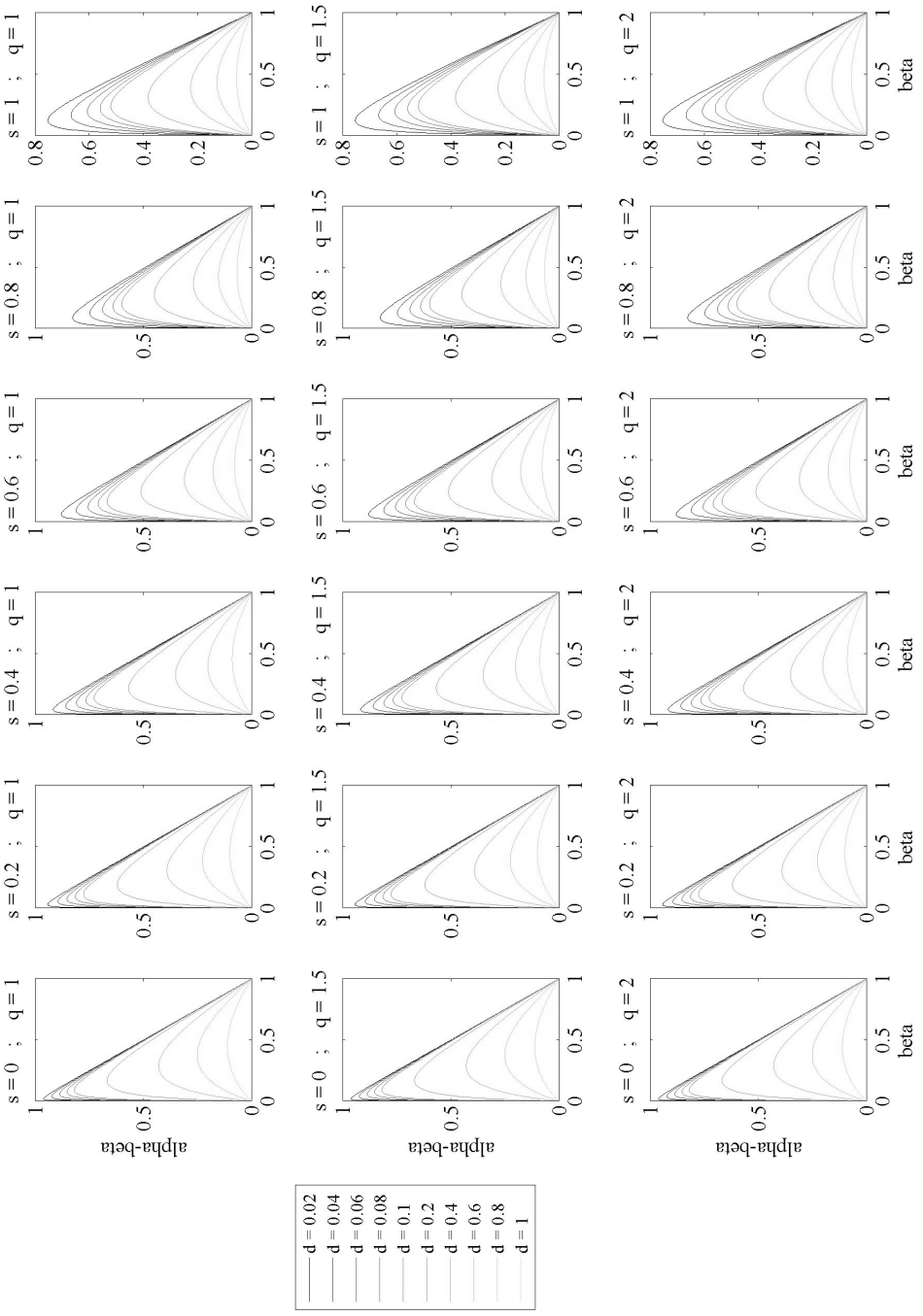

Figure D.3: Trend of the function $(\alpha(\beta) - \beta)$ with respect to the bed composition β varying the exponents s and q (and so m).

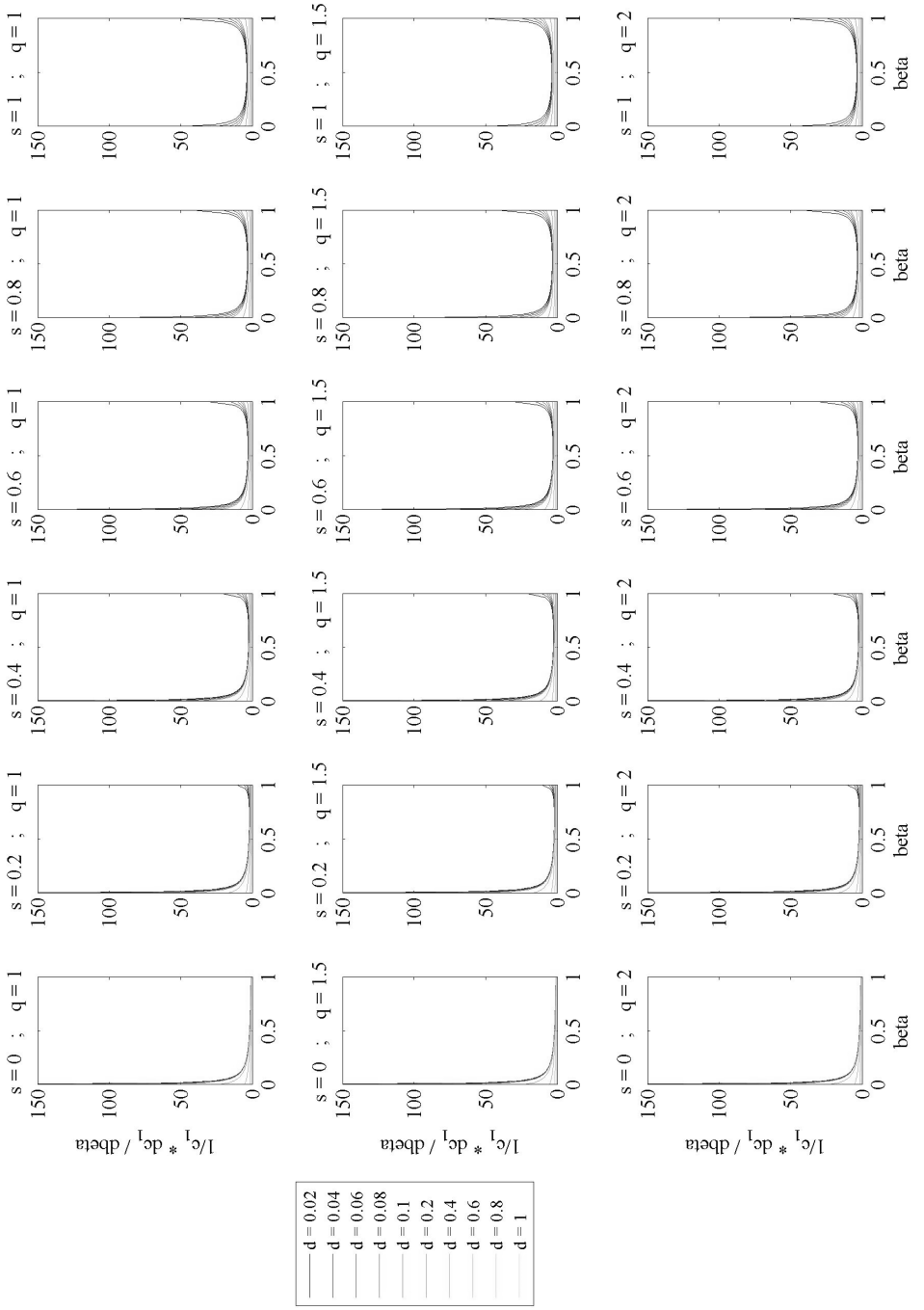

Figure D.4: Trend of the function $\frac{1}{c_1(\beta)} \frac{dc_1(\beta)}{d\beta}$ with respect to the bed composition β varying the exponents s and q (and so m).

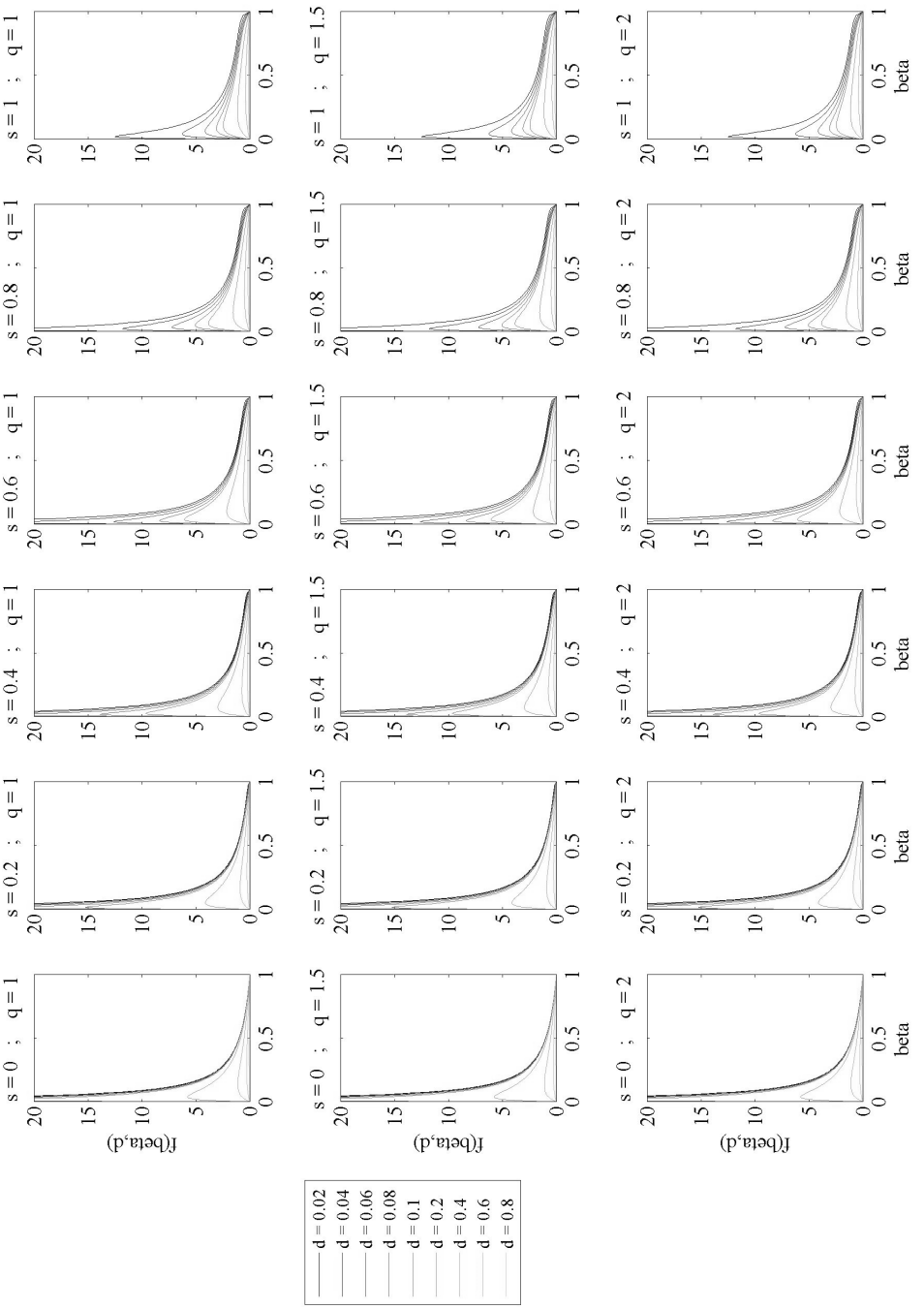

Figure D.5: Trend of the function $f(\tilde{\beta}(\tau), d)$ with respect to the bed composition β varying the exponents s and q (and so m).

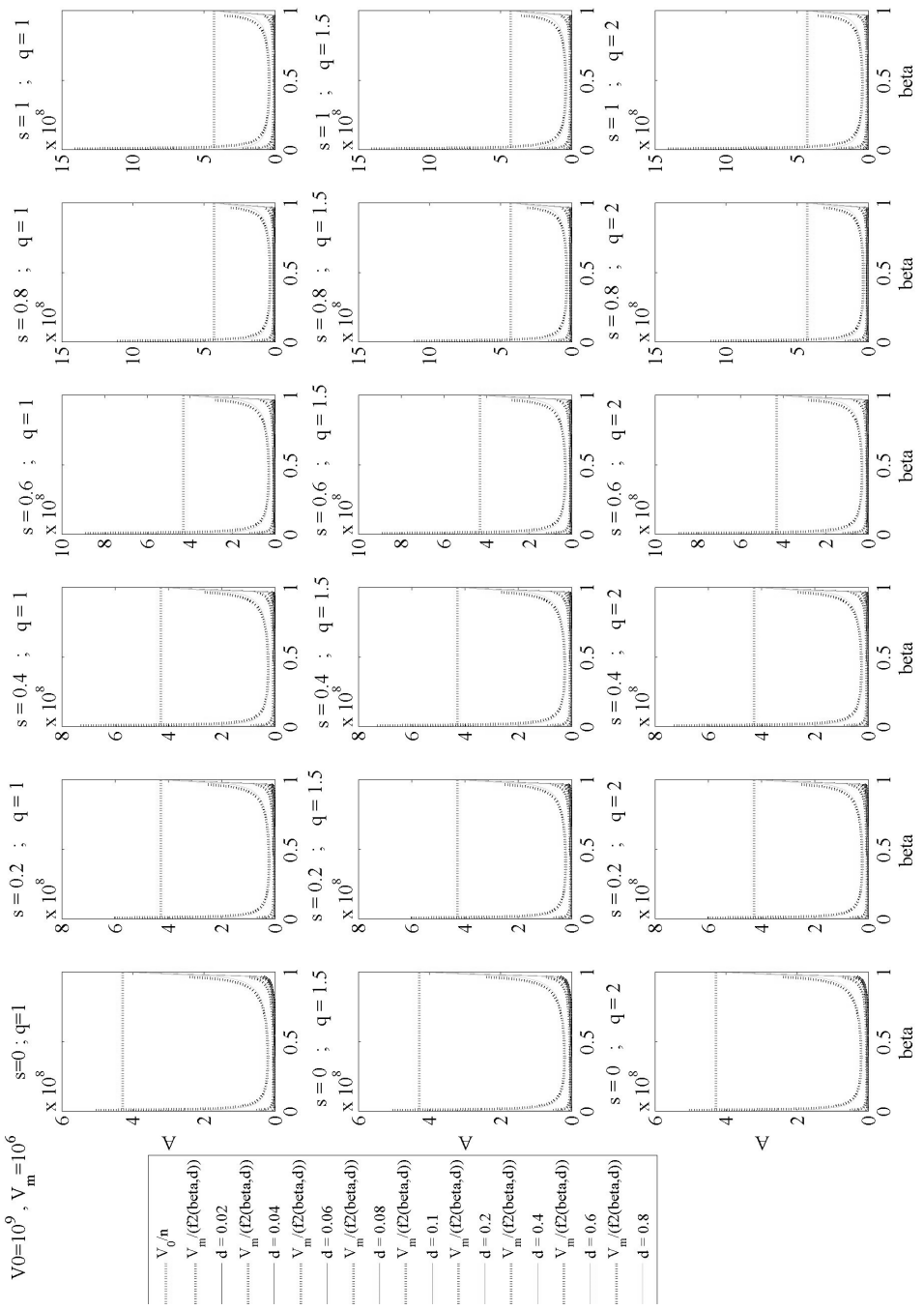

Figure D.6: Trend of the characteristic volume A with respect to the bed composition β varying the exponents s and q (and so m).

Bibliography

H. Aksoy and M.L. Kavvas. A review of hillslope and watershed scale erosion and sediment transport models. *Catena*, 64(2):247–271, 2005.

J.R.L. Allen. Reaction, relaxation and lag in natural sedimentary systems: General principles, examples and lessons. *Earth-Science Reviews*, 10(4):263 – 342, 1974.

P.A. Allen and P.L. Heller. *Dispersal and Preservation of Tectonically Generated Alluvial Gravels in Sedimentary Basins*. 2012.

N.E.M. Asselman. Fitting and interpretation of sediment rating curves. *Journal of Hydrology*, 234:228 – 248, 2000.

DIAO Autoritá di Bacino dell'Adige e dell'Alto Adriatico. Piano di gestione dei bacini idrografici delle alpi orientali. *Piano di gestione*, 2010.

C. Bellos and V. Hrissanthou. Numerical simulation of morphological changes in rivers and reservoirs. *Computers & Mathematics with Applications*, 45(1):453–467, 2003.

S. Brunelli. *Trasporto solido annuo dei corsi d'acqua in funzione delle loro caratteristiche idrologiche e morfologiche*. Master thesis. Universitá degli studi di Padova, 1987.

B.S. Choi. *Arma Model Identification*. Springer Series in Statistics. Springer London, Limited, 2012.

A. Crosato. Effects of smoothing and regridding in numerical meander migration models. *Water Resources Research*, 43(1), 2007.

J. De Vente and J. Poesen. Predicting soil erosion and sediment yield at the basin scale: scale issues and semi-quantitative models. *Earth-Science Reviews*, 71(1):95–125, 2005.

Provincia Autonoma di Bolzano. Cartografia provinciale. URL `http://www.provincia.bz.it/informatica/temi/cartografia-provinciale.asp`.

G. Di Silvio. *Validity and limitations of different transport models with particular reference to sediment transport*. Elsevier, 1986. Agricultural nonpoint source pollution : model selection and application : contributions to a workshop held in June 1984 in Venice, Italy, ISBN 04-449-95056.

G. Di Silvio. *Erosion and sediment dynamics from catchment to coast, a Northern prospective*. Number 82. UNESCO, 2008.

G. Di Silvio and M. Nones. Morphodynamic reaction of a schematic river to sediment input changes: Analytical approaches. *Geomorphology*, 2013.

G. Di Silvio and M. Peviani. *Modelling short- and long-term evolution of mountain rivers: An application to the torrent Mallero (Italy)*, volume 37 of *Lecture Notes in Earth Sciences*. Springer Berlin Heidelberg, 1991.

G. Di Silvio, L. Guarino, and M. Nones. Modello per l'analisi del bilancio di sedimenti a scala di bacino nel fiume Adige. *XXXI Convegno Nazionale di Idraulica e Costruzioni Idrauliche*, 2008.

G. Di Silvio, M. Franzoia, M. Nones, D. Bonaldo, Zaggia L., G. Lorenzetti, and C. Dallangelo. Evaluating sediment input of rivers flowing in the Lagoon of Venice. VII, 2011. Scientific Research and Safeguarding of Venice, 2007-2010 results.

Provincia Autonoma di Trento. Piano cave. URL `http://www.minerario.provincia.tn.it/piano_cave/`.

SEL e Edison. URL `http://www.seledison.bz.it/index.php?id=297&L=1`.

I.V. Egiazaroff. Calculation of non-uniform sediment concentration. *Journal of Hydraulic Div.*, (91): 225–248, 1965.

F. Engelund and E. Hansen. *A monograph on sediment transport in alluvial streams*. Teknisk Forlag, 1967.

H. Fang, M. Chen, and Q. Chen. One-dimensional numerical simulation of non-uniform sediment transport under unsteady flows. *International Journal of Sediment Research*, 23(4):316–328, 2008.

G. Fasolato, P. Ronco, and G. Di Silvio. How fast and how far do variable boundary conditions affect river morphodynamics? *Journal of Hydraulic Research*, 47(3):329–339, 2009.

G. Fasolato, P. Ronco, E. Langendoen, and G. Di Silvio. Validity of uniform flow hypothesis in one-dimensional morphodynamic models. *Journal of Hydraulic Engineering*, 137(2):183–195, 2011.

G. Gaeta. *Modelli Matematici in Biologia*. Springer, 2007.

F. Gentile, T. Bisantino, R. Corbino, F. Milillo, G. Romano, and G.T. Liuzzi. Monitoring and analysis of suspended sediment transport dynamics in the carapelle torrent (southern italy). *Catena*, 80(1): 1–8, 2010.

M Hirano. River bed degradation with armouring. *Trans. Jpn. Soc. Civ. Eng*, 3(2):194–195, 1971.

T.P.Q. Le, J. Garnier, B. Gilles, T. Sylvain, and C. Van Minh. The changing flow regime and sediment load of the Red River, Viet Nam. *Journal of Hydrology*, 334(1–2):199 – 214, 2007.

W.S. Merritt, R.A. Letcher, and A.J. Jakeman. A review of erosion and sediment transport models. *Environmental Modelling & Software*, 18(8):761–799, 2003.

D.N. Moriasi, B.N. Wilson, K.R. Douglas-Mankin, J.G. Arnold, and P.H. Gowda. Hydrologic and water quality models: use, calibration, and validation. *Transactions of the ASABE*, 55(4):1241–1247, 2012.

G Müller and U Förstner. General relationship between suspended sediment concentration and water discharge in the Alpenrhein and some other rivers. *Nature*, 217:244–245, 1968.

M. Nones, D. Bonaldo, G. Di Silvio, and L. Guarino. Sediment budget of rivers at watershed scale: the case of Adige river. *European Geosciences Union*, 2009.

C. Paola and R. Seal. Grain size patchiness as a cause of selective deposition and downstream fining. *Water Resources Research*, 31(5):1395–1407, 1995.

I. Park and S. Jain. Numerical simulation of degradation of alluvial channel beds. *Journal of Hydraulic Engineering*, 113(7):845–859, 1987.

R. Ranzi, T.H. Le, and M.C. Rulli. A rusle approach to model suspended sediment load in the Lo river (Vietnam): Effects of reservoirs and land use changes. *Journal of Hydrology*, 422:17–29, 2012.

J. Sieben. *Modeling of hydraulics and morphology in mountain rivers*. PhD thesis. Technische Universiteit Delft, 1997.

S.K. Sinha and G. Parker. Causes of concavity in longitudinal profiles of rivers. *Water Resources Research*, 32(5):1417–1428, 1996.

J.P. Syvitski, M.D. Morehead, D.B. Bahr, and T. Mulder. Estimating fluvial sediment transport: the rating parameters. *Water Resources Research*, 36(9):2747–2760, 2000.

J.P.M. Syvitski and A.J. Kettner. On the flux of water and sediment into the Northern Adriatic Sea. *Continental Shelf Research*, 27(3):296–308, 2007.

S. Tealdi, C. Camporeale, and L. Ridolfi. Long-term morphological river response to hydrological changes. *Advances in Water Resources*, 34(12):1643–1655, 2011.

Regione Veneto. Sit. a. URL http://www.regione.veneto.it/web/ambiente-e-territorio/sistema-informativo-territoriale.

Regione Veneto. Dighe e invasi. b. URL http://www.regione.veneto.it/web/ambiente-e-territorio/dighe-e-invasi.

DE Walling. Human impact on land–ocean sediment transfer by the world's rivers. *Geomorphology*, 79 (3):192–216, 2006.

A.B. Watts and M. Torné. Subsidence history, crustal structure, and thermal evolution of the Valencia Trough: A young extensional basin in the western Mediterranean. *Journal of Geophysical Research: Solid Earth (1978–2012)*, 97(B13):20021–20041, 1992.

W. H. Wischmeier and D.D. Smith. Predicting rainfall erosion losses - a guide to conservation planning. *Agriculture Handbook*, (537), 1978.

W. Zhang, S. Mu, Y. Zhang, and K. Chen. Temporal variation of suspended sediment load in the Pearl River due to human activities. *International Journal of Sediment Research*, 26(4):487 – 497, 2011.

A. Zuliani, L. Zaggia, F. Collavini, and R. Zonta. Freshwater discharge from the drainage basin to the Venice Lagoon (Italy). *Environment International*, 31(7):929–938, 2005.